Simulating the Dynamics and Influences of the West African Westerly Jet

Akintunde Israel Makinde
(MKNAKI002)

Dissertation submitted for the degree of
Master of Science
in the
Department of Environmental and Geographical Science,
University of Cape Town

Supervisor
A/Prof. Babatunde J. Abiodun

January 2022

Declaration I

I understand the meaning of plagiarism and know that it is wrong. Hence, I declare that all the work in this thesis has been done by me, and that information derived from other studies has been properly acknowledged and referenced.

Signed by candidate

Akintunde Israel Makinde

Declaration II

There are parts of this thesis that have been submitted and are awaiting review in the following publications:

- Makinde A. I., Abiodun B. J., James R., Washington R., Dyer E., and Webb T., 2021, 'How well do CMIP6 models simulate the influence of the West African westerly jet on Sahel precipitation?' Submitted to *Climate Dynamics*.
- Makinde A. I., and Abiodun B. J., 2022, 'Simulating the characteristics of the West African westerly jet using the Model Prediction Across Scale-Atmosphere (MPAS-A)'. Submitted to *International Journal of Climatology*.

Abstract

The West African westerly jet (WAWJ) is a key rainfall producing system over West Africa. While past studies have examined the dynamics of the WAWJ and its influences on Sahelian rainfall, there is no information on how well the jet is simulated by contemporary climate models. This thesis examines the capability of the Coupled Model Intercomparison Project version 6 models (CMIP6) and the Atmospheric component of Model Prediction Across Scale (MPAS) in simulating the WAWJ, its moisture transport over West Africa, and its influence on Sahelian precipitation. Three types of climate dataset (observation, reanalysis, and simulations) were analysed in the thesis. The observation dataset (from the Climate Research Unit or 'CRU') and the reanalysis dataset (from the European Centre for Medium-Range Weather Forecast Atmospheric Reanalysis, or 'ERA5') were used to evaluate 26 CMIP6 models (for 35 years: 1980–2014) and MPAS (for 30 years: 1985–2014). To investigate the sensitivity of the simulated WAWJ to model resolution, two additional simulations were performed with MPAS, focusing on WAWJ strong years (1989, 1994, and 1999) and weak years (1986, 1990, and 2000). This thesis defined the WAWJ as a low-level westerly jet (with average maximum speed of 5 m s^{-1}) at 925 hPa over the eastern Atlantic Ocean and over the West African coast and used standard statistical metrics to quantify the capability of the models in simulating the characteristics and influences of the WAWJ.

The majority of the CMIP6 models capture the temporal and spatial structures of the WAWJ and agree with ERA5 that the jet attains its maximum speed in August. However, most simulated jets form earlier and are stronger than the observed jet. While most of the CMIP6 models capture the link between the jet and temperature distribution over West Africa, they struggle to reproduce the relationship between the jet and precipitation distribution over the sub-continent, especially over the Sahel. Most models failed to replicate the increase in the moisture transport (i.e., the eastward and north-eastward transports) associated with a stronger WAWJ, as in ERA5. Some models capture the increased moisture transport but do not translate it to increased precipitation over the Sahel.

MPAS performs well in simulating various features in temperature, precipitation, and wind fields over West Africa, but with wet and warm biases over the region. It also simulates the WAWJ but the simulated jet forms too early and is too strong. In addition, the position and

dynamics of the simulated jet differ from the observed jet because the model fails to capture the local pressure gradient force that induces the WAWJ over the Atlantic Ocean. The model underestimates the relationship between the WAWJ and Sahelian precipitation because it limits WAWJ moisture transports to the southern part of Sahel, in contrast to the observation. The sensitivity simulations show that increasing the horizontal resolution of the model does not improve the MPAS simulation of the WAWJ or the WAWJ moisture transport to the Sahel. The results of the study have application in improving the climate models for seasonal predictions and future projections over West Africa, especially over the Sahel.

Acknowledgments

First and foremost, I acknowledge the greatness and supremacy of God. Secondly, I appreciate God's goodness and favour for offering His protection, provision, guidance, and wisdom in overseeing the successful completion of this degree. Thanks, and glory to His name.

Secondly, I wish to record my appreciation for my supervisor, A/Prof. Babatunde J. Abiodun for his mentorship, tutelage, support, encouragement, and patience. He has taught me so much with his life experiences and personal testimonies. I cannot adequately express or quantify the impact he has had on my life and my career. May God continue to bless and uphold you and the family. May He equip you the more as you are a blessing to this generation and beyond.

My sincere thanks must also go to the LaunchPAD (Priority on African Diagnostics) – the Climate Model Evaluation Hub for Africa – and the Foreign, Commonwealth & Development Office (FCDO) for their financial support, without which I would not have been able to complete this degree. I count myself fortunate to be part of the first phase of the LaunchPAD fellowship and, indeed, it was a launch pad for me and my career. I acknowledge all the members of the fellowship. Many thanks are due to Dr Rachel for her wonderful and encouraging coordination throughout the fellowship period. It was a great privilege to work with Dr Ellen Dyer and Dr Thomas Webb too. I wish to also say a big thank you to UK Aid for their financial responsibility towards the fellowship and the Met Office for their support. Thank you all.

My acknowledgements would be incomplete without also giving credit to the Climate Systems Analysis Group (CSAG), as well as the Centre for High-Performance Computing (CHPC) for the contribution of computing resources. I equally want to thank all the institutions that provided the data for this work: the European Centre for Medium-Range Weather Forecasts (ECMWF) Atmospheric Reanalysis for the ERA5 data; the Climate Research Unit (CRU) for the CRU TS v4 data; the National Centers for Environmental Prediction (NCEP) Climate Forecast System (CFS) for the CFSR data through the National Center for Atmospheric Research (NCAR) Research Data Archive (RDA); the World Climate Research Programme (WCRP) and its working group on the couple modelling for CMIP6 data through the Earth System Grid Federation (ESGF) archive. I also need to acknowledge Phillip Mukwenha for his

technical support, patience, and unrelenting willingness to help, and Roland Takong for the numerous MPAS tutorials, his fixing of errors, and generous debugging support.

I would like to also thank my peer-review group members; Paige Donkin, Roland Takong, Maoyi, and Sawadogo, for the knowledge shared and for debating our analyses together. I am grateful to my fellow graduate student, Paige Donkin, for her many wonderful discussion, intellectual insights, and encouragement. She is such a good friend who has excellent teamwork skills, a hard worker with a keen sense of quality, and pays attention to every detail. We have shared everything together on this journey, from meetings to seminars. Many thanks to the Egbebiyi Family, Dr Temitope and Mrs. Oluwabukola Egbebiyi, for their kind encouragement, moral, and spiritual support.

Finally, an enormous thank you is due to my family. Most importantly, I wish to acknowledge my mother, who shifted roles and took up a variety of responsibilities to lay the good foundations that ensured not one of her children is without a degree. To my Father, for being a vessel through which God has made this glorious seed come alive. No less, I wish to thank my partner, who with patience and understanding waited and trusted the plan and God's purpose for this successful journey. Lastly, to my siblings, Arc. Bayo, Mr. Leye, Nurs. Kemi, and Dapo, I want to record my gratitude for the unity, love, care, deep understanding, and courage with which we are pushing through. I pray for God's speed and help in all ramifications.

To everyone else who has helped me on this journey but whom time and space do not allow me to mention: Thank you.

Dedication

To the Almighty God, the Alpha and Omega,

who because of His love for me and the world, gave up

his only Son on the Cross as my substitute

that I may live and have eternal life.

John 3:16

Table of Contents

List of Figures

List of Tables

List of Abbreviations

ADW – Angular-distance weighting

AEJ – African easterly jet

AEWs – African easterly waves

AGCM – Atmospheric general circulation model

AOGCM – Atmosphere-ocean coupled general circulation model

AR1 – Assessment Report One

ARW – Advance Research Weather Research and Forecasting

AWEs – African easterly waves

CAM-EULAG – Community atmospheric model with EULAG dynamics

CFSR – Climate forecast system reanalysis

CHPC – Centre for High Performance Computing

CLLJ – Caribbean low-level jet

CLJs – Coastal low-level jets

CMIP5 – Coupled Model Intercomparison Project, Phase 5

CMIP6 – Coupled Model Intercomparison Project, Phase 6

CRU – Climate Research Unit

ECMWF – European Centre for Medium-Range Weather Forecast

ENSO - El Niño-Southern Oscillation

ERA5 – ECMWF Atmospheric Reanalysis version 5

ESGF – Earth System Grid Federation

GCM – Global climate model (or global circulation model)

GDP – Gross Domestic Product

GPLLJ – Great Plains low-level jet

IPCC – Intergovernmental Panel on Climate Change

ITCZ – Intertropical Convergence Zone

ITD – Intertropical discontinuity

LAM – Limited area model

LLJs – Low-level jets

LW – Longwave

MCS – Mesoscale convective system

MPAS – Model prediction across scale

MPAS-A – MPAS Atmosphere

NAO – North Atlantic Oscillation

NCAR – National Center for Atmospheric Research

NCEP – National Center for Environmental Prediction

NLLJs – Nocturnal low-level jets

OGCM – Oceanic general circulation model

PGF – Pressure gradient force

RCM – Regional climate model

RDA – Research data archive

RMSE – Root mean square error

RRTMG – Rapid radiative transfer model for GCMs

SALLJ – South American low-level jet

SCVT – Spherical Centroidal Voronoi Tessellation

SHL – Sahara heat low

SST – Sea surface temperature

SW – Shortwave

TEJ – Tropical easterly jet

TLLJ – Turkana low-level jet

VGCM – Variable resolution global climate model

WAHL – West African heat low

WAM – West African monsoon

WAWJ – West African westerly jet

WCRP – World Climate Research Program

WRF – Weather research and forecasting

WRF-NRCM – Weather research and forecasting nested regional climate model

WSM6 – Weather research and forecasting single-moment 6-class

YSU – Yonsei University planetary boundary layer scheme

Chapter 1: INTRODUCTION

1.1 Background

West Africa (4^{o}N:15^{o}E, 28^{o}N:17^{o}W), a sub-region north of the equator in the western part of Africa, consists of seventeen countries (Figure 1.1) including Benin, Burkina Faso, Cabo Verde, Gambia, Ghana, Guinea, Guinea-Bissau, Cote d'Ivoire, Liberia, Mali, Mauritania, Niger, Nigeria, Senegal, Sierra Leone, Togo and Saint Helena (Beauchemin, 2011; Egbebiyi, 2016; Niang et al., 2017; USAID, 2018). The subregion, which is approximately 6 million km^2 in area, covers about one-fifth of the landmass on the entire continent (Egbebiyi, 2016; Shvili, 2021). There is a great diversity of landscapes in West Africa, ranging from the alluvial valleys in Senegal and Ghana to the sandplains and low plateaus of the Sahel, and the hills of Togo to mountains reaching over 1,500 metres in Guinea and 1,800 metres in Niger (*Physical Geography*, n.d.). Some important topographical features in the region include the Adamawa Highlands (2,042m), Fouta Djallon (1,537m), the Guinea Highlands (1,656 m), Jos Plateau (1,690m), the Mandara Mountains (1,142m), the Nimba Mountains (1,752m), the Plateau of Djado (1,120m) in northern Niger, and the Sierra Leone Mountains (1,948m) (Ferguson, 1985). West Africa, which is the most populous region in Africa with an estimated population of 412 million people (as of 2021), is projected to have a population of 796 million people by 2050 (United Nations, 2019).

The economy of West Africa is largely based on farming, with about 80% of the population depending on the rain-fed agriculture that accounts for about 96% of the overall crop production in the region for their livelihood (Antwi-Agyei et al., 2021; Egbebiyi et al., 2019; Omotosho & Abiodun, 2007). The agricultural sector provides employment for roughly 60% of the population and contributes around 35% of the GDP of West African nations (Antwi-Agyei et al., 2021; Osabohien et al., 2021). Furthermore, West Africa produces approximately 30% of the entire continent's total food requirement.

Nevertheless, the agriculture, food security, and many socio-economic activities in West Africa are under the threat of devastating impacts of extreme weather and climate events (particularly extreme rainfall, drought, and heatwaves), which are fuelled by climate variability (Abatan, 2011; Adaawen, 2021; Antwi-Agyei et al., 2021; Egbebiyi et al., 2019; Taylor et al., 2017).

These impacts are usually most severe in the Sahel, where food shortages are recurrent. For instance, in 2010 and 2012, more than 15% of the population of the Sahel region faced food insecurity due to drought (in addition to environmental degradation, population displacement, and wars) (FAO 2012; Boyd et al., 2013; Masih et al., 2014; Diouf et al., 2015; Mbow et al., 2021). Notwithstanding extreme climate events, serious concerns also exist regarding the scarcity of pastoral resources (grazing and water) in the region, and the increasingly negative impacts of climate change. The occurrence of droughts and other weather extremes simply make it even harder for farmers to produce the crops and livestock needed to sustain the growing population (Graves et al., 2019). Hence, any reliable plan pertaining to socio-economic development in West Africa requires a better knowledge of climate variability and change over the subcontinent.

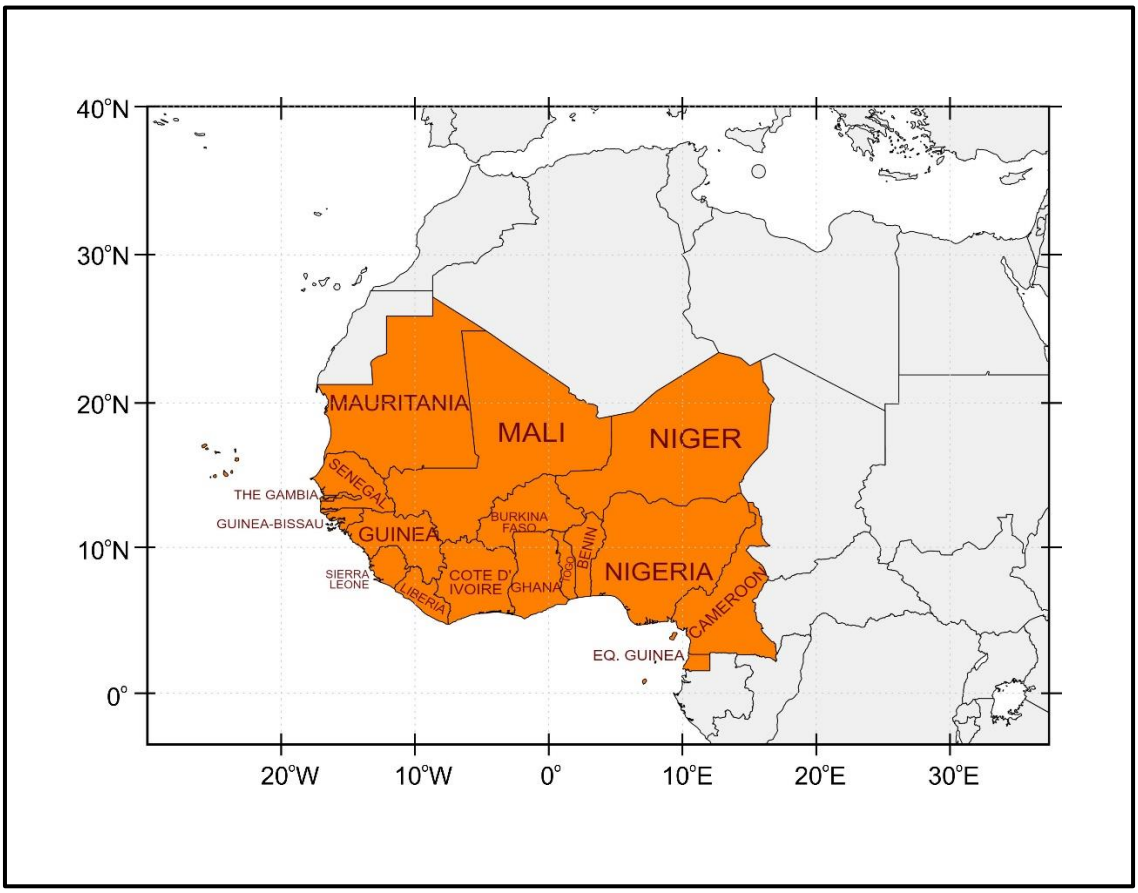

Figure 1.1: West Africa and the seventeen countries that make up the subregion (modified after https://mapchart.net/world.html).

1.2 The Climate of West Africa

The climate of West Africa is characterised by wet and dry seasons that vary from arid desert conditions in the north to humid tropical monsoon conditions along the coastal regions in the south (Figure 1.2). The region's climate is marked with uniformly high sunshine and high temperatures in the lowlands with a mean annual temperature above 18^{o}C and about 26^{o}C in the areas within 10^{o} around the equator. While the temperature can be as high as 58^{o}C during the day, it can be as low as 4^{o}C at night in places such as the northern part of Mali and Niger (Ferguson, 1985; USGS EROS, 2016). In the Sahel, a transitional zone between the arid Sahara (desert) to the north and the belt of humid savannas to the south, monthly mean temperatures vary from a maximum of 33–36^{o}C to a minimum of 18–21^{o}C, with a projection that the temperature will have risen by approximately 3^{o}C by 2050 (Graves et al., 2019).

Generally, West Africa's rainfall decreases latitudinally from the equator to higher latitudes and varies from year to year, as well as on decadal time-scales, with varying length of wet seasons (Gbobaniyi et al., 2014; Maranan et al., 2018). For instance, it rains abundantly throughout the year in the Gulf of Guinea, with no defined dry season (Afiesimama et al., 2006; Bichet & Diedhiou, 2018; Joly & Voldoire, 2010; Muhammed, 2013), whereas in places like Mali and Niger (to mention only two), precipitation is limited only to a wet season. As one progresses to the northern edge of the Sahel, precipitation decreases in both quantity and duration (Lebel & Ali, 2009). The Sahel gets approximately 200–600mm of rainfall a year, most of which falls between May and September (Jnr, 2014; Lebel & Ali, 2009; Le Houerou, 1980; Panthou et al., 2014; Visser & Sterk, 2007). West Africa's rainfall patterns are influenced by many factors, including ocean currents and topography (Quenum et al., 2020). For instance, places with higher mountains – like the Jos Plateau in Nigeria and the Fouta Djalon Highlands in Guinea – receive more precipitation than lowlands on the same latitude. In addition, sea surface temperature (SST) variability and anomalies affect the Sahelian rainfall on interannual and decadal time scales (Buontempo et al., 2012).

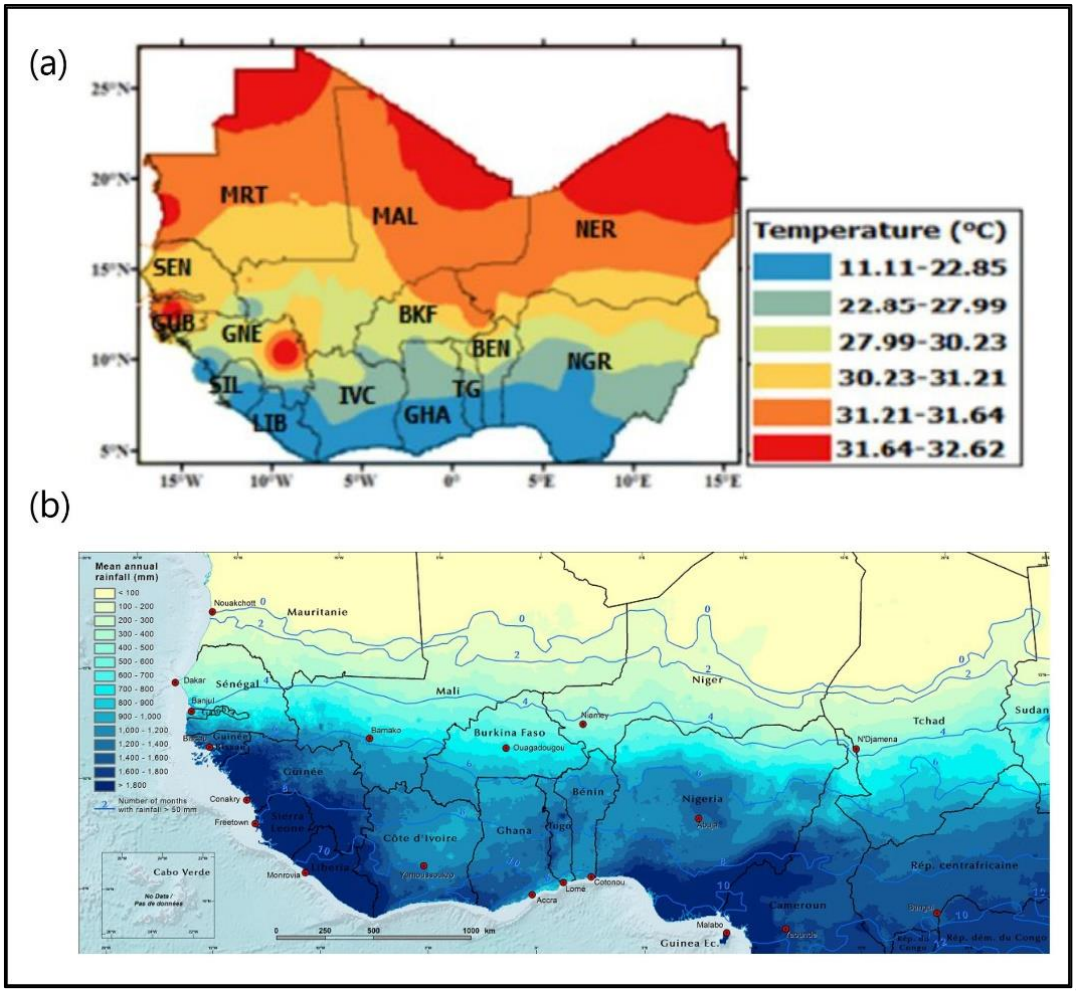

Figure 1.2: Spatial distribution of annual mean (a) temperature and (b) rainfall over West Africa (modified after the following sources: (1) Ojo et al., 2021; (2) Atlas at https://eros.usgs.gov/westafrica/node/157. Last accessed 17 January 2022).

1.3 Impacts of West African rainfall variability

The high variability in West African rainfall is a bottleneck to socio-economic developments in the region. It fuels extreme weather and climatic events (e.g., droughts, dry spells, extreme rainfall, and heatwaves) that often degrade the environment, damage water resources, destroy agricultural products (e.g., crops and pasture), threaten food security, encourage disease epidemics (such as malaria and meningitis), disrupt hydro-electric power generation, and destroy human lives – especially in the Sahel, as illustrated in Figure 1.3 (Abiodun et al., 2012; Akpoti et al., 2016; Atiah, Mengistu Tsidu, et al., 2020; Ballo et al., 2021; Campion & Venzke, 2013; Diasso & Abiodun, 2017; Druyan, 2011; Gautam, 2006; Geist & Lambin, 2004; Graef

& Haigis, 2001; Janicot, 1992; Kumi & Abiodun, 2018; Lebel et al., 2000; Nicholson, 2000, 2013a; Oguntunde et al., 2018; Sylla et al., 2010; Tarhule, 2005; Tschakert et al., 2010). For instance, the Sahelian drought of 2007, which was described as the worst natural disaster to strike the region for decades, caused approximately 325,000 deaths (Ahmadalipour & Moradkhani, 2018). Between 1988–2010, the Savannah zone (particularly Ghana) recorded 15 flood events resulting in about 244 casualties and the displacement of around 692,700 people. In the more recent flooding that took place in 2015 in Accra, Ghana, an estimated 152 people were killed and over 8,000 were displaced (Asumadu-Sarkodie et al., 2015; Karley, 2009; Kayaga et al., 2021). In Nigeria in 2012, 33 of the 36 states in the country were flooded, claiming about 363 lives and negatively impacting approximately 7 million people, not to mention causing roughly $500,000 of economic loss to damages (Komolafe et al., 2015). Six years later, severe floods affected about 210,000 people, destroying 82,000 homes and devastating crops and livestock (Ajibade et al., 2013; Guha-Sapir et al., 2013; Koike, 2019; Komolafe et al., 2015; Okoloye et alf., 2013). In a more recent example, the flooding of Lake Chad and its tributaries in October 2019 caused the displacement of thousands of people along the Chad and Cameroon border (McOmber, 2020). In the same year, flooding of the Niger River killed 57 and negatively impacted roughly 211,366 people, also damaging approximately 16,000 houses (Elagib et al., 2021).

In addition to fuelling extreme events, the high rainfall variability devastates planning and management across a range of socio-economic sectors (including, but not limited to agriculture, water resources, health services, and sporting activities). Agriculture, which forms the economic backbone of West African countries, is predominantly rain-fed and highly prone to suffering the effects of rainfall variability (Abiodun et al., 2012; Nicholson, 2013a; Rosegrant et al., 2002; Shiferaw et al., 2014). Furthermore, any variability in annual rainfall (e.g., the amount, onset, cessation, and duration of the rainy season) usually impacts agricultural practices by influencing things such as seed sowing, germination, and overall crop production. For instance, in 2005, a rainfall deficit (in addition to insect invasion) destroyed the harvest in Niger (Devereux, 2009, 2019). Similarly, in 2010, the Sahelian droughts deteriorated soil quality and destroyed vegetation (Jnr, 2014), putting approximately 10 million people at risk of acute hunger and resulting in more than 25% of refugee children in Chad becoming malnourished (Vogel, 2010). Again, in 2012 and 2013, rainfall variability in the region led to serious famine, exposing about 18 million people to the risk of hunger and subjecting 1.4 million children to severe malnutrition (Essoungou, 2013b).

Moreover, studies have shown that the frequency and severity of extreme events associated with rainfall variability are increasing and becoming more widespread (Dietz et al., 2006; Elagib et al., 2021; Essoungou, 2013a; Quenum et al., 2019). These studies also indicate that the trend may persist into the future as climate change and variability continue to fuel extreme weather and climatic events. Therefore, a greater understanding of the causes of rainfall variability in the region will provide a more informed assessment of the range of future rainfall variability that West African societies will have to mitigate against (by reducing exposure and vulnerability and enhancing resilience). This thesis is a modest attempt to move in that direction.

Figure 1.3: Impact of extreme weather and climate events (droughts, dry spells, extreme rainfall, and disease epidemics) in the Sahel (modified after the following sources: (1) https://cpb-eu-w2.wpmucdn.com/edublog.mgfl.net/dist/a/14/files/2015/05/Rural-Land-Degradation.compressed-1k178t6.pdf; (2) https://ourworld.unu.edu/en/desertification-crisis-affecting-168-countries-worldwide-study-shows; (3) https://reliefweb.int/report/niger/coping-floods-niger; (4) https://www.theguardian.com/global-development/2021/apr/28/almost-30-million-will-need-aid-in-sahel-this-year-as-crisis-worsens-un-warns; (5) https://www.thepledge.ng/hunger-in-africa-continues-to-rise-fao/. Last accessed 17 January 2022).

1.4 Atmospheric systems influencing West African rainfall

Several atmospheric systems interact in complex ways and at various spatial and temporal scales to induce or modulate rainfall over West Africa (Figure 1.4). While some of these systems are mesoscale or synoptic scale features that reside within the West African region, some are global circulation features, and others are regional-scale features located outside the West African region. Examples of global circulation features that influence West African rainfall are the Hadley Cell (Fontaine et al., 1995; Freitas et al., 2017 ; de Oliveira et al. 2018; Jackson et al. 2020) and the Ferrel Cell, a residual mass transport created by the breaking of transient eddies from the mid-latitude systems. The eddies usually manifest as 'dry intrusion' events in the mid-troposphere over the Sahel and impact Sahel convection (Roca et al. 2005; Lafore et al. 2011). The regional-scale circulation features that remotely modulate West African rainfall through atmospheric teleconnection include El Niño-Southern Oscillation (ENSO) (Joly & Voldoire, 2009; Okonkwo et al., 2015; Preethi et al., 2015) and North Atlantic Oscillation (NAO) (Diatta et al., 2020; Lüdecke et al., 2021), as well as others. However, the focus of the present discussion will be on the atmospheric systems that reside within the West African region.

1.4.1 West African monsoon

The West African monsoon (WAM) is an important system influencing West African rainfall (Figure 1.2). The WAM, a regional-scale atmospheric system, involves a seasonal shift in surface and lower-level wind direction over West Africa. It is associated with the replacement of the cool dry north-easterly wind by the moist warm south-westerly wind in summer. While the north-easterly wind brings dust and harmattan in the wintertime over the region, the south-westerly (or summer monsoon) brings moisture from the eastern Atlantic onto the continent and contributes to the annual precipitation. The two trade winds converge in a band called the Intertropical Convergence Zone (ITCZ) over the ocean, or intertropical discontinuity (ITD) over the continent. The ITCZ is characterised by the formation of deep convection and an associated rain belt over West Africa. The WAM system, which is driven by the meridional gradient of horizontal temperature between the Atlantic Ocean and the continent, varies from year to year and the variation affects rainfall all over West Africa (Afiesimama et al., 2006; Son & Seo, 2020). At the intraseasonal scale, the onset of the WAM is characterised by an abrupt shift in the latitudinal position of the ITCZ (from a quasi-stationary position at about 5^oN to 10^oN) (Hastenrath 1995; Sultan et al., 2003). Precipitation and convection are also

significantly affected (Redelsperger et al., 2002). As the northern boundary of the ITCZ extends northward, the monsoon flow becomes stronger and convection within the ITCZ is enhanced (Sultan et al., 2003). Hence, the monsoon system (WAM) transports abundant moisture (by the warm and moist south-westerlies from the Atlantic Ocean) onto West Africa. As a result, the WAM provides most of the rainfall that serves as a major source of potable water for people and livestock and a supply for rain-fed agricultural activity in West Africa (Sultan et al., 2005; Monerie et al., 2016). Generally speaking, the West African rainfall is controlled by the interaction and latitudinal movement of the WAM and the ITCZ (Fig 1.4).

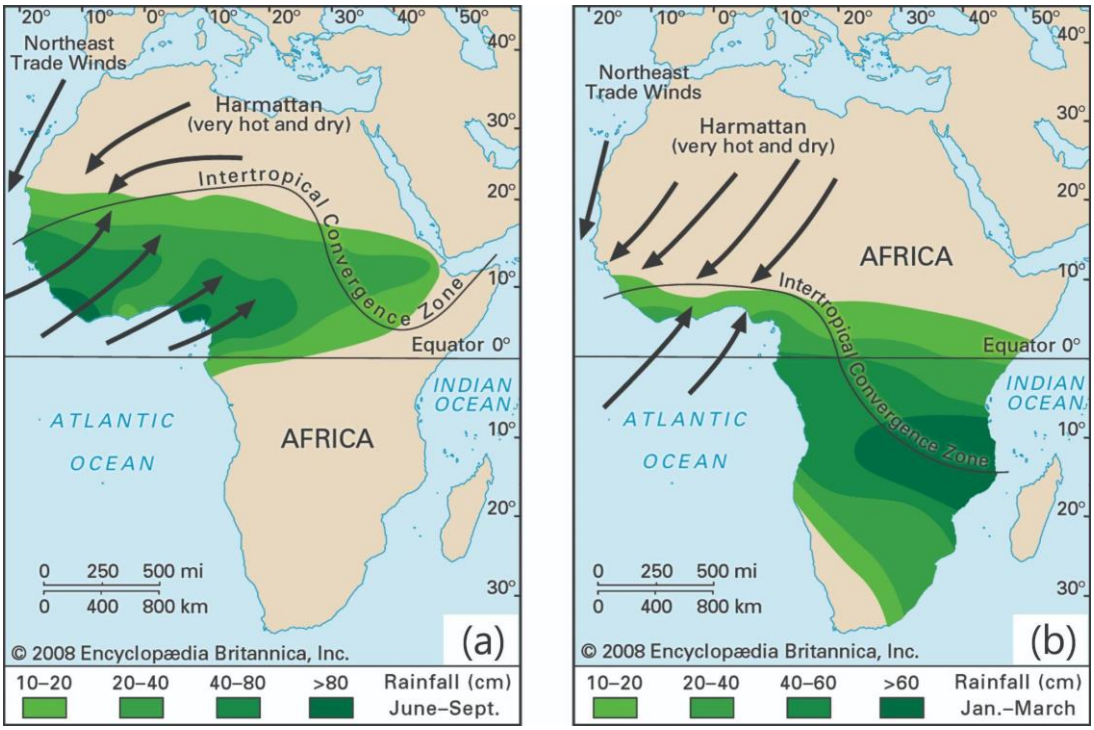

Figure 1.4: West African monsoon wind and rainfall patterns in (a) June–September and (b) January–March (adapted from Encyclopaedia Britannica at https://www.britannica.com/science/West-African-monsoon#/media/1/640047/126422. Last accessed 17 January 2022).

1.4.2 African easterly jet

The African easterly jet (AEJ) is another important climatic feature over West Africa (Figure 1.5). Along with the WAM and the ITCZ, this maximum easterly wind between 600–700 hPa, with a mean wind speed usually in the order of 10–12m s^{-1}, modulates rainfall in the Sahel and over the entire West Africa at large (Cook, 1999; Omotosho and Abiodun 2007; Cornforth et al., 2009; Dezfuli & Nicholson, 2011; Hosten, 2018). The jet forms over northern Africa (to the north of the monsoon trough) as a result of the meridional surface moisture and the positive meridional temperature gradient between the Gulf of Guinea and the Sahara Desert (Cook, 1999; Tompkins et al., 2005; Cornforth et al., 2009; Dezfuli & Nicholson, 2011; Sylla et al., 2011; Kebe et al., 2020). From March to October, the jet has a mean intensity of 15m s^{-1} (with the highest intensity occurring in August), and its meridional position varies from 10^{o} to 20^{o}N between June and August (Burpee, 1972; Thorncroft & Blackburn, 1999; Tompkins et al., 2005; Hosten, 2018). On average, the jet has maximum zonal wind speeds located mainly to the west (Hosten, 2018). Analysis of the jet in August at 600 hPa shows a distinctive zonally oriented double-core (western; 20°W-5°E and eastern core; 5°E and 30°E) structure in some years (Nicholson & Webster, 2007; Dezfuli & Nicholson, 2011; Hosten, 2018). While the western core is relatively stationary in those years, the eastern core (at the mean position of 20^{o}E) experiences large latitudinal shifts (both northward and southward) relative to the western core (Dezfuli & Nicholson, 2011). In August, the AEJ is pushed north-westward and its horizontal and vertical wind shear are enhanced (Grodsky, 2003; Pu and Cook, 2010; Dezfuli and Nicholson, 2010). The horizontal instability of the AEJ leads to the generation of African easterly waves (AEWs). The low-level convergence associated with AEWs usually lifts up the warm moist south-westerly monsoon air to initiate deep convections (e.g., thunderstorms and mesoscale convective systems, 'MCS'), which are known for heavy precipitation in West Africa - especially over the Sahel. Hence, any variation in the position and strength of the AEJ causes variabilities in precipitation at interseasonal and interannual time scales in various regions, especially in the Sahel (Jenkins et al., 2005; Sylla et al., 2011). It also causes interseasonal fluctuations in the position of the monsoon rain belt over West Africa (Cook, 1999; Nicholson and Webster, 2007; Sylla et al., 2009, 2011).

1.4.3 West African westerly jet

The West African westerly jet (WAWJ) also modulates precipitation over the Sahel and West Africa at large (Figure 1.5). The WAWJ is a low-level westerly jet that forms over the eastern

Atlantic and the West African coast. The jet is said to form when the westward extension of the continental thermal low (the West African heat low, or 'WAHL') overlays the Atlantic marine ITCZ (Pu and Cook, 2010). The WAWJ transports moisture from the eastern Atlantic onto the subcontinent (especially at 8–11°N), as well as enhances moisture transport by the WAM and pushed it further north of the ITCZ, reaching about 20^{o}N over the western Sahel (Fontaine, 2003; Omotosho and Abiodun, 2007; Nicholson, 2013; Lélé et al., 2015; Lélé and Leslie, 2016). As a result, variation in the strength of the WAWJ influences precipitation over West Africa, especially over the Sahel region (Kidson & Newell, 1977; Cadet & Nnoli, 1987; Grodsky et al., 2003; Nicholson and Grist, 2003; Fontaine 2003; Fontaine, 2003; Gu & Adler, 2004; Omotosho and Abiodun 2007; Pu & Cook, 2012; Lélé et al., 2015; Liu et al., 2019).

However, as West African rainfall is a product of these atmospheric systems and their complex interactions, for any atmospheric model to capture the West African rainfall spatial pattern and temporal variability, it needs to correctly simulate those atmospheric systems and their interactions. This thesis explicitly aims to improve knowledge in that area.

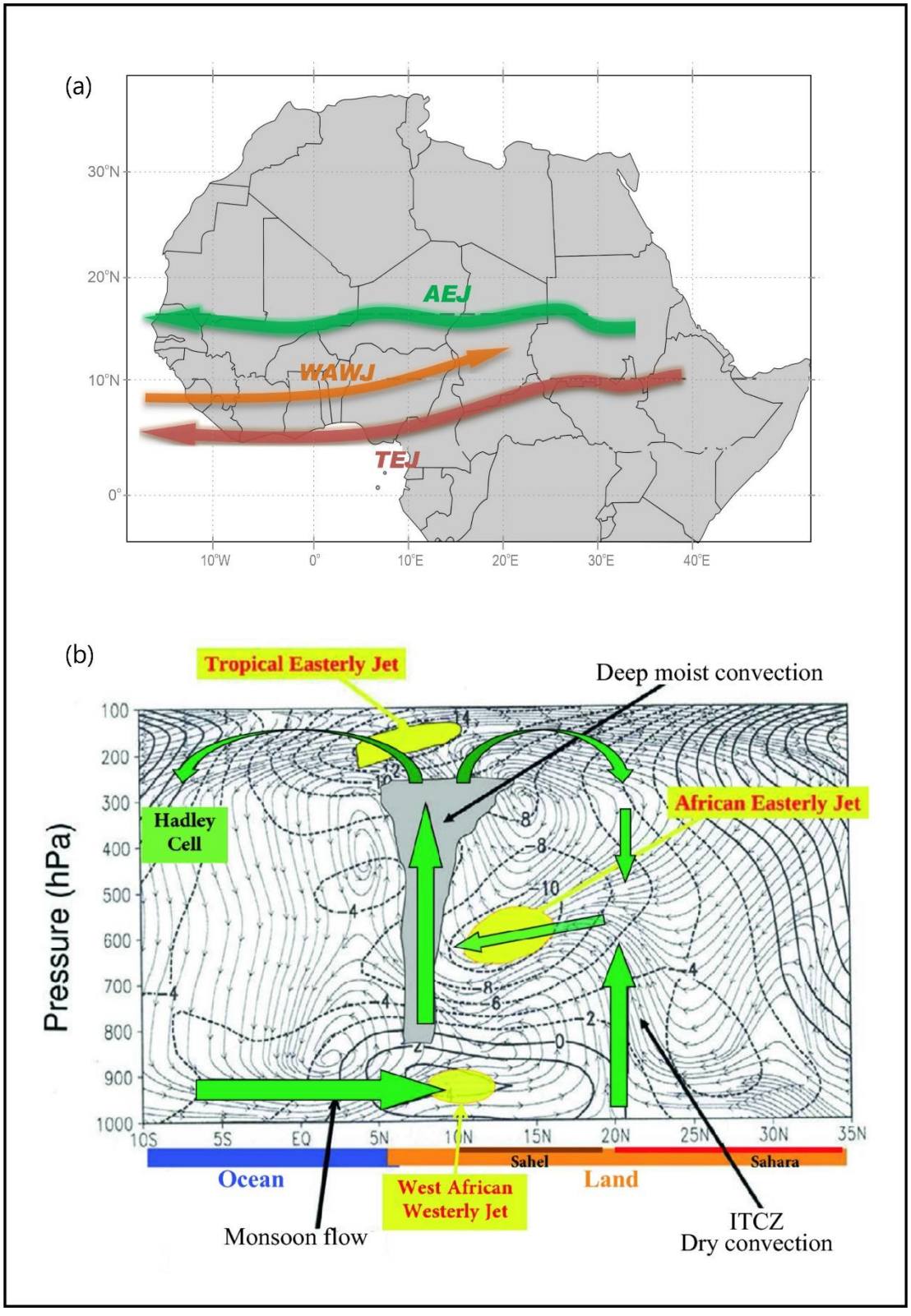

Figure 1.5: (a) Schematic and (b) vertical profile of major rainfall-producing systems over West Africa (modified after Sylla et al., 2013).

1.5 Atmospheric models

Atmospheric models are the most viable tools for simulating and studying atmospheric systems, features, and processes-including their complex interactions (Figure 1.6) and influence on variables (Zhang & Moore, 2015). There are three major types of atmospheric model, namely: global climate models (also known as global circulation models, general circulation models, or 'GCMs'); regional climate models (also known as limited area models or 'RCMs'); and variable resolution GCMs (also known as stretched-grid GCMs or 'VGCMs').

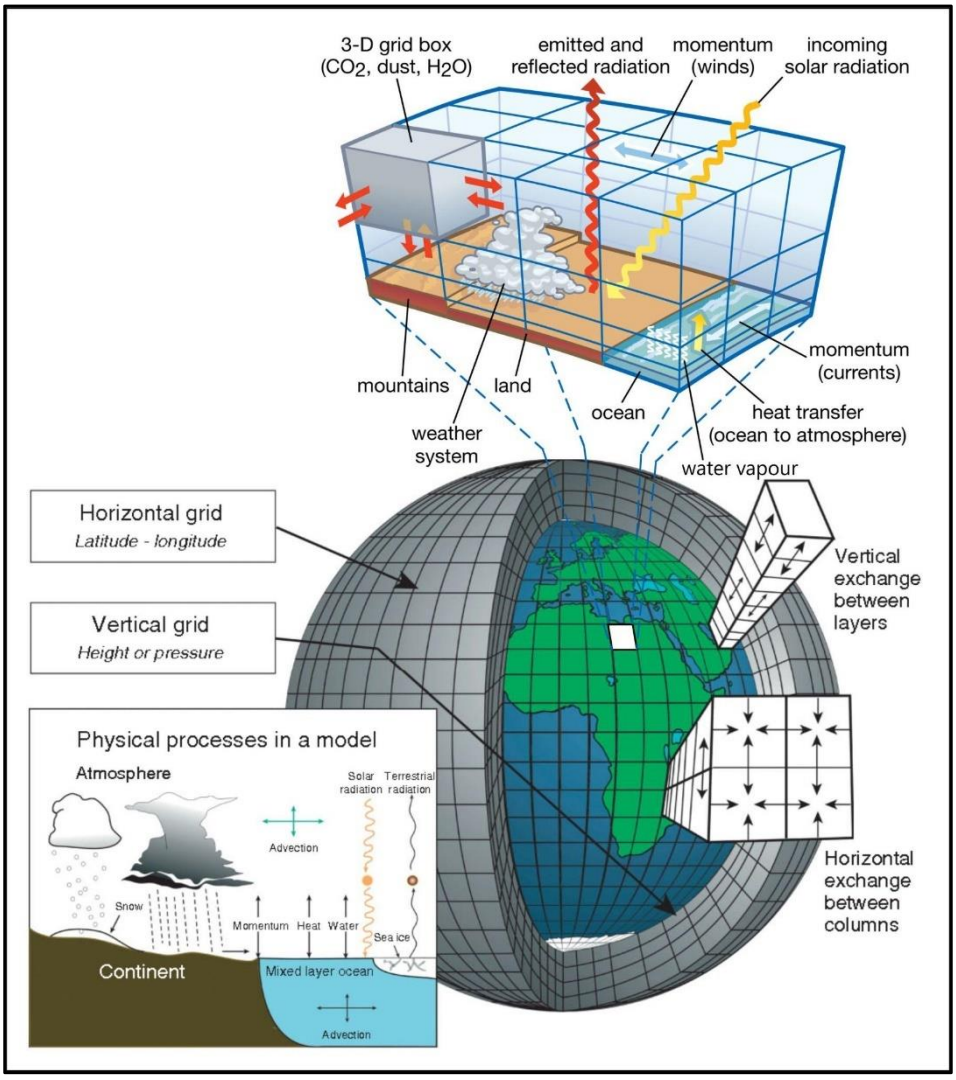

Figure 1.6: Schematic representation of the physical processes, their complex interactions, and cartesian grid structure used in finite-difference GCMs (modified after the following sources: (1) Edwards (2011); (2) https://www.britannica.com/science/global-warming/Theoretical-climate-models#/media/1/235402/109625. Last accessed 17 January 2022).

1.5.1 Global climate models

The GCM is a mathematical model that solves equations representing the physical processes of the atmosphere and ocean to understand atmospheric and ocean dynamics and their feedback. Due to the nonlinearity of these equations, GCMs employ numerical methods to obtain an approximate solution and then divide the atmosphere and/or ocean into discrete 3-dimensional grid cells which represent computation units. These grid cells are usually in the range of 100–300km in size. Therefore, GCMs use parameterisation and assumptions for processes that occur on a scale too small for the grid cells or which cannot be resolved directly.

GCMs can be subdivided into three groups, namely: atmospheric global climate models (AGCMs), which simulate the atmosphere and land surfaces using imposed SST; oceanic global climate models (OGCMs), which simulate the ocean and sea-ice using imposed fluxes from the atmosphere; and atmosphere-ocean coupled global climate models (AOGCMs), which combine the two submodels and eliminate the need for imposed fluxes and SST.

GCMs can be used to study the impacts of global circulations or teleconnections on precipitation over a region like West Africa (Zhao et al., 2021), as well as studying the trends in climate variables such as precipitation and temperature (Druyan, 2011; Sylla et al., 2016; Hassan et al., 2020; Macadam et al., 2020; Shiru et al., 2020). However, because of their coarse horizontal resolution (100–300km), GCMs cannot explicitly capture fine-scale features induced by local temperature-gradient, vegetation, orography, and coastlines (Abiodun et al., 2011; Raj et al., 2018; Iles et al., 2019). This usually compromises the accuracy of simulated regional precipitation patterns.

1.5.2 Regional climate models

RCMs are a numerical atmospheric model like GCMs that are used for regional applications, as the name implies. However, RCMs only simulate a portion of the globe (a region) and are therefore forced by specified lateral and oceanic conditions derived from a GCM that simulates atmospheric, oceanic, and land surface processes or observation and/or reanalysis datasets (Leung et al., 2003; Rummukainen, 2010). In other words, RCMs downscale global information provided by a GCM or coarse-scale observations to local- or fine-scale, limited to an area or a region. Hence, RCMs can typically be run at a higher resolution (i.e., smaller grid cell size, usually in the order of 12.5km) and at a faster rate than GCMs (Akinsanola et al., 2015; Giorgi et al., 2021). In this way, RCMs address the need to understand and simulate

climatic processes and phenomena that are not accounted for by global models (Gutowski et al., 2020; Stefanidis et al., 2020).

RCMs have been used for providing regional climate information for climate predictability studies, seasonal climate prediction, and studying the impact of land-cover changes (Wang et al., 2004; Giorgi, 2006; Abiodun et al., 2012; Lawal et al., 2015; Egbebiyi, 2016; Naik & Abiodun, 2016). However, RCMs suffer from uncertainties associated with their internal mechanisms, as well as inherited from the driving GCMs. In addition, RCMs currently lack a feedback mechanism because the nesting of the RCMs within GCMs occurs only in one direction – from the GCM to the RCM (Noguer et al., 1998; Sylla et al., 2009; Akinsanola et al., 2015).

1.5.3 Variable resolution global climate models

VGCMs offer an alternative approach to nested LAM (limited area model) in order to perform high-resolution simulation at a reduced computational cost compared to increasing the GCM's resolution (Kramer et al., 2020). Unlike GCMs, VGCMs allows for unified model hierarchy (Zarzycki et al., 2014) and high spatial resolutions in areas of interest, such as tropical areas of West Africa where vegetation variations, complex topography, coastlines, and MCS are the dominant features forcing precipitation (Mathon and Laurent, 2001). VGCMs employ grid-stretching methods ranging from non-uniform grid mapping (e.g., CAM-EULAG) to unstructured centroidal Voronoi meshes (e.g., MPAS) as the basis for the horizontal discretisation in the fluid-flow solver. As a result, the variable resolution grid structure allows high-resolution areas to easily blend into low-resolution areas without the usual boundary constraints that plague conventional regional climate models (Ringler et al., 2008).

Virtually all VGCMs conserve quantities such as mass, since their numerical schemes are uniform at the global scale, regardless of grid spacing (Zarzycki et al., 2014). In addition, VGCMs, through their variable resolution capability and single unified framework (rather than two separate models), ameliorate issues like one-way interaction and the potential inconsistency associated with the traditional nesting of an RCM into a GCM (Huang et al., 2016).

Over the past few decades, VGCMs have performed better than uniform resolution models. For instance, CAM-EULAG does a better job of simulating the monsoon season, capturing the rain belt associated with the ITCZ, and reproducing the observed global rainfall pattern over West

Africa than traditional GCMs with the same grid (Abatan, 2011; Abiodun et al., 2011). Furthermore, the recently developed Model for prediction across scale (MPAS) has the capability of simulating the spatial and temporal CO_2 variation at a global scale, as well as representing the observed atmospheric CO_2 spatial structures related to the midlatitude synoptic weather system (Zheng et al., 2021). In addition, MPAS performs well in reproducing the dynamics of the WAM and its associated precipitation over West Africa (Heinzeller et al., 2016). However, there is little or no information on the capability of MPAS in simulating the WAWJ and its moisture transport.

1.6 Aim and objectives

1.6.1 Aim

The aim of this thesis is to examine the capability of contemporary GCMs and the new VGCM in simulating the WAWJ and the associated moisture transports over West Africa, and to investigate the sensitivity of the simulated WAWJ to increase in horizontal grid resolution.

1.6.2 Objectives

The objectives of the thesis are as follows:

- To examine the performance of contemporary GCMs in simulating the characteristics of the WAWJ and its moisture transport over West Africa.
- To investigate how well the GCMs capture the relationship between the WAWJ and precipitation over West Africa.
- To study the capability of the new VGCM (i.e., MPAS) in simulating WAWJ dynamics.
- To examine the sensitivity of the simulated WAWJ to an increase in horizontal resolution in MPAS.

1.7 Structure of dissertation

The remaining part of this dissertation is structured as follows: Chapter Two reviews past studies on the dynamics and the influence of the WAWJ on Sahel precipitation; the performance of coupled model intercomparison project, phase 6 (CMIP6); and the capability of the stretch-grid model for prediction across scales (MPAS). Chapter Three describes the data

and methods used for the study. Chapters Four and Five present the results and discussion of the study. Specifically, Chapter Four discusses how well the CMIP6 simulations represent the characteristics of the WAWJ and its influence on Sahel precipitation, as well as the moisture transport by the jet, while Chapter Five discusses the capability of MPAS in simulating the characteristics of the WAWJ and of the sensitivity of the simulation to increase in horizontal resolution. Finally, Chapter Six provides the conclusion of the thesis and recommendations for future studies.

Chapter 2: Literature Review

This chapter provides a comprehensive review of the literature that was relevant to the writing of this thesis. This includes an overview of the progress and challenges in simulating West African climate, the characteristics and influence of low-level jets (LLJs) around the world, and the capability of climate models to simulate atmospheric features over West Africa. It also considers the results of past studies conducted into the sensitivity of simulated African climatic features to variations in the horizontal resolution of climate models.

2.1 Progress and challenges of simulating West African climate

Modelling the West African climate has historically depended on coarse-grid GCMs, which cannot fully account for all the characteristics of the atmospheric systems and processes at the regional-to-national scale (Lebel et al., 2000; Gallée, 2004; Paeth et al., 2008, 2011; Roehrig et al., 2013; Vellinga et al., 2016). The West African climate involves complex multi-scale interactions among various atmospheric features and processes that range from mesoscale to planetary-scale (Cook & Vizy, 2006; Biasutti, 2013; Roehrig et al., 2013). As a result, the simulation of climate systems in West Africa is sensitive to a horizontal resolution of atmospheric models. All in all, this makes it challenging for GCMs with a coarse resolution to adequately simulate the West African climate system (Abiodun et al., 2011; Raj et al., 2019).

Despite the advancement in resolution and complexity of GCMs (from 300km grid spacing since the first Intergovernmental Panel on Climate Change, IPCC, assessment report [AR1] in 1990 to 100km grid spacing, as at IPCC AR6), GCM still struggles to reproduce regional-scale features that involve interactions between the large-scale circulation and regional or mesoscale features induced by local temperature-gradient, vegetation, orography, and coastlines (Abiodun et al., 2011; Raj et al., 2019; Iles et al., 2020; TRS Briefing1, 2021). For instance, several studies have discussed the biases of CMIP6 ensembles in simulating the characteristics of precipitation over West Africa (e.g., Almazroui et al. 2020; Monerie et al. 2020). Iyakaremye et al. (2021) have shown that while the majority of the CMIP6 models reasonably simulate observed temperature over West Africa in general, only 20% of these models have a very strong spatial correlation with observed monthly mean temperatures over the Sahel region. The model bias in temperature, which is up to 3^{o}C over the Sahel region, was attributed to the inability of

the models to adequately represent the complex topography of Africa and their inability to represent the variable surface fluxes of latent and sensible heat over West Africa (Iyakaremye et al., 2021; Li et al. 2021). Monerie et al. (2020) showed that CMIP6 models do not simulate the monsoon system to propagate northward enough over West Africa, which has been offered as a possible explanation for why the models underestimate precipitation over the Sahel. This bias was also identified in CMIP5 models and was attributed to a warm bias over the Atlantic cold tongue and a cold bias in the Sahara (Foltz et al., 2019). Klutse et al. (2021) showed that, although the majority of the CMIP6 models perform well in simulating the mean maximum dry spell length and wet days over West Africa, more than 95% of them overestimate the mean maximum wet spell length over the Sahel and Sahara. It was noted that some of the models overestimate the mean maximum dry spell length too. Furthermore, Cook & Vizy (2006) evaluated how 18 coupled GCM simulations, at the process level, represent the climatology and the interannual variability of the WAM in the second half of the 20th-century. The authors found that while the models accurately captured the summer precipitation climatology over North America and Europe, they struggled to capture the WAM over Africa and failed to place precipitation maximum over the African land surface.

Simulations at resolutions sufficiently fine to capture these high-impact phenomena are computationally expensive and may find it difficult to gain sufficient enough advances to reach a uniform, cloud-resolving global resolution. However, the novel approach to high-resolution climate modelling represented by VGCM has been discussed in the literature and is being evaluated over West Africa. Several studies (Abiodun et al., 2011; Lim et al., 2014; Vellinga et al., 2016; Druyan & Fulakeza, 2018; Raj et al., 2019) have documented how VGCM, which offers the capability to increase resolution over an area of interest, improves the simulation of some of the regional-scale features. Such features include AEJ, MCS, AEW, the ITCZ, and the WAWJ, among others. For example, Abiodun et al. (2011) showed that increasing the resolution of a VGCM (called CAM-EULAG) locally over West Africa improves the quality of the simulated AEJ and monsoon system from the model. Specifically, the increase in resolution makes the simulated monsoon circulation penetrate further inland and produce better summer precipitation patterns. Through a process-based evaluation, Raj et al. (2019) also found that a high-resolution atmospheric general circulation model (HiRAM, with 25km resolution) performs better than the parent model (ESM2M, with 2.5^o x ~2^o resolution) in representing the spatial distribution and intensity of the WAM rainfall. The position of the AEJ and WAM rain belt, as well as the two-cell structure of the convection over West Africa, are better simulated

in HiRAM than ESM2M. However, there is a dearth of information on the capability of VGCM to simulate the WAWJ and its moisture transport.

2.2 Characteristics of low-level jets

In the lower troposphere, low-level jets are important features and play a significant role in moisture transport. It is useful to examine their characteristics to gain more insight into WAWJ and its role in moisture transport. Previous studies have identified and discussed the characteristics of various LLJs over different parts of the world (Parish et al., 1988; Weaver & Nigam, 2011; Ranjha et al., 2013; Oliveira et al., 2018; Borvarán et al., 2021; Gadde & Stevens, 2021). All these studies agree that LLJs, which are narrow streams of maximum wind speed within the lower troposphere, are mesoscale-flow phenomena. LLJs are characterised by sharp maxima in the vertical profile of wind speed, evident in the lowest few kilometres of the atmosphere (Rife et al., 2010; Ranjha et al., 2013; Oliveira et al., 2018). Most LLJs are supergeostrophic and strong vertical wind shear is associated with their presence, which affects turbulent exchange between the atmosphere and the surface (Baas, 2009; Baas et al., 2009; Borvarán et al., 2021; Gadde & Stevens, 2021).

Two types of LLJ are documented in the literature. The first type is the nocturnal low-level jet (NLLJ). The NLLJ is a warm-season atmospheric boundary layer phenomenon that forms at night under the condition of clear-skies when there is strong radiative cooling and synoptic winds are weak (Ruchith & Ernest Raj, 2015; Shapiro et al., 2016). Examples of NLLJs are the Great Plains low-level jet (GPLLJ), the South American low-level jet (SALLJ), and the Turkana low-level jet (TLLJ).

The second type of LLJ is the coastal low-level jet (CLJ). The CLJ, unlike the NLLJ, is a LLJ confined to the marine atmospheric boundary layer with a horizontal width exceeding hundreds of kilometres off the coast, while the vertical extent is relatively small and has a mid-afternoon wind speed maximum (Ranjha et al., 2015). CLJs, which form due to thermal gradients between the land and the ocean, as well as geostrophic balances of Coriolis deflection, are influenced by many local factors, including land-sea temperature contrasts, upwelling, coastal terrain, and large-scale atmospheric dynamics (Parish, 2000; Ranjha et al., 2013). Studies (Ardanuy, 1979; Marengo et al., 2004; Parish et al., 1988; Ranjha et al., 2013) have shown that, except in Antarctica, CLJs are common features along the mid-latitude west coasts of every continent

and along the east coasts of some regions. Examples of CLJs are the Caribbean low-level jet (CLLJ), the Indian monsoon low-level jet (MLLJ), and the WAWJ.

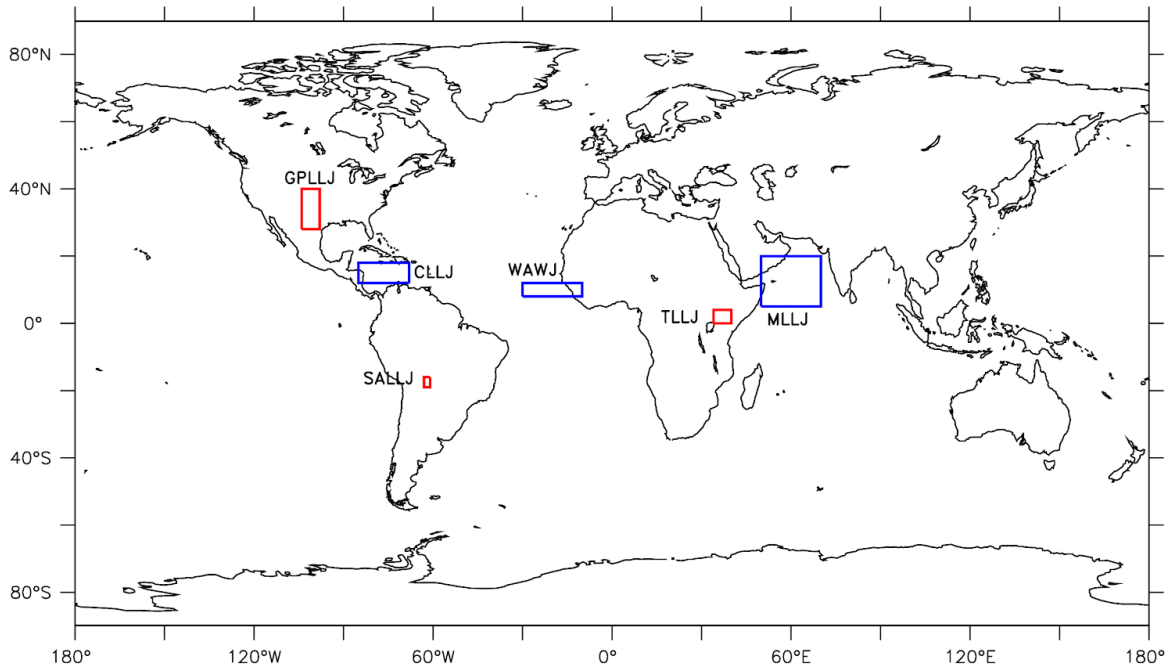

Figure 2.1: Locations of the selected nocturnal low-level jets and coastal low-level jets reviewed in the thesis. The low-level jets (i.e., The Great Plains low-level jet, GPLLJ; South American low-level jet, SALLJ; and the Turkana low-level jet, TLLJ) are indicated with red boxes while the coastal low-level jets (The Caribbean low-level jet, CLLJ; Monsoon low-level jet, MLLJ; and the West African Westerly Jet, WAWJ) are indicated with blue boxes. The location of the jets is derived from Pu & Cook (2010) and Torres-Alavez et al. (2021).

2.2.1 Great Plains low-level jet (GPLLJ)

The GPLLJ, a low-level southerly flow from the Gulf of Mexico into the Great Plains, is a prominent feature of the summer climatology over the central United States (Song et al., 2005; Cook et al., 2008; Berg et al., 2015; Smith et al., 2018, 2019). Song et al. (2005) find that the GPLLJ, which generally forms during the night and early morning (Mitchell et al., 1995; Cook et al., 2008), occurs on about 60% of the warm-season nights. According to Berg et al. (2015) and Cook et al. (2008), the GPLLJ plays an important role in the summer precipitation distributions and regional-scale moisture transport over the central United States. It is

responsible for about 70–80% of the moisture transport from the Gulf of Mexico over the Great Plains and 50% of the total moisture transport near the Great Lakes and the northeast United States (Algarra et al., 2019; Smith et al., 2018). Weaver & Nigam (2011) argue that any variability in the strength, location, and timing of the GPLLJ has a significant influence on the regional hydroclimate of the central United States (Burrows et al., 2019).

While examining the corridors of warm-season precipitation in the central United States, Tuttle & Davis (2006) discovered that the exit region of the GPLLJ strongly correlates with the corridors. In addition, they found that the jet enhances convergence and lifting, as well as frontogenesis and showed that the strength of the GPLLJ is strongly positively correlated with rainfall intensity in the region. Furthermore, Torres-Alavez et al. (2021) have indicated that the jet, which contributes to the occurrence of thunderstorms and severe weather over the Great Plains of the United States, has become more intense and frequent over recent years.

2.2.2 South American low-level jet (SALLJ)

The SALLJ, a northerly low-level jet with wind maximum between 10^{o}–20^{o}S, is located immediately to the east of the Andes mountains and is a key feature of the South American climate. This jet has a strong diurnal oscillation and is frequent in the spring and summer, transporting considerable amounts of moisture from the Amazon to the La Plata basins of south-eastern South America (Saulo et al., 2000; Marengo, 2002; Nicolini et al., 2002). Campetella & Vera (2002) have shown that due to the proximity of the Andes mountains, the SALLJ exhibits a northwest - southeast orientation during winter, and the seasonal changes in cyclone activity have a significant impact on the location of maximum SALLJ. Several studies (Marengo, 2002; Falvey & Garreaud, 2005; Salio et al., 2007; Torres-Alavez et al., 2021) have documented the characteristics and the importance of the jet to the regional weather and hydrology of the subtropical region, particularly the agriculturally productive regions of southern Brazil and northern Argentina. For instance, Salio et al. (2007) reported that the SALLJ contributes to convection initiation and enhances the mesoscale convective system over the central South American region. In addition, the authors argued that through a feedback system involving latent heat release and convergence at the exit region of the jet, the SALLJ sustains organised convective systems for a longer lifetime.

Campetella & Vera (2002) have shown that the southward flow associated with the SALLJ from the tropical latitudes enhances precipitation, as well as strengthening and intensifying

low-level cyclones through diabatic heat release and enhanced penetration of warm air advection east of the cyclone centre over south-eastern South America. Furthermore, Guedes do Nascimento et al. (2016) and Montini et al. (2019) have shown that the moisture transported over the La Plata Basin by the jet, is paramount to socio-economic activity in the region, which is based primarily on agriculture and hydropower generation. This fact is critical because the basin, which covers five countries (including Argentina, Bolivia, Brazil, Paraguay, and Uruguay), produces approximately 70% of the combined GDP of the countries located there.

2.2.3 Turkana low-level jet (TLLJ)

The TLLJ is a south-easterly low-level jet with an average speed of about 30m s^{-1} in the Turkana channel, Northern Kenya (Kinuthia & Asnani, 1982; Nicholson, 2016). The jet is a semi-permanent feature of the semi-arid climate that occurs on an average of 79% of the days between May–October and becomes strongest between the June–September dry season (Nicholson, 2016). Indeje et al. (2001) has explained that orographic forcing is a primary factor in the development of the TLLJ. However, its formation is also helped by the large-scale monsoon flow. Thermal and frictional forcing are responsible for the maintenance of the jet—while the channel's depth determines the jet's vertical structure and the location of the jet core (Hartman, 2018).

A number of studies have examined the relationship between the TLLJ and rainfall variability in the region. For instance, while investigating the dynamics of the jet, Indeje et al. (2001) discovered that the downward vertical velocity associated with the middle of the jet, which decreases moisture flux convergence and increases temperature flux divergence, inhibits the formation of mesoscale circulation. As a result, the TLLJ causes dry conditions over the Lake Turkana Basin (Indeje et al., 2000). In the exit region of the jet, while the jet is at its peak in the early hours of the day, Vizy & Cook (2019) observed an enhanced low-level convergence and a transient shift of the zonal moisture gradient to the west. Consequently, rainfall peaks over eastern South Sudan in the morning but peaks in the late afternoon to evening over western South Sudan. In a recent study, King et al. (2021) found that over the last 30–40 years, the TLLJ strength has weakened, which may have significant implications for rainfall in the region, especially in northwest Kenya, if such trends continue.

2.2.4 Caribbean coastal low-level jet (CLLJ)

The CLLJ is one of the atmospheric features that influences the climate of the Central America region. The CLLJ, a region of strong easterly winds at 925 hPa, spans about 500km in width from the western Caribbean to the Lesser Antilles (Muñoz et al., 2008; Hidalgo et al., 2015). It is a summer and winter feature over the basin and has a semi-diurnal cycle with a minimum at 0200 UCT and a maximum at 1400 UCT. The strength varies semi-annually, with peaks in February and July (Muñoz et al., 2008; Amador, 2008; Cook & Vizy, 2010; Hidalgo et al., 2015).

Muñoz et al. (2008) highlight that the formation of the jet is influenced by the high mountains to the south of the Caribbean Sea that affect the meridional gradient of temperature and favour a strong easterly wind. Additionally, they report that the jet strength is enhanced by the subsidence over the subtropical North Atlantic, which occurs as a result of the shift of the ITCZ that is associated with the Central American monsoon. Several studies (Wang, 2007; Mestas-Nuñez et al., 2007; Cook & Vizy, 2010; Muñoz & Enfield, 2011; Hidalgo et al., 2015) have associated the CLLJ with precipitation in the region. For instance, Mestas-Nuñez et al. (2007) found that in the summer, the CLLJ effectively transports moisture into the central United States. The greatest amount of moisture is transported between May–September into the Gulf of Mexico, as well as into the Caribbean basin (Muñoz et al., 2008; Cook & Vizy, 2010). In addition, Mestas-Nuñez et al. (2007) establish a link between the jet's interannual variability and the interannual variability of precipitation in the central United States. Additionally, during the strong CLLJ, Cook & Vizy (2010) have found anomalous moisture transport northward across the Gulf of Mexico into the central United States, which enhances rainfall over Louisiana and Texas. However, when the jet is weak, the anomalous flow crosses the southern Caribbean in a westward direction, resulting in a significant decrease in rainfall over the south-central United States (Mestas-Nuñez et al., 2007; Martin & Schumacher, 2011). Meanwhile, Vichot-Llano et al. (2021) have projected an intensification in the strength and width of the jet—they predict that the jet will strengthen and expand both eastward and northward in the near and more distant future.

2.2.5 Indian Monsoon low-level jet (MLLJ)

The MLLJ is one of the atmospheric features and an important moisture component of the monsoon circulation over India (Joseph & Sijikumar, 2004; Aneesh & Sijikumar, 2016; Xavier

et al., 2018; Viswanadhapalli et al., 2020). The MLLJ, which is sometimes referred to as the 'Somali jet', 'Findlater jet', or 'cross-equatorial low-level jet', is a region of strong south-westerly cross-equatorial wind (with an average core speed of $30m^{-1}$ at 850 hPa) that develops over the Arabian Sea during the Indian summer monsoon (Swathi et al., 2020; Viswanadhapalli et al., 2020). Joseph & Sijikumar (2004) and Xavier et al. (2018) have highlighted that orography, friction, and variation in pressure are important factors in the jet's formation and development (Joseph & Sijikumar, 2004). Significantly, Viswanadhapalli et al. (2020) have also shown that the jet is crucial for the transport of moisture from the ocean onto the subcontinent. Therefore, as is the case for all of the regions mentioned above, the MLLJ is important for the livelihood of an enormous number of people, as well as for the economy of densely populated India, the second-largest agricultural producer in the world.

Sathiyamoorthy & Mahesh (2013) discovered that moisture converges with decreasing wind speed at the exit region of the jet and produces low clouds that are predominant at the jet's exit region. As a result, the jet produces and modulates rainfall and is crucial for the large-scale distribution of precipitation over the region (Xavier et al., 2018; Swathi et al., 2020; Viswanadhapalli et al., 2020). It has, therefore, been reported by Xavier et al. (2018), that any changes in the strength and character of the MLLJ can cause episodes of heavy rainfall over the south-western coast of India, and variability in precipitation over the Indian subcontinent as a whole. Furthermore, Viswanadhapalli et al. (2020) have argued that the jet is crucial to the formation and the maintenance of monsoon inversion layers over the Arabian Sea (Wu et al., 2017; Dwivedi et al., 2021). In addition, Dwivedi et al. (2021) have shown that the jet enhances upwelling over the Arabian Sea by exerting a drag on the surface water. This, in turn, creates a large temperature gradient between the sea and the land - and the feedback strengthens the jet (Swathi et al., 2020). The upwelling makes the Arabian Sea one of the most productive oceanic regions in the tropics (Joseph & Sijikumar, 2004; Swathi et al., 2020).

2.2.6 West African Westerly Jet

The characteristics and dynamics of the WAWJ have also been documented (Grodsky, 2003; Pu & Cook, 2010, 2012; Issa Lélé et al., 2015; Lélé & Leslie, 2016; Liu et al., 2020). These studies agree that the jet is a summer atmospheric feature and a major source of rainfall over the Sahel zone during the boreal summer. Pu & Cook (2010) defined the jet as a low-level jet located off the coast of West Africa at 925 hPa and found that the jet develops at the beginning of June, reaches a maximum speed of $6m\ s^{-1}$ in August, and dissipates in mid-October.

Additionally, they found the jet has a weak semidiurnal cycle with minima speed at 0600 UTC and 1800 UTC and maxima speed at 1200 UTC and 0000 UTC. While studying the dynamics of the WAWJ, Pu & Cook (2010, 2012) clearly distinguished the WAWJ from the monsoon flow and found a strong link between the jet and the diurnal (Liu et al., 2020), decadal, and interannual rainfall variability in the Sahel. They also argued that the WAWJ plays a crucial role in the atmosphere-ocean-land surface interactions in West Africa. Using moisture budget analysis, Liu et al. (2020) quantified the moisture transport associated with the WAWJ and found that the jet, which transports moisture from the eastern Atlantic onto the subcontinent (especially at 8–11^{o}N), has a strong relationship with West African precipitation on seasonal and diurnal timescales.

While analysing the intensity, location, and structure of the tropical rain belt as a factor in interannual rainfall variability over West Africa, Nicholson (2008) found that the wet and dry years in the Sahel are associated with the weakening and contraction of the tropical rain belt. In other studies, Nicholson (2008, 2009) linked the intensification (weakening) of the rain belt, which is associated with wet (dry) years in the Sahel, with the northward (southward) displacement of the AEJ and anomalously strong (weak) tropical easterly jet (TEJ). Meanwhile, several studies (Grist & Nicholson, 2001; Nicholson & Grist, 2001; Dezfuli and Nicholson 2010; Kebe et al., 2020) have argued that during the WAWJ strong (wet) periods, the WAWJ displaces the AEJ (and its associated disturbances) northward and modulates the interannual variability of the AEJ. Thus, it is claimed that the WAWJ enhances both the horizontal and vertical wind shear over the Sahel. However, while all these studies have shown that the WAWJ plays a pivotal role in rainfall variability over the Sahel, none of them have investigated how well the jet is represented in contemporary climate models. The present study aims to address this gap by examining how well CMIP6 models and MPAS represent the WAWJ.

2.3 Applications of the model for prediction across scales (MPAS)

Some studies (e.g., Hagos et al., 2013; Heinzeller et al., 2016; Kramer et al. 2018; Maoyi and Abiodun, 2021) have demonstrated the capability of MPAS to simulate different atmospheric features. For instance, Michaelis et al. (2019) showed that MPAS (at high variable resolution of 15 km to 60 km over northern and southern hemisphere, respectively) reasonably reproduces large-scale atmospheric features in the Northern Hemisphere, such as the upper-tropospheric jets, maritime sea-level pressure pattern, and annual precipitation patterns across the tropics. While examining the capability of MPAS in simulating the characteristics of the Botswana

High, Maoyi & Abiodun (2021; 2022) showed that MPAS (with relatively high variable resolution of 48-km over Southern African and 240-km grid spacing over the rest of the globe) is capable of replicating the major features of climatology over southern Africa, such as temperature, rainfall, geopotential height at 500 hPa, and vertical motion. The model has also been shown to capture the temporal and spatial variation of the Botswana High, and its impact on droughts and deep convections over the region. Furthermore, Landu et al. (2014) showed that MPAS, at high resolution of 30 km, is capable of simulating West African systems by examining the structure of the ITCZ in the model's dynamical core. The authors' results showed that MPAS simulates maximum precipitation over the tropical region forming an ITCZ-like structure. Other researchers, such as Weber and Mass (2019), have shown that MPAS (at the convection-permitting scale of 3 km horizontal resolution) demonstrates an improvement in forecast precipitation statistics as well as enhanced multiweek predictive skill in tropical areas and to some extent in extratropical regions. In addition, the MPAS reproduced the Madden-Julian oscillation (MJO) better at the 3-km scale than at the 15-km grid scale. Furthermore, the authors claimed that the model accurately represents terrain features and orographic precipitation at the convection-permitting scale, as well as provides more realistic propagation of extratropical mesoscale convective systems, and improved representation of gravity wave drag effects produced by terrain (Davis et al. 2003; Smith et al. 2006). However, there is little or no information about the capability of MPAS to simulate the WAWJ and its moisture transport over West Africa.

Chapter 3: Data and Methodology

This chapter describes the methodology of the thesis. It consists of three sections. The first section presents the study domain, and the second section describes which datasets were analysed. The final section describes the methods, experiments, and analytical procedures used to analyse the datasets.

3.1 Study area

The study domain for this thesis is the West African domain (4^oN - 20^oN and 40^oW - 20^oE), as defined in the thesis (Figure 3.1). This domain is wider than the usual West African domain (4^oN - 20^oN and 20^oW - 20^oE) used in some previous studies (Omotosho & Abiodun, 2007; Abiodun et al., 2012; Egbebiyi, 2016) because it extends westward to include the WAWJ area. Hence, the study domain consists of the West African subcontinent, the WAWJ area (as defined by Pu & Cook, 2010, and Liu et al., 2020), and part of the North Atlantic Ocean. Following previous studies (Omotosho & Abiodun, 2007; Abiodun et al., 2012; Egbebiyi, 2016), West Africa is divided into three distinct climate zones: the Sahel (12–20°N), Savannah (8–12°N), and the Guinea Coast (4–8°N).

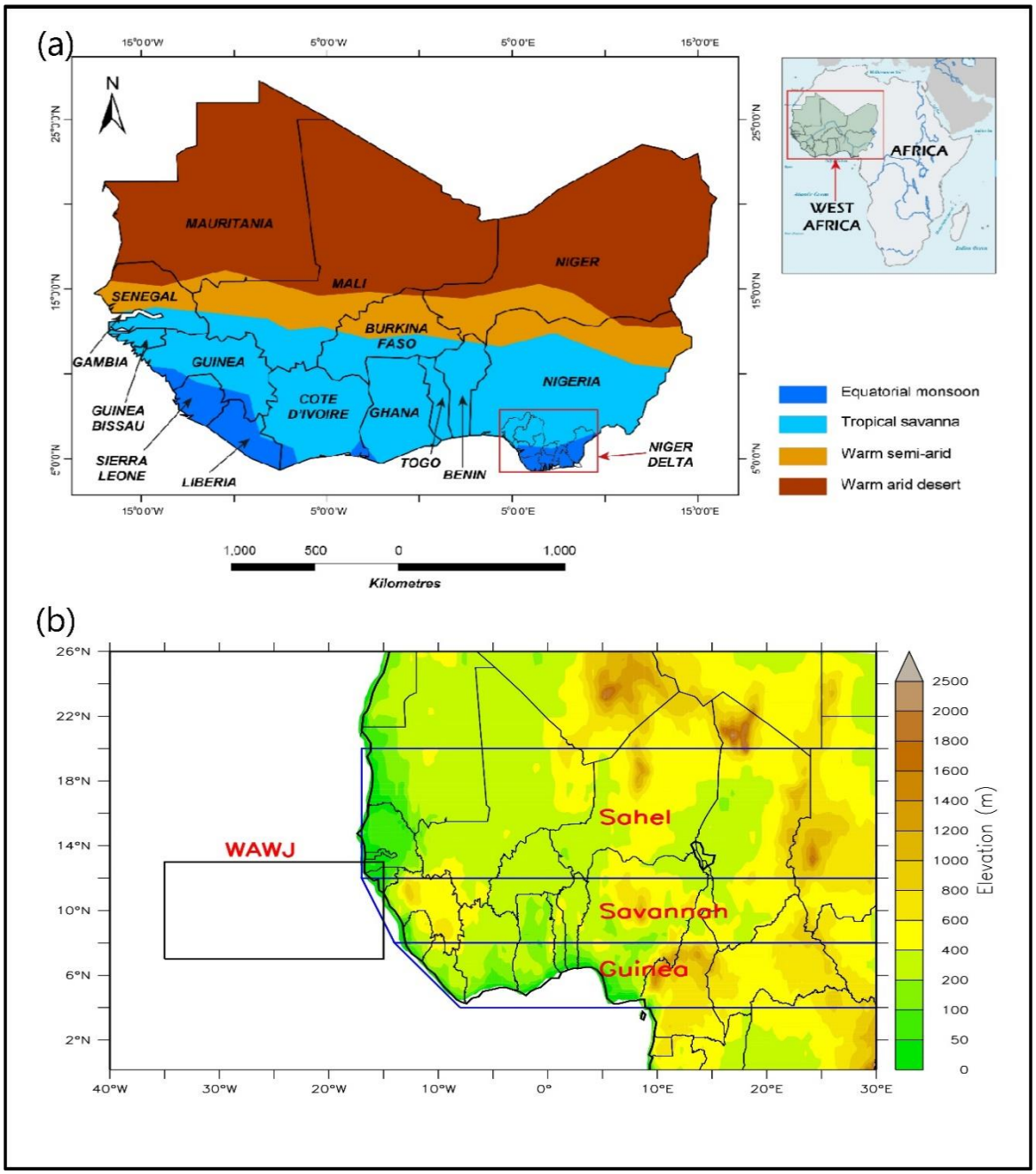

Figure 3.1: Study domain: (a) West African climate classes (modified after Onojeghuo et al. 2017); (b) West Africa topography (in metres) showing West Africa the climatic zones (Sahel, Savannah, and Guinea), and the WAWJ area as used in the study (modified after Diasso and Abiodun 2017)

3.2 Data

This thesis analysed three types of datasets: observation, reanalysis, and model simulation.

3.2.1 Observation dataset

The observation dataset is the Climatic Research Unit gridded Time Series, version 4 (CRU TS v4; hereafter CRU, https://crudata.uea.ac.uk/cru/data/hrg/). The CRU dataset is a widely used climate dataset with a grid resolution of 0.5° x 0.5° and covers all land domains of the world except Antarctica. CRU provides monthly gridded datasets as far back as 1901 for 10 observed and derived variables using a normalised series from a network of about 10,000 ground stations (Trenberth et al., 2013; Harris et al., 2020). The latest version of the dataset (version 4) uses a more streamlined process with an improved angular-distance weighting (ADW) interpolation technique that boosts the interpolation efficiency and accuracy. In addition, this version employs a fully customised process to facilitate nuanced interpretation of the gridded values and full traceability that improves quality control of the dataset. The CRU dataset has been applied in many studies over West Africa. The rainfall products detect and measure rainfall patterns better, especially in the Savannah zone (Atiah, et al., 2020a; Atiah, et al., 2020b). In this thesis, CRU monthly rainfall and near-surface (2-metre) temperature products for the period of 1980–2014 were used to evaluate the reanalysis and the model simulation dataset over West Africa.

3.2.2 Reanalysis dataset

The role of reanalysis in climate research and monitoring applications is now widely recognised and has been routinely used, together with other datasets (Bojinski et al., 2014; Hersbach et al., 2020). Reanalysis is a combination of observations and past short-range weather forecasts (through data assimilation) to provide the most complete picture of the past weather and climate. They are globally complete and consistent in time (Hersbach et al. 2019). The reanalysis dataset used in the present study is the 5th generation European Center for Medium-Range Weather Forecast reanalysis (hereafter, ERA5) obtained from the Copernicus Climate dataset website (https://cds.climate.copernicus.eu). ERA5, which is a replacement of the ERA-Interim reanalysis, embodies a detailed record of the atmosphere, land surface, and ocean waves globally from 1950 up to the present date. The new reanalysis, which combines vast amounts of historical observations into global estimates using advanced modelling and data assimilation systems, has a significantly enhanced high spatial resolution of 30km grid across

the globe on 137 levels from the surface up to the height of 80km with an hourly output (Hersbach et al., 2020; Jiao et al., 2021). ERA5 has been shown to be amongst the best performing reanalysis products by many studies (Albergel et al., 2018; Wang et al., 2018, 2019; Tarek et al., 2020; Hersbach et al., 2020; Jiao et al., 2021) because it provides quality precipitation data over space and time against radar and precipitation gauge observations (Beck et al., 2018).

The ERA5 data used in this study include the monthly precipitation and near-surface temperature. The zonal and meridional component of the wind, vertical velocity, and geopotential height were also utilised from the ERA5 dataset. The ERA5 reanalysis data were used to evaluate how well the models simulate the climatological structure and the interannual variability of the WAWJ, as well as its influence on rainfall variability in the Sahel and West Africa.

3.2.3 Climate simulation datasets

Two types of climate simulation dataset were used for the study. The first simulation dataset is from CMIP6. The CMIP6 dataset consists of an ensemble of standard global climate simulations that allow results from each simulation to be directly compared across different models to see where they agree or disagree (Touzé-Peiffer et al., 2020). A number of CMIP standards, model experiment protocols, formats, and distribution mechanisms were developed to ensure the outputs of climate models were accessible to a wide research community (Covey et al., 2003; Eyring et al., 2016; Zhongming et al., 2019; Touzé-Peiffer et al., 2020).

For this study, monthly data from twenty-six coupled atmosphere-ocean global climate simulations (Table 3.1) were downloaded from the Earth System Grid Federation (ESGF) website of CMIP6 (https://esgf-node.llnl.gov/search/cmip6/). These GCM simulations were chosen based on model resolutions and the availability of the atmospheric variables needed in the thesis. Only two GCM simulations have a 250km resolution; the rest have a resolution of 100km. The variables used in the analysis were temperature, precipitation, wind (zonal and meridional components), vertical velocity, geopotential height, and specific humidity. For the evaluation, all datasets were regridded to 0.5^{o} x 0.5^{o} horizontal resolution and analysed for a 35-year period (1980–2014). The second climate simulation dataset was obtained with atmospheric component of MPAS (or MPAS-A; hereafter MPAS). A detailed description of MPAS and the model experimental setup for obtaining the dataset is given in the next section.

3.3 MPAS model description

The MPAS version 7.0, a newly developed variable resolution global climate model, is a fully compressible non-hydrostatic model that scales on massively parallel systems. Through the use of a single scalar density function, MPAS employs the sphere discretisation method using the unstructured spherical centroidal Voronoi tessellation (SCVT) algorithms to generate variable-resolution, as well as global quasi-uniform resolution meshes (Du et al., 1999; Zhao et al., 2016, 2019). As a result, the variable resolution grid structure allows high-resolution areas to easily blend into low-resolution areas without the usual boundary constraints that plague conventional regional climate models, and without exhibiting the obvious problems in the mesh-transition zones (Ringler et al., 2008; Skamarock et al., 2012). Hence, MPAS eliminates the problems associated with traditional rectilinear grids and deploys a subset of the atmospheric physics employed in the Weather Research and Forecasting (WRF) (Du et al., 1999; Ringler et al., 2008; Sinkovits & Duda, 2016; Maoyi & Abiodun, 2021). Furthermore, the use of the Voronoi meshes – as with the icosahedral meshes – eliminates the polar filtering that is required with latitude-longitude meshes that converge grid lines at the pole, and allows parallelisation and good scaling performance on massively parallel architectures, such as on high-performance computing systems (Skamarock et al., 2012).

MPAS solver uses height-based terrain-following vertical coordinates and a split-explicit time integration scheme that employs the 3rd Order Runge-Kutta method and a forward-backward method with a smaller time step for acoustic modes (Wicker & Skamarock, 2002; Klemp et al., 2007; Skamarock & Klemp, 2008). The non-hydrostatic fluid-flow solver spatially discretises the continuous equations on an unstructured C-grid centroidal Voronoi mesh (illustrated in Fig 3.2). As a result, quasi-uniform meshes, as well as variable-resolution meshes, can be constructed for the sphere, for regional domains on the sphere, and for cartesian planes (Ringler et al., 2008; Skamarock et al., 2012). This technique guarantees its accuracy in applications on the sphere, in non-hydrostatic cases on cartesian domains, and distinguishes MPAS from other models.

Skamarock et al. (2012) tested the MPAS solver for non-hydrostatic flows on cartesian planes and for large-scale flows and found that the solver is as accurate as existing non-hydrostatic solvers for non-hydrostatic-scale flows and has accuracy comparable to existing global models using icosahedral (hexagonal) meshes for large-scale flows. Ringler et al. (2010, 2011) evaluate MPAS atmospheric dynamical core using the standard shallow-water test case suite for both

quasi-uniform and variable resolution meshes, respectively. They report that the performance of the MPAS dynamical core for the full suite of meshes (from quasi-uniform resolution to highly variable resolution meshes) is notable with conservation of mass and quantities, like the potential vorticity to within machine precision and total available energy to within a time-truncation error.

Table 3.1: Simulations (Alias), model names, and key references of CMIP6 models used in this thesis. All simulations have a quasi-horizontal resolution of 100 km except two simulations (GISSE and UKESM) with a quasi-horizontal resolution of 250 km.

Simulation	**Model Name**	**Variant**	**Reference**
AWICM	AWI-CM-1-1-MR	r1i1p1f1	Semmler et al. (2018)
BCCCS	BCC-CSM2-MR	r1i1p1f4	Wu et al. (2018)
CAMSC	CAMS-CSM1-0	r1i1p1f6	Rong (2019)
CASES	CAS-ESM2-0	r1i1p1f8	Chai (2020)
CES-A	CESM2	r1i1p1f10	Danabasoglu (2019)
CES-B	CESM2-WACCM	r1i1p1f11	Danabasoglu (2019)
CES-C	CESM2-WACCM-FV2	r1i1p1f12	Danabasoglu (2019)
CIESM	CIESM	r1i1p1f3	Huang (2019)
CMCCC	CMCC-CM2-SR5	r1i1p1f4	Lovato and Peano (2020)
E3S-A	E3SM-1-0	r1i1p1f6	Bader et al. (2019)
E3S-B	E3SM-1-1	r1i1p1f7	Bader et al. (2019)
E3S-C	E3SM-1-1-ECA	r1i1p1f8	Bader et al. (2020)
ECE-A	EC-Earth3	r1i1p1f2	EC-Earth (2019)
ECE-B	EC-Earth3-Veg	r1i1p1f3	EC-Earth-Veg (2019)
FGOAL	FGOALS-f3-L	r1i1p1f5	Yu (2019)
FIOES	FIO-ESM-2-0	r1i1p1f7	Song et al. (2019)
GFDLC	GFDL-CM4	r1i1p1f9	Guo et al. (2018)

GISSE	GISS-E2-1-G	r1i1p5f1	NASA-GISS (2018)
HADGE	HadGEM3-GC31-LL	r1i1p1f3	Ridley et al. (2019)
INM-A	INM-CM4-8	r1i1p1f1	Volodin et al. (2019)
INM-B	INM-CM5-0	r1i1p1f2	Volodin et al. (2019)
MPIES	MPI-ESM1-2-HR	r1i1p1f5	Jungclaus et al. (2019)
MRIES	MRI-ESM2-0	r1i1p1f9	Yukimoto et al. (2019)
SAMUN	SAM0-UNICON	r1i1p1f10	Park and Shin (2019)
TAIES	TaiESM1	r1i1p1f11	Lee and Liang (2020)
UKESM	UKESM1-0-LL	r9i1p1f2	Tang et al. (2019)

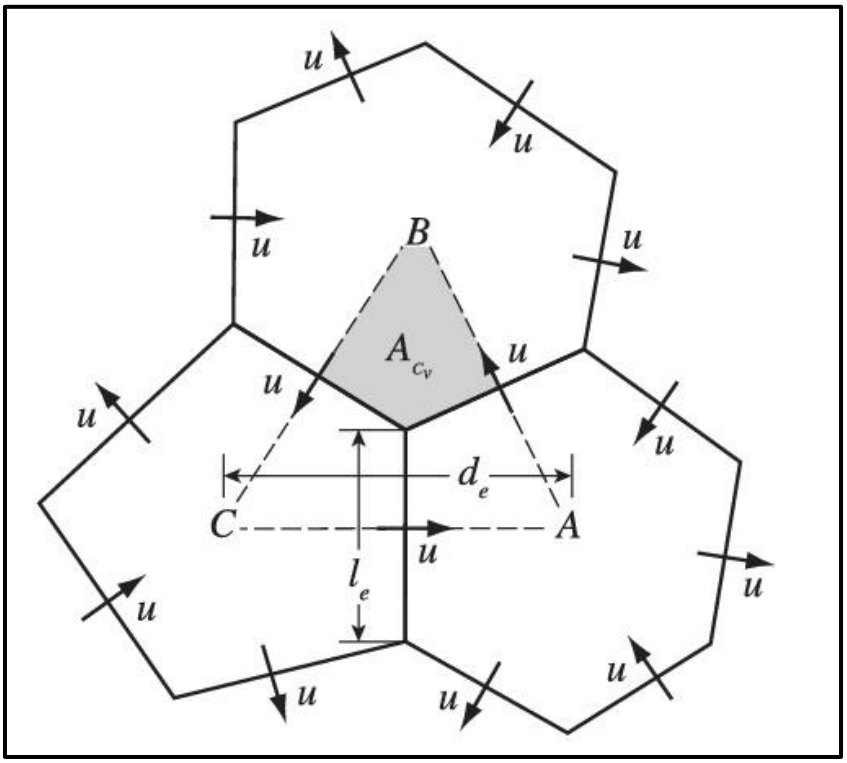

Figure 3.2: Illustration of the horizontal C-grid staggered Voronoi mesh (adapted from Skamarock et al., 2012).

MPAS utilises the atmospheric physics from the Advanced Research WRF model, which has benefitted from the work of hundreds of scientists. The physics schemes are largely based on the configurations used for the ARW Nested Regional Climate Model (WRF-NRCM) and tropical cyclone predictions. In newer versions of MPAS, these parameterisation schemes for various processes have been grouped into suites of schemes that have been tested together. The default physics suite is called the 'mesoscale reference' suite. It contains the schemes listed in Table 3.2. This suite has been tested to be appropriate for mesoscale resolutions (> 10km cell spacing).

Table 3.2: The set of parameterisation schemes used by the 'mesoscale reference' physics suite.

Parameterisation	**Scheme**	**References**
Convection	New Tiedtke	Kong et al. (2022); Zhang & Wang (2017)
Microphysics	WSM6	Hong & Lim (2006); Kim et al. (2021)
Land Surface	Noah	Campbell et al. (2020); Ek et al. (2003)
Boundary Layer	YSU	Burgering et al. (2013); Gilliam & Pleim (2010)
Surface Layer	Monin-Obukhov	Monin (1954); Zheng et al. (2014)
Radiation, LW	RRTMG	Cai & Yu (2012); Kong et al. (2022)
Radiation, SW	RRTMG	Cai & Yu (2012; Kong et al. (2022)
Cloud fraction for radiation	Xu-Randall	Ridout (2013); Ridout et al. (2021)
Gravity wave drag by orography	YSU	Burgering et al. (2013); Gilliam & Pleim (2010)

3.4 MPAS model experimental set-up

In this thesis, MPAS was applied to perform three simulation experiments (Table 3.3). The first experiment was to assess the capability of MPAS in simulating the West African climate and the climatology of the WAWJ. For this experiment (designated as MPAS experiment), MPAS simulation used quasi-uniform grid-mesh with 60km quasi-uniform resolution over the globe (containing 163,842 horizontal grid cells; Figure 3.3a) and covered a 30-year period (December 1984–31 December 2014; December 1984 simulation was discarded a model spin-up). The second and third experiments (hereafter, MPAS60 and MPAS15) were to test the sensitivity of the MPAS simulation of the WAWJ to changes in model horizontal resolution. While the MPAS60 experiment used a quasi-uniform resolution grid (as in the MPAS experiment), the MPAS15 experiment used a variable-resolution grid-mesh with 15km resolution over West Africa and 60km over the rest of the globe (containing 535,554 horizontal grid cells; Figure 3.3b), with the refinement region centred at 0^{o} longitude, 0^{o} latitude (Figure 3.3c). The simulation of the sensitivity experiments (MPAS60 and MPAS15) focused on the three years of strong WAWJ (1989, 1994, and 1999) and three years of weak WAWJ (1986, 1990, and 2000) as indicated by ERA5 results and, in each year, the simulation covered a period of two months (July and August; July simulation was discarded as a model spin-up). The August simulation was used because the WAWJ reaches its maximum intensity in August (Pu & Cook, 2010, 2012).

Table 3.3: The three simulation experiments, their period, and the meshes used in the study.

Experimental simulation	**Analysis period**	**Grid mesh**
MPAS	30 years (1985–2014)	Quasi-uniform resolution
MPAS60	1 month (August; 1986, 1989, 1990, 1994, 1999, 2000)	Quasi-uniform resolution
MPAS15	1 month (August; 1986, 1989, 1990, 1994, 1999, 2000)	Variable-resolution

All the experiments (MPAS, MPAS60, and MPAS15) used the MPAS default physics options (i.e., the mesoscale reference suite; Table 3.2), which are the recommended parameterisation schemes for simulations with horizontal grid size greater than 10km. The simulation was initialised with the climate forecast system reanalysis (CFSR) surface and pressure level dataset and forced with 6 hourly CFSR SST and sea-ice data. The simulation used 41 vertical pressure levels and output the results at a 3-hour interval.

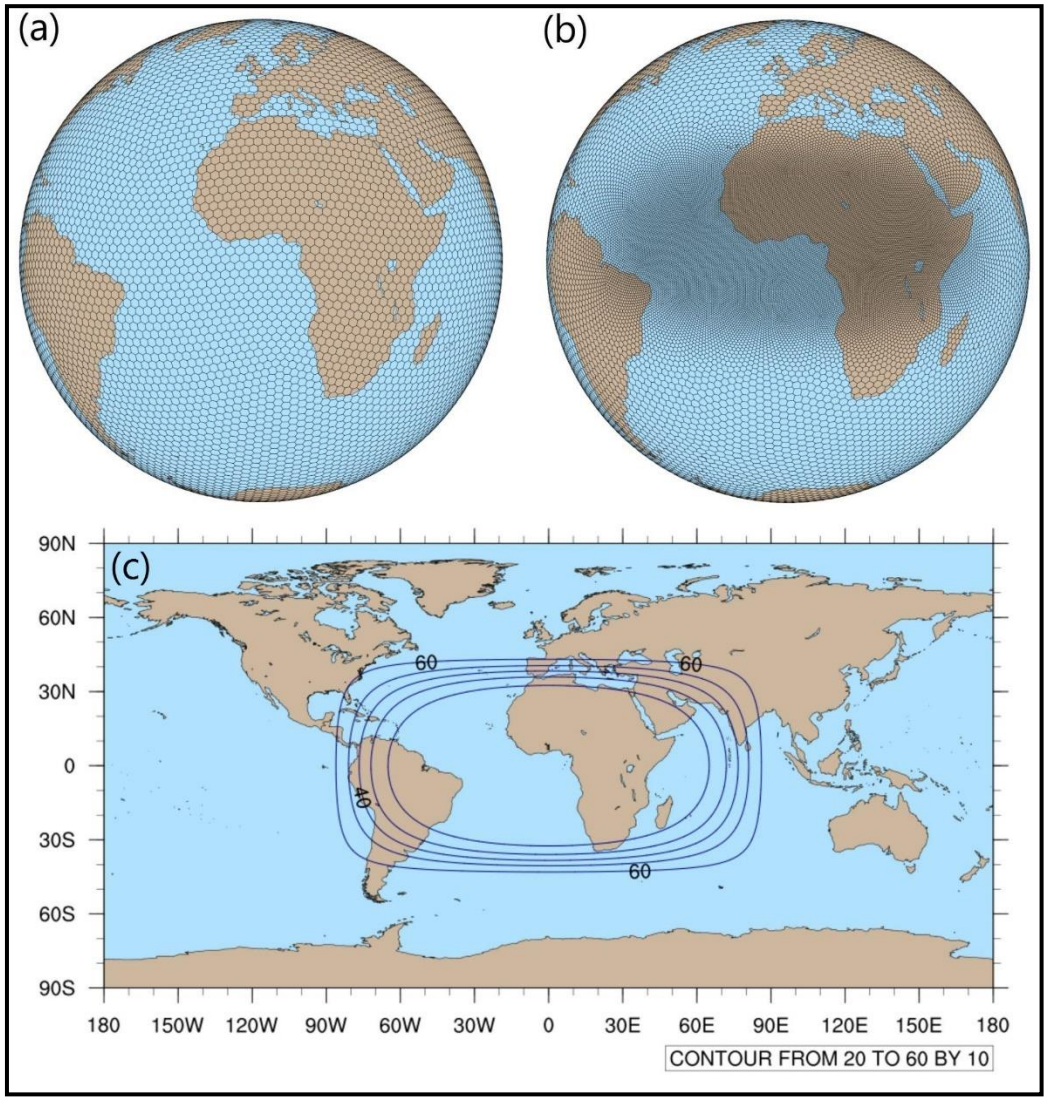

Figure 3.3: The MPAS mesh grid used in the thesis. Panel (a) and (b) show the grid structure for the quasi-uniform and variable resolution grid-mesh. Panel (c) shows the refinement region (which is centred at 0^{o} longitude, 0^{o} latitude) and the smooth transition of the horizontal resolution from 15km to 60km; for clarity, the contours vary from 20km (at the centre) to 60km at 10km interval.

3.5 Method

3.5.1 Identification and characterisation of the WAWJ

Following previous studies (Liu et al., 2020; Pu & Cook, 2010, 2012), this thesis defines the WAWJ as a low-level westerly jet (i.e., at 925 hPa) over the eastern Atlantic and the West African coast. Using this definition, the thesis identified and compared the characteristics of the WAWJ in ERA5 reanalysis and CMIP6 simulation datasets over the period of 35 years (1980–2014). The analysis focused on the climatological structure and interannual variability of the jet, as well as the relationship of the jet with other climate variables over West Africa. The core area (averaging region) of the jet is defined as a 7^{o} x 2^{o} (longitude x latitude) area over the WAWJ region. This box area encompasses the core of the jet without extending outside the jet region. While the size of the area is the same for all the datasets, the location differs among the datasets.

For the climatological structure, the study considered the vertical, horizontal, and annual structure of the jet. In the vertical structure analysis, the vertical profile was examined, as well as the longitude-vertical and latitude-vertical distributions of the jet, using the jet core area as the averaging region. In the horizontal analysis, the zonal wind greater than or equal to 2m s^{-1} was extracted and the wind values over the continent were masked out. The capability of the CMIP6 simulations to reproduce the spatial pattern in the reanalysis was quantified with correlation, and percentage bias was calculated. For ERA5 and the majority of CMIP6 simulations, the jet core is at 925 hPa and its maximum strength is in August. So, for most of the analyses reported in this paper, the 925 hPa was used as the default level, August as the default month, and the average zonal wind over the core area as the WAWJ strength.

3.5.2 Interannual variability of the WAWJ and its influence on precipitation

In the annual variation analysis, the study calculated the maximum zonal wind over the core area of the jet in August for all the years for each dataset as the WAWJ strength and compared it with that of Sahel precipitation. The interannual variability of the WAWJ was represented by the anomalies of the WAWJ strength (at 925 hPa in August), while the interannual variability of Sahel precipitation was designated by the standardised precipitation over the Sahel (averaged over 18^{o}W–30^{o}E, 10^{o}N–20^{o}N in August). The characteristics of the WAWJ time-series (the WAWJ strength) were quantified with the trend and standard deviation, while the relationship between the WAWJ and precipitation time-series was quantified with the

correlation coefficient. The capability of the models' (i.e., CMIP6 and MPAS) simulations to reproduce the WAWJ interannual variability, as well as the influence of the variability on the Sahel precipitation were examined.

To examine the relationship between the WAWJ and the spatial distribution of climate variables (i.e., temperature and precipitation) over West Africa, a correlation between the jet strength and the climate variables at each grid point over West Africa was performed in August at 925hPa (CMIP6:1980–2014, MPAS:1985–2014). The spatial distribution of the correlation coefficient calculated for each simulation dataset was compared with the one obtained for the ERA5 dataset. The comparison was quantified with statistical metrics, including correlation (r) and root-mean-square-error (RMSE). To explain the relationship between the jet and climate variables, the spatial distribution of the difference between the composites of climate variables (precipitation, temperature, and moisture flux) during the WAWJ positive and negative modes (i.e., positive modes minus negative modes) were calculated. For each dataset, the WAWJ positive modes are the three years with the highest WAWJ strength anomalies, while the negative modes are the three years with the lowest WAWJ strength anomalies.

3.5.3 Analysis of WAWJ dynamics

To investigate the dynamics and formation of the WAWJ, the thesis calculates the different terms in the horizontal momentum balance equation:

$$\frac{du}{dt} = -\frac{\partial \Phi}{\partial x} + fv + R_x \quad (1)$$

and

$$\frac{dv}{dt} = -\frac{\partial \Phi}{\partial y} - fu + R_y \quad (2)$$

where the first term on the right-hand side of equations (1) and (2) is the horizontal geopotential height gradient term and the Φ is geopotential height. The second term is the Coriolis term, where $f \equiv 2\Omega sin\text{ø}$ is the Coriolis parameter, $\Omega \equiv 7.292 \times 10^{-5}\, rads^{-1}$ is the angular speed at which the earth rotates, and ø is the latitude. Lastly, the third represents horizontal friction.

Furthermore, the geostrophic wind is obtained as:

$$u_g = -\frac{g}{f}\frac{\partial \Phi}{\partial y} \quad \text{and} \quad v_g = \frac{g}{f}\frac{\partial \Phi}{\partial x} \tag{3}$$

and the ageostrophic wind is defined as

$$u_a = u - u_g \qquad \text{and} \quad v_a = v - v_g \tag{4}$$

where u and v are the zonal and meridional wind components, $g \equiv 10\, ms^{-1}$ is the acceleration due to gravity.

Chapter 4: Representation of West African Westerly Jet and its influence on Sahel Precipitation in CMIP6

This chapter presents and discusses the results of our analysis on evaluating the capability of twenty-six GCMs in the coupled model intercomparison project-version six (CMIP6) to simulate WAWJ and its influence on precipitation over West Africa, particularly the Sahel. In this chapter, the discrepancies between the observed data are discussed. The spatial, vertical, and temporal structure of the jet is analyzed along with the interannual variation of the jet and Sahel precipitation. The influence of WAWJ on the spatial distribution of climate variables over West Africa is investigated.

4.1 Temporal structure of the WAWJ

The ERA5 reanalysis reproduces the annual cycle of the WAWJ (Figure 4.1), including the five-stage evolution of the jet as reported in Pu and Cook (2010). The jet has a core speed of about 2.5 m s^{-1} in Stage 1 (June), intensifies steeply as its core speed increases from 2.5 m s^{-1} to 4.3 m s^{-1} in Stage 2 (June–July), attains its peak strength of about 5 m s^{-1} in Stage 3 (August), and weakens as its core speed reduces to about 2.7 m s^{-1} in Stage 4 (September). Despite the differences in the temporal resolution of the data used in Pu and Cook (2010) (i.e., daily) and the present study (i.e., monthly), the strength of the jet obtained here agrees with that reported in Pu and Cook (2010) at each stage. This implies that the characteristics of the jet can be described with monthly datasets.

The majority of the CMIP6 simulations depict the five-stage evolution and the peak of the jet (Figure 4.1). However, there are notable biases in the results. Firstly, the jet develops too fast in the models. For example, the jet already attains Stage 3 (speed $\geq$ 4.0) in February in 6 models (23%); in March in 7 models (27%); in April in 8 models (31%); and in May in 2 models (8%). Only 3 models (ECE-A&B and CIESM) simulate Stage 3 in August as depicted in ERA5 results. Second, the jet is too strong in most models. The peak strength of the jet is more than 5 m s^{-1} in 15 models (58%) and even more than 8 m s^{-1} in 8 models (31%). Third, the weakening of the jet (Stage 4; speed < 4.0 m s^{-1}) is prolonged in most models. Only 5 models (19%) simulate Stage 4 of the jet in September; 12 models (46%) simulate it in October; and 2 (8%)

feature it in November. Four models (CASE, HADGE, INM-A&B, and MRIES) fail to simulate the temporal structure of the jet as in ERA5. For instance, in MRIES, the jet first features in March (instead of June), intensifies steeply and reaches maximum speed in April (instead of August), and disappears in August (instead of September).

4.2 Spatial structure of the WAWJ

The ERA5 reanalysis also captures all the spatial structures of the WAWJ in August (Figure 4.2) as in Pu and Cook (2010). In ERA5, the WAWJ extends from 6°–12°N and from 5°–35°W, but the jet core is located around 8°N and 20°W. The jet is associated with an offshore extension of the thermal low, as indicated by the trough (i.e., 780-gpm contour) extending from over the continent to around 30°W over the ocean. Most CMIP6 models produce a westerly jet off the coast of West Africa but the capability of the models to replicate the spatial structure varies, as depicted by the spatial correlation (r) of the simulated structure with the reanalysis and by associated simulation bias (i.e., percentage bias or 'PBIAS'), indicated in the bottom left panels of Figure 4.2. While 9 models (35%) feature a strong to very strong positive correlation ($r \geq 0.7$) with the ERA5 reanalysis, 8 models (31%) have a weak positive correlation ($0.4 \leq r \leq 0.6$), and 9 models (35%) show poor correlation ($-0.3 \leq r \leq 0.3$). Most models overestimate area coverage and the core strength of the jet. Their PBIAS range from 1% (in ECE-A) to 57% in (CES-C). For example, in CES-C (which shows the highest PBIAS), the jet stretches from 5°–14°N and 15°–40°W with a core strength of more than 8 m s^{-1}. Only 4 models (GISSE, INM-A & B, and MRIES) feature negative PBIAS (-27% to -8%). In MRIES (which has the largest negative bias) the jet only stretches from 7°–11°N and 15°–23°W with a core strength of less than 4 m s^{-1}.

4.3 Vertical structure of the WAWJ

The latitude-height cross-section of the zonal wind along the jet's longitudes in August further confirms the agreement between the ERA5 and Pu and Cook (2010) results (Figure 4.3). In both, the jet extends from the surface to about 750 hPa but the core of the jet (about 4 m s^{-1}) is at 925 hPa (Figure 4.3). The African easterly jet (AEJ) core is located above (600 hPa) and north (centred on 16°N) of the WAWJ. This agrees with the finding of Grist and Nicholson (2001) that equatorial westerlies (including the WAWJ) displace the AEJ (and its associated disturbances) northward and modulate the interannual variability of the AEJ. The study also found that the northward displacement of the AEJ coincides with wet years in the Sahel because

it enhances both the horizontal and vertical wind shear over the Sahel. The majority of the models capture the vertical structure of the jet as in the ERA5 reanalysis and the seasonal northward shift of the AEJ. However, the models show different capabilities in simulating the vertical extent of the WAWJ and the associated northward shift of the AEJ. The jet extends to 750 hPa (or above) in only 13 models (50%) and to 800 hPa in 6 models (23.1%). However, one model (MRIES, which simulates the weakest WAWJ) features the jet below 900 hPa and puts the jet core at 1000 hPa.

The longitude-height cross-section of the zonal wind speed along the jet's latitudes in August shows the jet core (4 m s^{-1}) between 25°–15°W in the ERA5 (Figure 4.4), which is 2 m s^{-1} weaker and extends more westward than in Pu and Cook (2010). This small discrepancy could be because this study used averaged values over 8°–10°N, whereas Pu and Cook (2010) used values along a single latitude (9.5°N). However, as in Pu and Cook (2010), the ERA5 result distinguishes the WAWJ from the WAM westerly component maxima over land. While the WAWJ core is located between 15°–25°W, the WAM core is located between 9°–15°E. Some of the models capture the vertical structure of the jet in the longitudinal cross-section. However, the majority of the models fail to clearly distinguish the WAWJ from the WAM. For instance, the CES-C model features the westerly flow maximum from about 28°W–12°E overland without any distinction. The INM-A model failed to capture the WAWJ at all and only features a westerly flow maximum at 10°E.

4.4 Inter-annual variability of the WAWJ

The capability of CMIP6 simulations to reproduce the interannual variability of the WAWJ as in ERA5 differs (Figure 4.5). ERA5 shows a strong positive trend (tr = 0.04 m s^{-1} yr^{-1}) in the interannual variability of the jet. This positive trend is related to the partial recovery of precipitation in the Sahel that began in the 1990s (Hagos & Cook, 2008; Pu & Cook, 2010 and 2012). The majority of the models capture the positive trend of the jet ranging from 0.01 m s^{-1} yr^{-1} (in INM-A) to 0.05 m s^{-1} yr^{-1} (in ECE-A and CES-B). However, 3 models (CAMSC, E3S-A, E3S-C) show a negative trend (tr ≤ -0.017 m s^{-1} yr^{-1}) of the jet. The jet in these models also shows a weak positive correlation with precipitation over West Africa, particularly over the Sahel. The standard deviation of the simulated WAWJ variability varies from 0.42 (in INM-A) to 1.5 (CES-C, E3S-C), with 16 models (61.5%) underestimating the variability. In ERA5, the interannual variability of the WAWJ is strongly correlated with that of the Sahelian rainfall (r = 0.76). While some 15 models (57.7%) agree with ERA5 on the correlation (i.e., r > 0.5), 11

models (42.3%) show weak to very weak correlations. Hence, the correlation of the WAWJ and Sahelian rainfall ranges from 0.1 (in INM-A, which features the lowest interannual variability of the WAWJ) to 0.83 (in CIESM).

4.5 WAWJ and the spatial distribution of climate variables over West Africa

Observation (ERA5 with CRU) shows that there is a strong relationship between the WAWJ strength and spatial distribution of climate variables (i.e., precipitation and temperature) in West Africa (Figs. 4.6 and 4.7). The jet features a strong correlation ($r > 0.6$) with precipitation over the Savanna and Sahel zones (10^{o}–30^{o}N and 20^{o}W–25^{o}E; Figure 4.6). However, the peak correlation ($r \approx 0.8$) obtained in this study is higher than that which is reported in Pu & Cook, 2012 ($r \approx 0.6$). The jet also has a strong dipole correlation with the surface temperature (Figure 4.7), featuring a positive correlation ($r \approx 0.6$) north of 20^{o}N but a negative correlation ($r \approx -0.7$) between 8^{o}–20^{o}N. While the positive correlation can be attributed to the role of the Saharan heat-low in the formation of the WAWJ (as discussed by Pu & Cook (2012) and reviewed in our introduction), the negative correlation (between 8^{o}–20^{o}N) is due to the influence of the jet on the temperature field through precipitation. Hence, the ERA5 (with CRU) results suggest that the stronger the intensity of the Saharan heat-low (i.e., the higher the temperature north of 20^{o}N), the stronger the WAWJ (due to associated stronger pressure gradient force between the continent and the Atlantic Ocean).

The stronger WAWJ transports more moisture eastward into the continent within the 5^{o}–10^{o}N band (Figure 4.8). Figure 4.8 shows more transport of moisture from this band (5^{o}–10^{o}N) in the northeast direction in the Sahel (north of 10^{o}–20^{o}N). This suggests that the increase in the eastward transport of moisture by the WAWJ provides more moisture for the north-eastward transport of moisture by the monsoon flow. The increase in moisture transport into the sub-continent increases precipitation and soil moisture, which results in lower temperatures within the 8^{o}–20^{o}N band (Figure 4.7). These results agree with previous studies (i.e., Pu & Cook, 2012) that linked the yearly variation in the WAWJ strength to interannual variability of precipitation in the Sahel.

It is worth noting that not all the CMIP6 models capture the relationship between the jet and spatial distribution of the climate variables as depicted in ERA5 (Figure 4.6 and Figure 4.7). While most models reproduce the observed strong correlation between the jet and climate variables, the pattern and magnitude of the correlation differ from ERA5. For instance, on the

relationship between the jet and precipitation (Figure 4.6), only 7 models (26.9%) feature a comparable pattern ($r \geq 5$; shown at the bottom left corner of Figure 4.6) with the correlation map of ERA5, namely: ECE-A (r = 0.5), ECE-B (r = 0.5), GFDLC (r = 0.5), CES-B (r = 0.5), CIESM (r = 0.6), MPIES (r = 0.5), and TAIES (r = 0.5). All these models (except TAIES) agree with ERA5 that the positive phase of the WAWJ produces a stronger eastward transport of moisture within the 8°–20°N band (from the west coast up to 25°E), a more north-eastward transport of moisture (from the band to north of 20°N), and higher precipitation over the sub-continent (north of 8°N). However, the north-eastward transport of moisture is weaker in these models than in ERA5, suggesting that their coupling of the WAWJ eastward transport of moisture and monsoon north-east transport of moisture may be weak in the models (Aadhar & Mishra, 2020; Hourdin et al., 2015; Li et al., 2021; Stouffer et al., 2017). That may explain why the increase in precipitation during the stronger WAWJ is limited to south of 15°N in these models (Figure 4.8). The remaining models (73.1%) have a weak agreement with ERA5 on the relationship between the WAWJ and spatial distribution of precipitation; their correlation with ERA5 ranges from 0.1 (E3S-A and E3S-B) to 0.4 (FIOES). While some of these models (e.g., AWICM, CASES, and MPIES) capture the two distinct increases in moisture transports (i.e., the eastward and north-eastward transports) during the stronger WAWJ, the moisture increase does not translate to a commensurable increase in precipitation north of 10°N, as in ERA5. Other models fail to simulate the two distinct increases in moisture transports altogether. For instance, with the increase in the WAWJ, some models (e.g., CES-C and UKESM) simply produce an increase in the eastward transport of moisture, while others (e.g., BCCCS, INM-A, and CMCC) simulate the increase in the north-eastward transport over the whole of West Africa. Three models (E3S-A, E3S-B, and E3S-C) do not produce any coherent pattern in moisture transport over the domain at all (see Figure 4.8). It is important to note that the latitudinal location of the jet and its core does not have any influence on the performance of these models.

The CMIP6 simulations perform better at linking the jet with the spatial distribution of temperature than with the spatial distribution of precipitation (Figure 4.7). Only 6 models (23.1%) show a weak agreement ($r < 0.5$) with ERA5 results, namely: FIOES (r = -0.1), INM-A (r = 0.1), CAMSC (r = 0.2), CES-C (r = 0.2), HADGE (r = 0.2), and E3S-C (r = 0.4). While HADGE and INM-A show a positive correlation between the jet and the spatial distribution of temperature over most parts of the domain, E3S-C shows a negative correlation. CAMSC features a dipole correlation, but it features some negative correlations north of 20°N in contrast

to the ERA5 result. Not all the models that have good agreement with ERA5 (i.e., $0.5 \leq r \leq 0.7$) reproduce the dipole correlation pattern as in ERA5. For instance, 6 models (AWICM, FGOAL, GISSE, E3S-A, E3S-C, SAMUN, and TAIES) show very weak positive correlations ($r < 0.3$) between the jet and temperature north of 25°N. This suggests that these models may underestimate the link between the WAWJ and the SHL. However, ECE-A and ECE-B show the best agreement with ERA5 on the relationship between the WAWJ and spatial distribution of climate variables over the sub-continent.

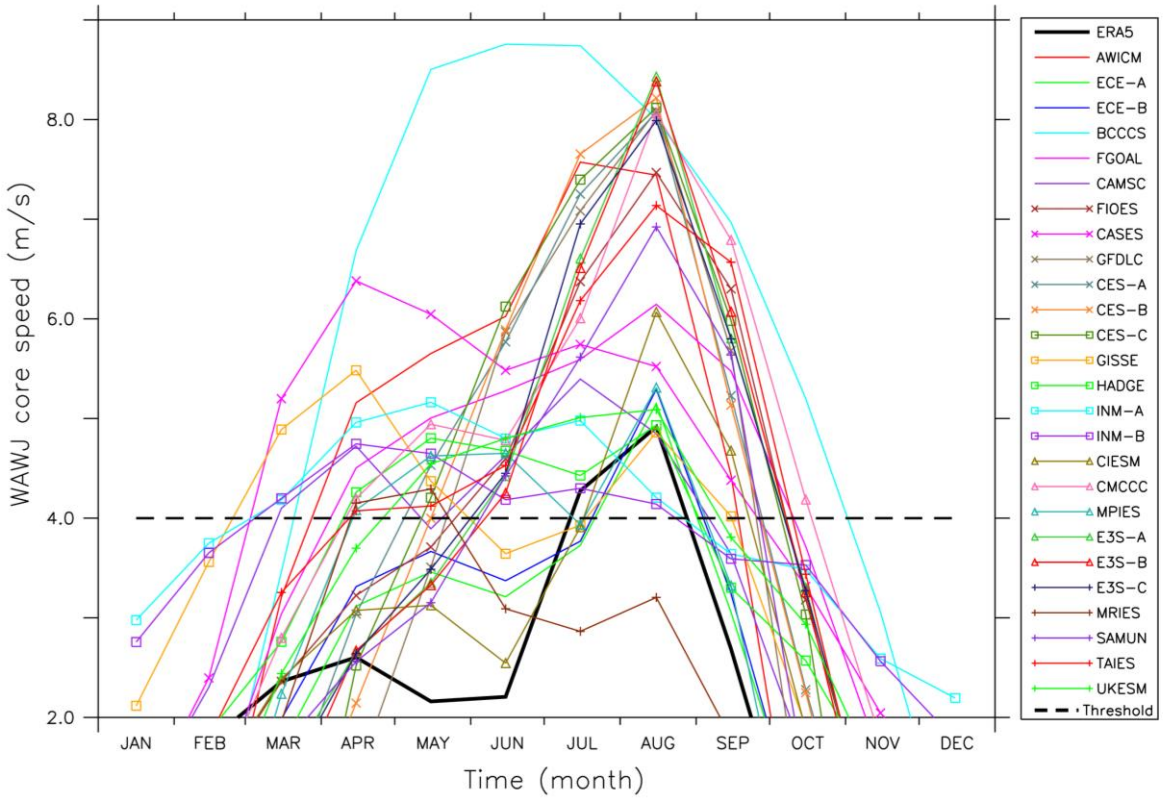

Figure 4.1: The magnitude and annual cycle of WAWJ core climatology from 1980–2014 at 925 hPa.

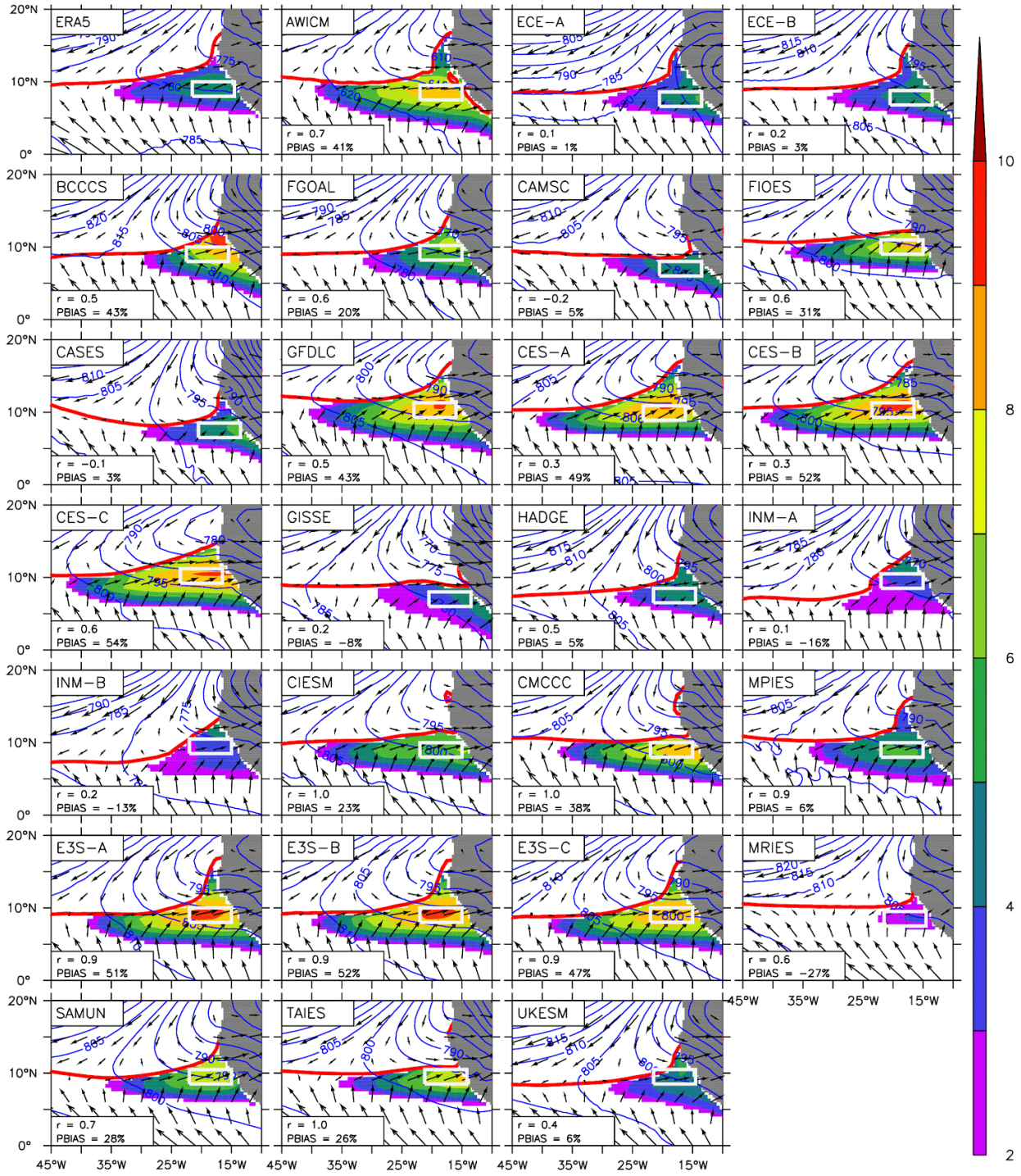

Figure 4.2: The spatial distribution of WAWJ (shading) climatology (1980–2014) and the associated ITCZ (Red), geopotential heights (contour), and wind patterns (vector) in August at 925 hPa.

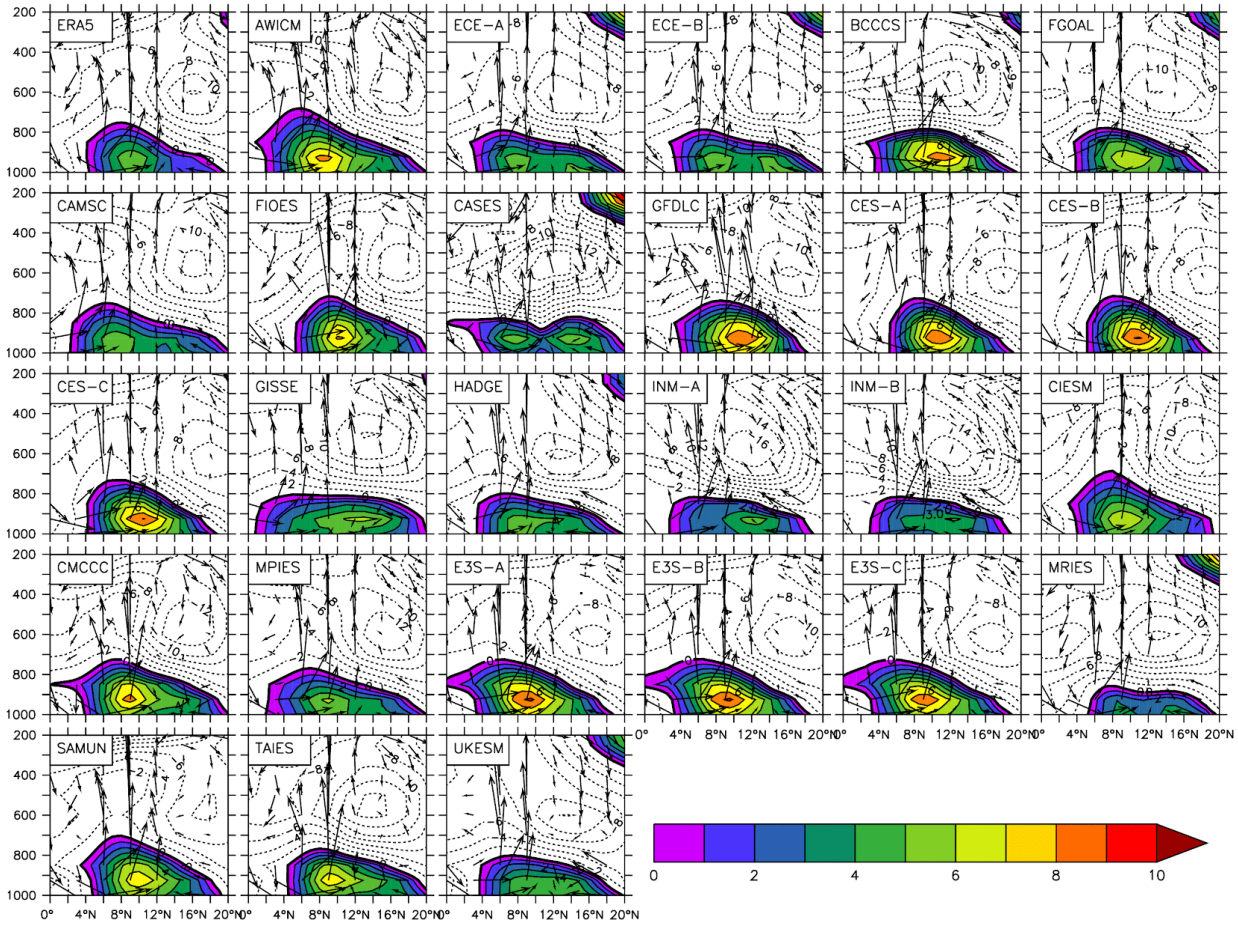

Figure 4.3: Cross-sections of zonal wind speed (m s^{-1}; contours; westerlies shaded) with vectors of meridional and vertical winds (multiplied by 10^2). The averaging regions used are shown (the white box) in Figure 4.2.

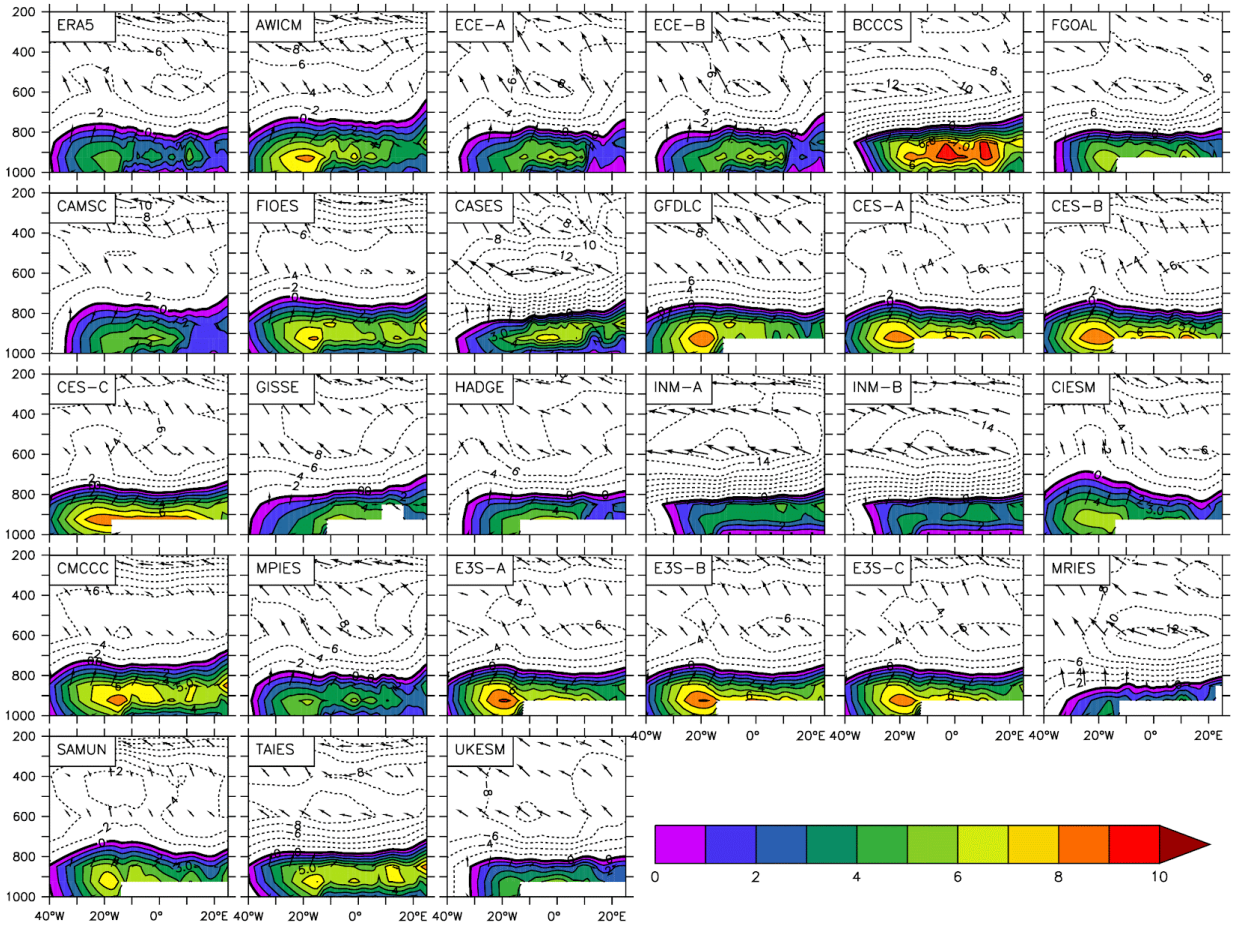

Figure 4.4: Cross-sections of zonal wind speed (m s^{-1}; contour; westerlies shaded) with vectors of zonal and vertical winds (multiplied by 10^2). The averaging regions used are shown in Figure 4.2.

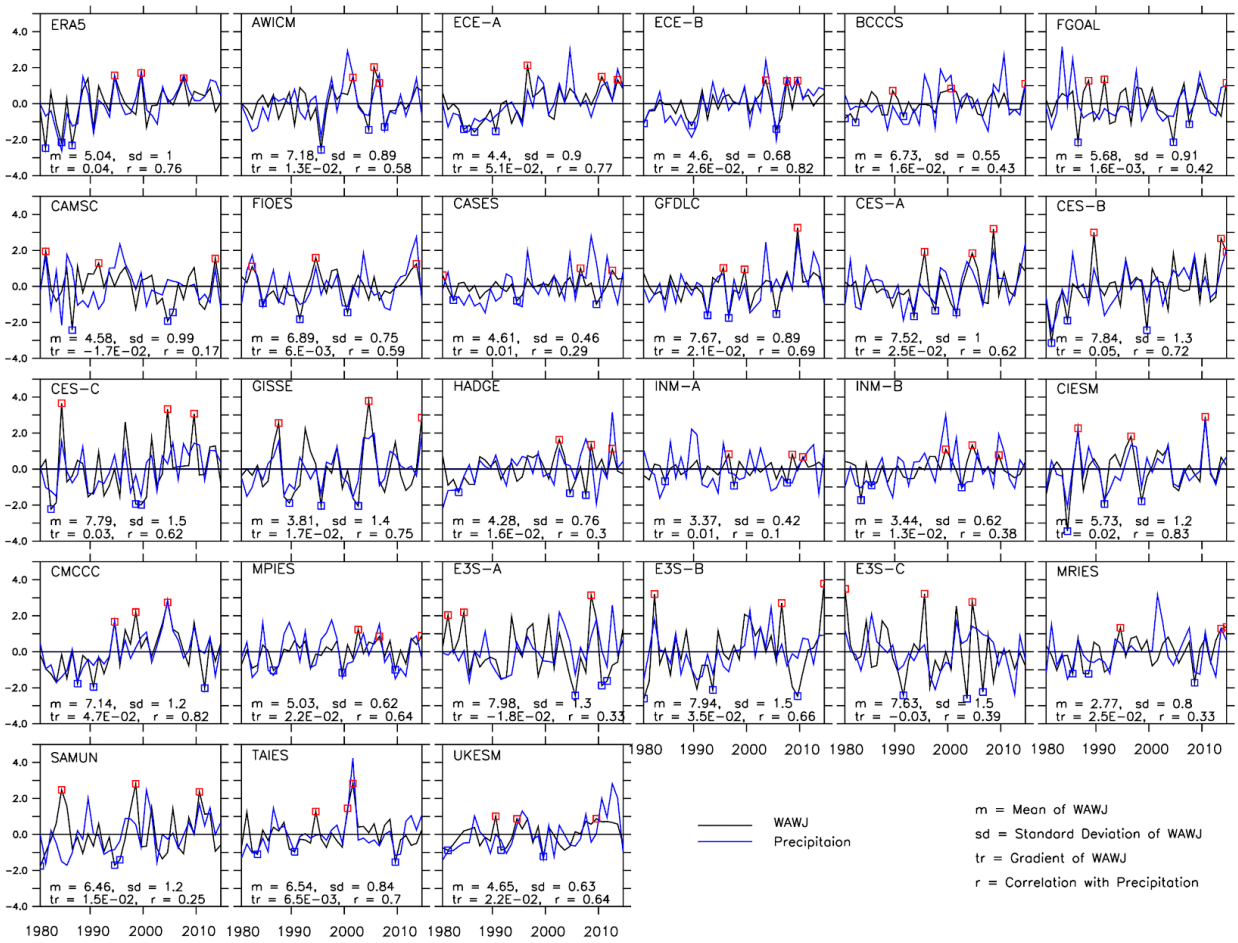

Figure 4.5: The temporal variation of WAWJ (anomaly, m s^{-1}) and Sahelian (domain; 10º-20ºN, 18ºW–30ºE) precipitation (standardised anomaly) in August as depicted by ERA5 (with CRU) and CMIP6 models.

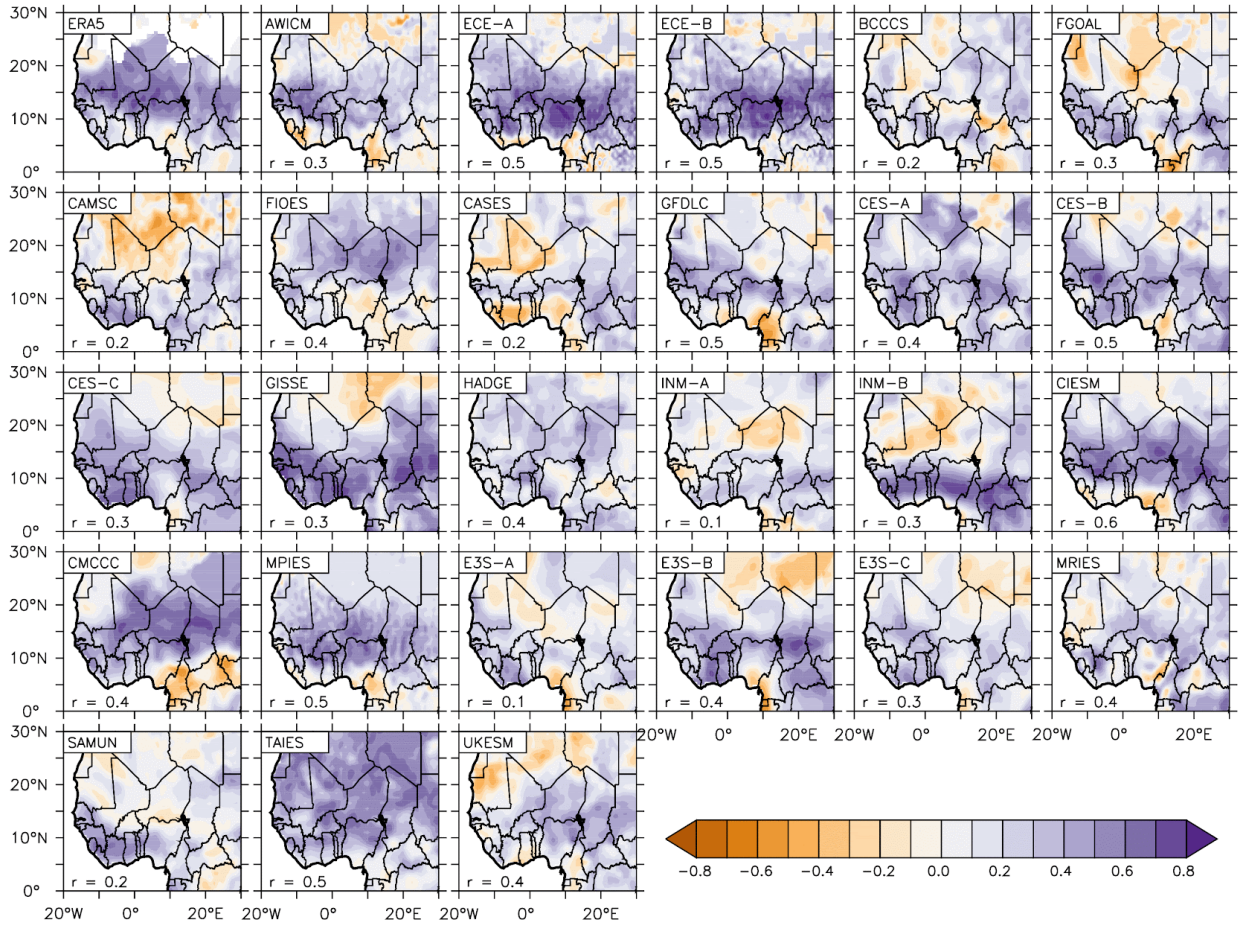

Figure 4.6: The spatial distribution of correlation between the WAWJ and precipitation (mm/month) over West Africa in August (1980–2014), as observed by ERA5 (and CRU) and simulated by the CMIP6 models. The similarity between the simulated and observed patterns is quantified and indicated with a correlation value in each panel.

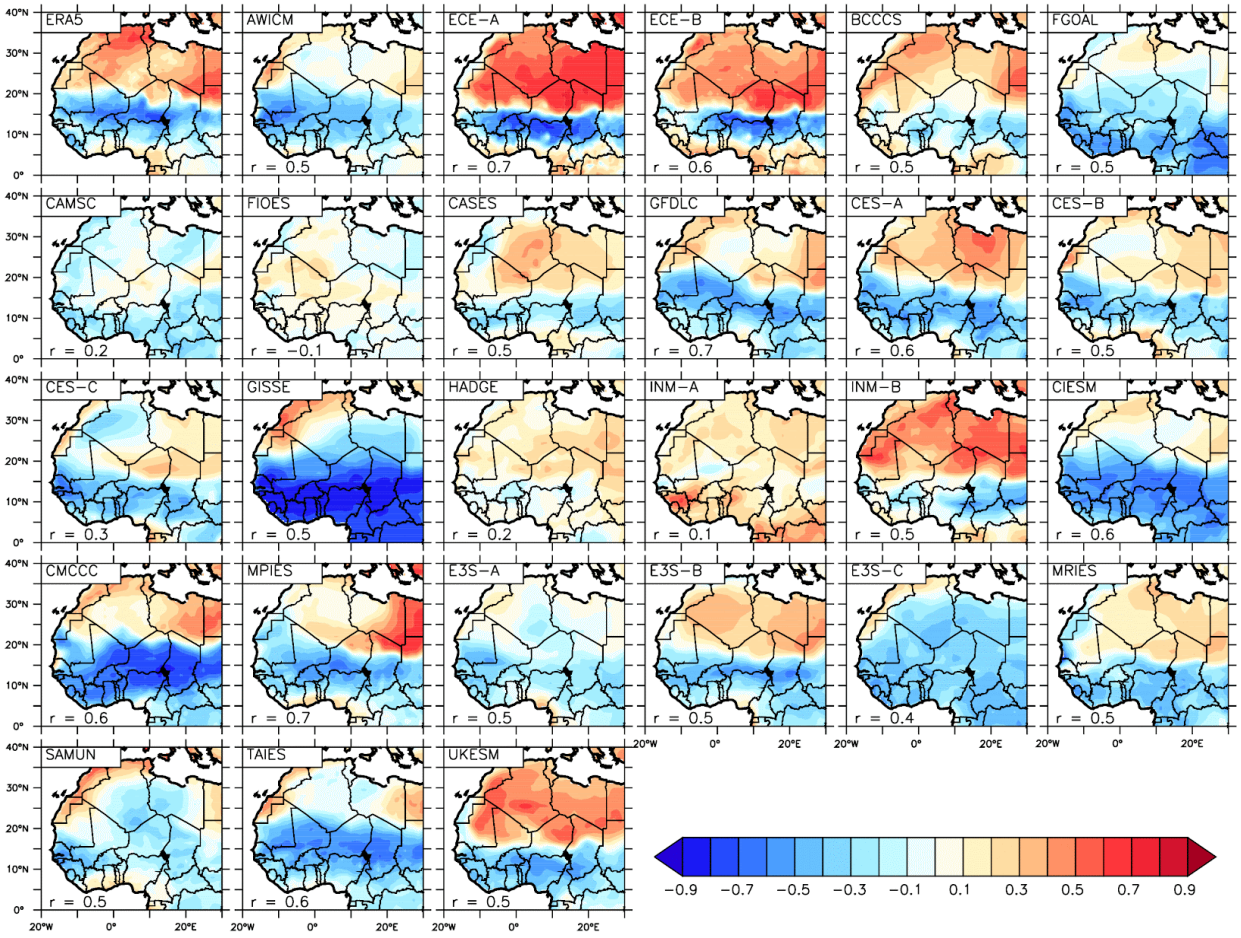

Figure 4.7: The spatial distribution of correlation between the WAWJ and temperature (°C) over West Africa in August (1980–2014), as observed by ERA5 (and CRU) and simulated by the CMIP6 models. The similarity between the simulated and observed patterns is quantified and indicated with correlation in each panel.

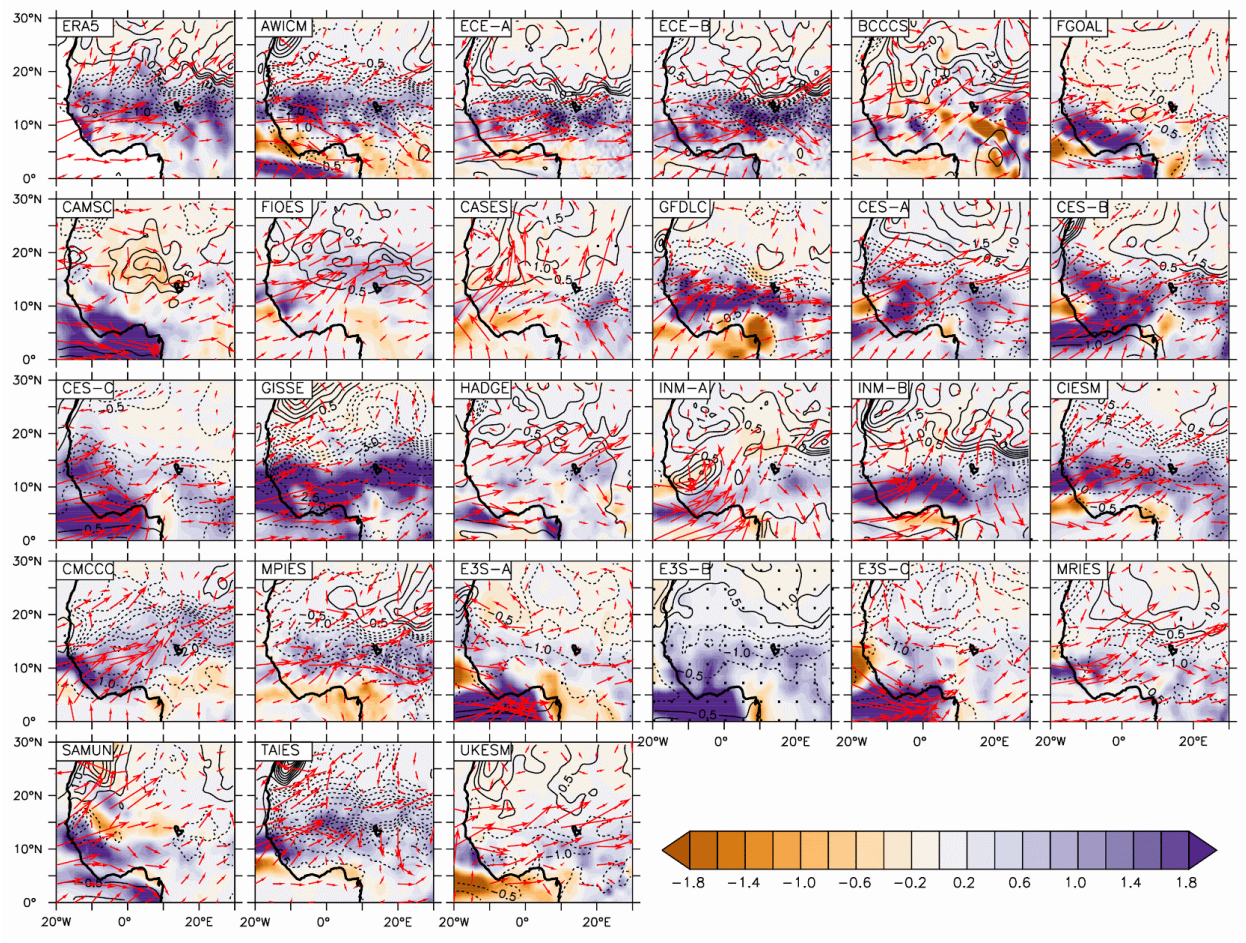

Figure 4.8: Difference of the composite of precipitation (mm/month; shade), temperature (°C; contour), and moisture flux (arrow) anomalies during positive and negative modes of the WAWJ (1980–2014).

Chapter 5: Simulation of West African Westerly Jet

This chapter discusses the results of the simulation and analysis of WAWJ in MPAS. In this chapter, the capability of the MPAS model in reproducing WAWJ and its influence on West African precipitation is investigated. First, the ability of MPAS to simulate West African climate is discussed, as well as the model biases. The characteristic of WAWJ, including the spatial and temporal structure and the interannual variation of the jet is studied. Second, the relationship between the jet and climate variables over West African is investigated. Finally, the sensitivity of the simulated WAWJ to MPAS horizontal resolution is discussed.

5.1 West African Climate

In reference to CRU and ERA5, MPAS gives a credible simulation of the West African climate in August. It reproduces all the essential features in precipitation ($r \simeq 0.8$), temperature ($r \simeq 0.9$), 925 hPa geopotential height ($r \simeq 0.8$), and 925 hPa wind fields (Figure 5.1). For instance, in the precipitation field (Figure 5.1a & 5.1b), MPAS simulates the general meridional gradient in the rainfall pattern over West Africa and adequately captures the position of the ITCZ, depicted by the peak rain band at about 10^{o}N. This is consistent with previous studies that show that ITCZ reaches its northernmost quasi-stationary position of 10^{o}N in August (Sultan et al., 2003; S. E. Nicholson, 2019). Furthermore, in the temperature field (Figure 5.1c & 5.1d), MPAS captures the location (at about 15^o–30^{o}N) and the magnitude of the Saharan heat low (SHL) including the temperature gradient associated with the SHL as in the observation. In addition, it reproduces the monsoon circulation system, characterized by the warm moist south–westerly and the cool dry north–easterly.

Nevertheless, there are notable biases in the model results. For instance, the model simulates a SHL that spreads across the zonal length of the domain (15^{o}W–35^{o}E). This warm bias may be attributed to the failure of the model to capture the southward intrusion of the cold mid-latitude system into West Africa. A strong southward flow is evident around 20^o to 30^{o}N and 15^o to 30^{o}E in ERA5 but not in MPAS (Figure 5.1e & 5.1f). The mid-latitude system is associated with the upper-level mid-latitude Rossby wave propagating westward over the Mediterranean (Flaounas et al., 2012; Lavaysse et al., 2010). Previous studies have shown that the mid-latitude

Rossby wave usually induces a warm ridge to the west and a cold trough to the east, causing a southward surge of cold air from Libya into the Sahara, thereby favoring the collapse of the SHL east of the Sahara (Vizy & Cook, 2009; Chauvin et al., 2010; Alamirew, 2018). This process seems to be absent in the MPAS simulation. In addition, the monsoon flow has a less meridional component in MPAS than in ERA5. For instance, while the monsoon flow is south-westerly in ERA5, it is almost westerly in MPAS (Figure 5.1e & 5.1f). This may be attributed to the stronger zonal geopotential gradient in MPAS than in ERA5. However, the MPAS monsoon would transport less moisture from the Gulf of Guinea into West Africa, feature less convergence with the north-easterly flow over the Sahel, and produce less precipitation over the continent in MPAS than in ERA5. Furthermore, the model overestimates temperature minima over the Guinea highlands, Jos plateau, and the Cameroon mountains, and grossly underestimates the rainfall maxima over these mountains. This result is consistent with the previous findings that the MPAS struggles to resolve the complex topography of West Africa (Heinzeller et al. 2015, Maoyi and Abiodun 2021). Most importantly, MPAS fails to reproduce the high-temperature gradient in the 10^{o} – 15^{o}N zone as depicted in ERA5 (Figure 5.1c & 5.1d). The presence of the high-temperature band in ERA5 may be attributed to two factors. First, it may be attributed to westward transports of warm air from the SHL (over the continent) into the Atlantic Ocean beyond 35^{o}W (Figure 5.1c & 5.1e); MPAS limits the transport of this heat to 20^{o}W (Figure 5.1d & 5.1f). Secondly, it may be due to warming of the atmospheric boundary layer by the ocean, because this region falls at the north-half of the high-SST band over the ocean (i.e., 5^{o} – 15^{o}N) in ERA5. In MPAS, the warming of the atmospheric boundary layer by the ocean is limited to the west of 25^{o}W (Figure 5.1g & 5.1h). However, in ERA5, the heavy precipitation from ITCZ produces a strong cooling of the atmospheric boundary air in the zone 5^{o} – 10^{o}N, leading to a strong temperature gradient between this zone and the zone of the high-temperature band. This strong temperature gradient is also absent in MPAS. As will be discussed later, this strong local meridional temperature gradient may play a crucial role in the formation of WAWJ.

5.2 The West African Westerly Jet

Figure 5.2 shows that MPAS simulates WAWJ that is comparable to that of ERA5. Nevertheless, the characteristics of the jet differ in MPAS and ERA5 results. For instance, in the annual cycle (Figure 5.2a), the jet develops faster in the MPAS than in ERA5. While the jet already attains the mature stage (i.e., speed ≥ 4.0 m s^{-1}) by May in MPAS, it does not attain

this stage until July in ERA5. Although the jet attains its peak strength in August in both datasets, it is stronger in MPAS (> 7.5 m s^{-1}) than in ERA5 (< 5.0 m s^{-1}). In the spatial distribution of the jet, the correlation between MPAS and ERA5 is poor (r = 0.1), because MPAS locates the core of the jet north of its position in ERA5 and underestimates the area coverage of the jet. Furthermore, in MPAS, the jet core is attached to the continent, whereas in ERA5, the jet core is a localized maximum wind off the coast. Therefore, it is obvious that the dynamics of WAWJ differ in the MPAS and ERA5.

To investigate the dynamics, Figure 5.3 presents the spatial distribution of the pressure gradient force (PGF) term in equation (1). The figure reveals that the WAWJ is forced by different pressure gradient force (PGF) patterns in MPAS and ERA5 (Figure 5.3). Although the PGF patterns of the two datasets are similar in June ($r \geq 0.7$), they are less strongly related in in July to September ($r \leq 0.6$) and their highest discrepancy occurs in August (r = 0.5). In July (Figure 5.3a & 5.3b), both datasets feature a tongue of low PGF (2 m s^{-2}) that stretches from the low latitudes (4^oN) to the higher latitudes (up to 10^oN) over the North Atlantic Ocean, except that the tongue is narrower and has south-east to north-west orientation in MPAS. ERA5 shows that the PGF max has broken into cells with the biggest and strongest cell at 6^oN in July. This cell intensifies (14 x 10^{-5} m s^{-2}) and shifts northward (to 9^oN) in August, then weakens in September. The PGF maximum, which can be attributed to the strong meridional temperature discussed in the previous section, is responsible for the formation of WAWJ in ERA5. However, MPAS does not feature this intensifying PGF maximum, instead, it consistently features the tongue of low PGF (2 x 10^{-5} m s^{-2}) from June to September. Hence, the formation of WAWJ in MPAS can be attributed to the pressure gradient induced by the westward extension of the continental trough over the coast. This suggests that, in the MPAS simulation, the dynamics of WAWJ are similar to that of the monsoon. Meanwhile, the ERA5 results and previous studies (i.e., Pu & Cook, 2010; W. Liu et al., 2020) indicate that the dynamics of WAWJ differ from that of the monsoon flow.

Nevertheless, both datasets (ERA5 and MPAS) agree on the direction of forces over their WAWJ areas (Figure 5.4). For instance, over the ERA5 WAWJ area (21.5^oW–14.5^oW, 8.5^oN–10.5^oN), the PGF is mainly northward (magnitude: 14 x 10^{-5} m s^{-2}; Figure 5.3e) and the Coriolis force is south-eastward (magnitude: 12 x 10^{-5} m s^{-2}; Figure 5.4a). This implies that the WAWJ is a sub-geostrophic wind, with the associated geostrophic wind directed eastward (magnitude: 6 m s^{-1}; Figure 5.4c) and the ageostrophic wind (induced by acceleration and friction forces)

directed north-westward (magnitude: 3 m s^{-1}; Figure 5.4e). Over the MPAS WAWJ area (23°W–16°W, 10.5°N–12.5°N), the PGF points northward and north-east directions (magnitude: 20 x 10^{-5} m s^{-2}; Figure 5.3f), and the Coriolis force is south-eastward (20 x 10^{-5} m s^{-2}; Figure 5.4b). In MPAS, the WAWJ is also sub-geostrophic with the associated geostrophic wind directed south-eastward (magnitude: 7 m s^{-1}; Figure 5.4d) and the ageostrophic wind part directed mainly northward (3 m s^{-1}; Figure 5.4e). The directions of the PG and Coriolis forces associated with WAWJ found in this thesis agree with those reported in Pu & Cook (2010), except that Pu & Cook (2010) found that the WAWJ is super-geostrophic instead of sub-geostrophic found here. The discrepancy may be attributed to the difference in the time step of the reanalysis datasets analyzed in both studies. While Pu & Cook (2010) analyzed the daily dataset, the present study analyzed the monthly dataset, which is an average of daily data. The averaging would smoothen the peak values observed in the daily data sets.

5.3 The relationship between WAWJ and climate variables over West Africa

ERA5 and MPAS agree on a strong relationship between the interannual variation of WAWJ and Sahel precipitation in August (Figure 5.5). However, the relationship is stronger ($r > 0.75$) in ERA5 than in MPAS ($r = 0.65$). The spatial distribution of the correlation between WAWJ and precipitation over West Africa (Figure 5.6) shows that WAWJ has a strong positive correlation ($r > 0.5$) with precipitation north of 10°N (i.e., Savanna and the Sahel) in both ERA5 and MPAS, except that the peak of the correlation ($r > 0.70$) spreads over the Savanna and Sahel in ERA5 but concentrates over the southern part of Sahel (i.e., 12°N–14°N) in MPAS. Both datasets indicate a negative correlation between WAWJ and precipitation over the Guinea zone, but while the negative correlation is spotty in ERA5 ($r \approx -0.4$), it covers the entire Guinea zone in MPAS ($r \approx -0.8$). There is a clear disagreement between MPAS and ERA5 regarding the relationship between WAWJ and temperature over the region. In ERA5, WAWJ features a positive correlation with temperature in the zone 10°N–25°N (i.e., the same area where it has a positive correlation with precipitation) but a negative correlation north and south of this area. Contrarily, in MPAS, WAWJ has a negative correlation with temperature south of 20°N but a positive correlation north of this latitude. These further stresses that the WAWJ in MPAS behaves like the monsoon flow, which is driven by the meridional temperature gradient between the Gulf of Guinea and the sub-continent. The composite analysis of WAWJ shows that, in both ERA5 and MPAS, a stronger WAWJ induces a stronger transport of moisture westward from the Northeast Atlantic into the West African continent in the zone 8°N–16°N.

However, over the continent, the moisture is further transported northward into the northern part of Sahel in ERA5, but not in MPAS. This may explain why the correlation between WAWJ and Sahelian rainfall is weaker in MPAS than in ERA5.

5.4 Sensitivity of the simulated WAWJ to MPAS horizontal resolution

MPAS fails to simulate the WAWJ as in ERA5 because it does not capture the local PGF that induces WAWJ over the Atlantic Ocean. Hence, it is of interest to investigate if increasing the model resolution over the study domain would assist the model in capturing the WAWJ as in ERA5.

The increase in horizontal resolution does not improve the MPAS simulation of WAWJ (Figure 5.7 - 5.9). Despite the increase, MPAS15 still fails to capture the spatial distribution of the jet (Figure 5.7) ($r \simeq 0.1$) because it does not simulate the localized PGF that induces WAWJ (Figure 5.8). It still attributes its WAWJ to the westward extension of the continental trough, thereby positioning the jet north of the observed position. Furthermore, the MPAS15 is not sensitive to the differences in the characteristics of WAWJ during the jet's strong and weak years as in ERA5. ERA5 indicates that localized PGF that induces WAWJ is higher in strong years (> 12 m s^{-2}) than in weak years (< 10 m s^{-2}), which explains why the jet is more established (i.e., covering a wider area with a stronger core) in the former than in the latter. However, it is difficult to link the changes in the localized PGF in the weak and strong years to the difference in SST patterns (or 2m temperature patterns) in these years because the differences in the patterns are not substantial. This may be because the calculation of the composites has weakened the temperature gradient. It could also be that there are other factors responsible for the inter-annual variability of the jet. However, while MPAS simulations capture the 2m temperature for both the strong and weak years as in ERA5, the simulations do not reproduce the associated localized PGF.

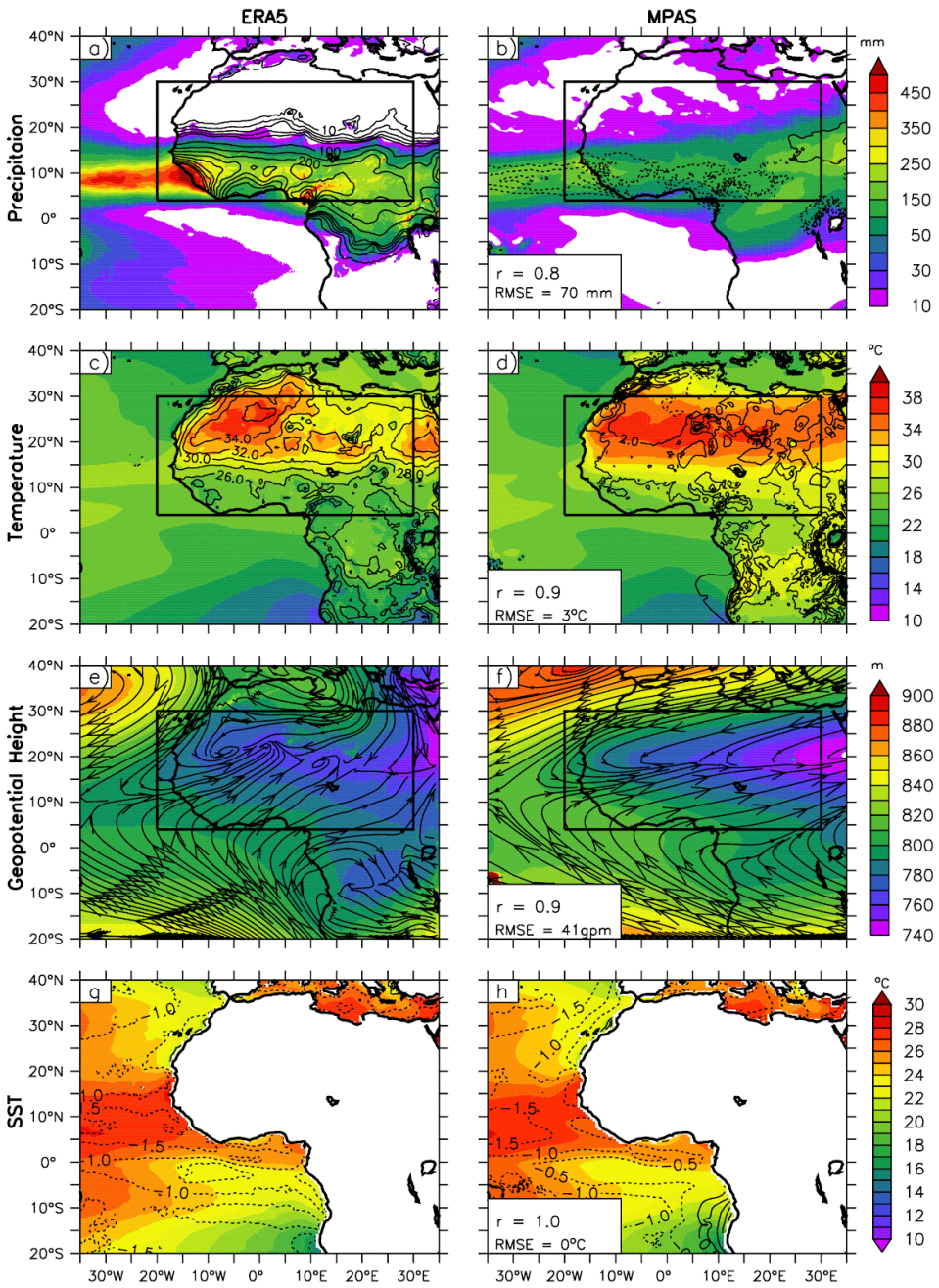

Figure 5.1: Spatial distribution of precipitation (mm month^{-1}; shade), 2–meter temperature (^{o}C; shade), geopotential height (gpm; shade) at 925 hPa, and sea surface temperature (^{o}C; shade) over West Africa in August (1985–2014) as depicted by ERA5 and MPAS. In panels (a) and (c), the contours show the corresponding CRU results; in panels (b) and (d), the contours are the difference between MPAS and ERA5 and, in panels (g) and (h), the contours are the difference between the 2–meter temperature and SST (i.e., temperature minus SST).

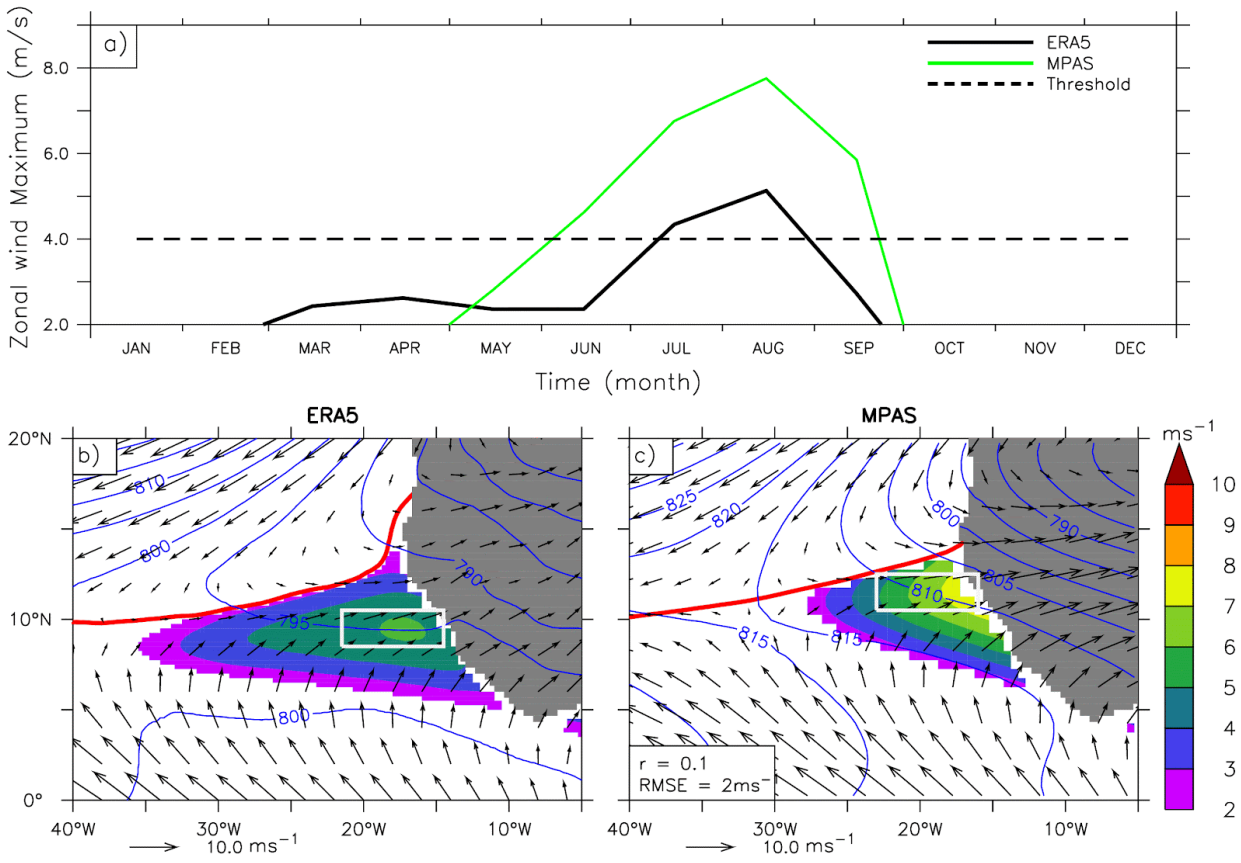

Figure 5.2: The climatology of WAWJ (1985–2014) as depicted by ERA5 and MPAS: (a) the annual cycle of WAWJ and (b) the spatial distribution of WAWJ in August (shaded). In panel (a), the dashed line indicates the threshold for defining the jet mature stage. In panels (b) and (c), the white rectangle shows the location of the jet core, the blue contours show the 925 hPa geopotential height while the arrows show the corresponding winds, and the red line shows the ITCZ.

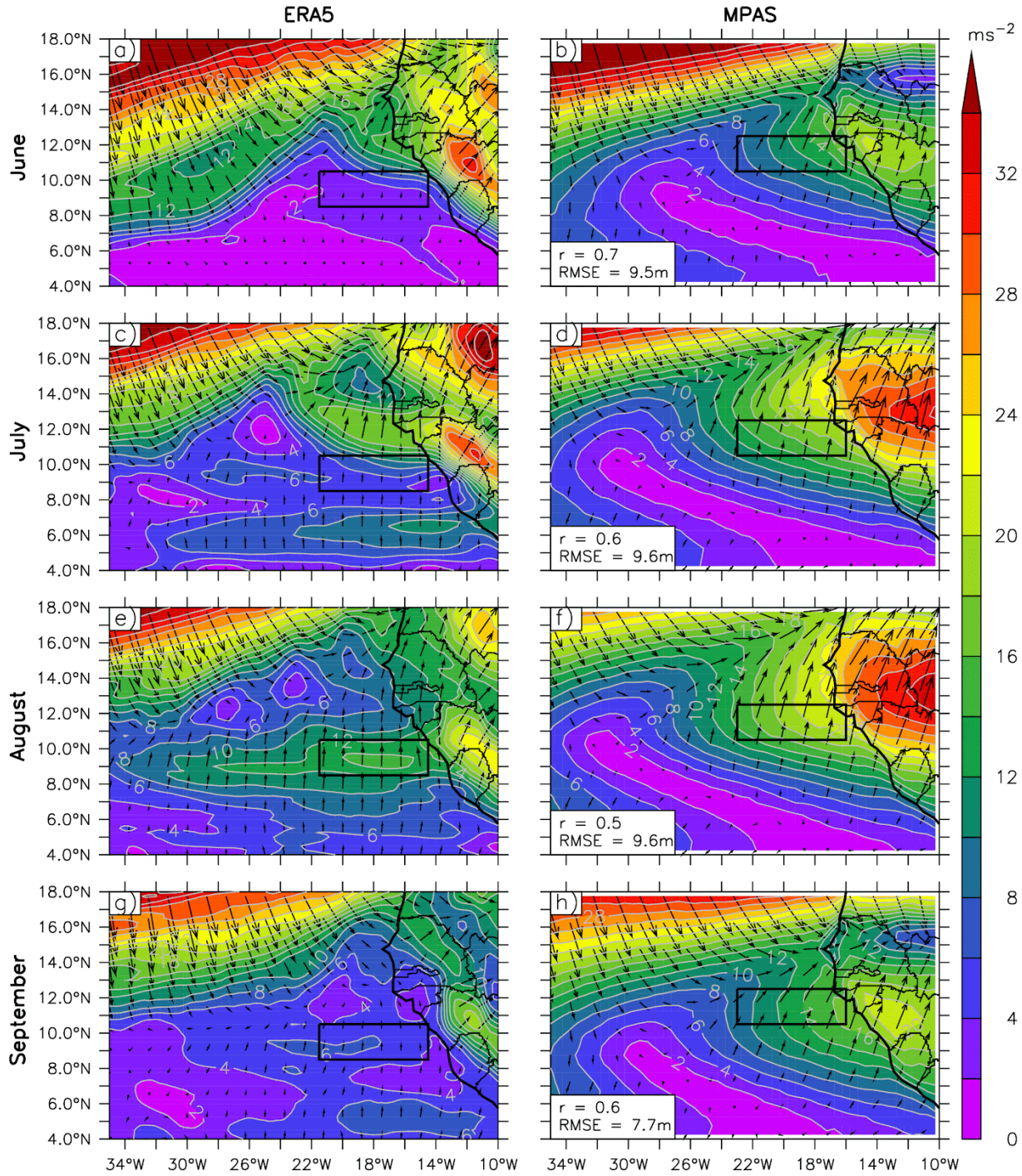

Figure 5.3: The spatial distribution of the pressure gradient term in equation (1) over the WAWJ domain from June to September (1985–2014) as depicted by ERA5 and MPAS. The arrows show the direction while the shading indicates the magnitude (multiplied by 10^5).

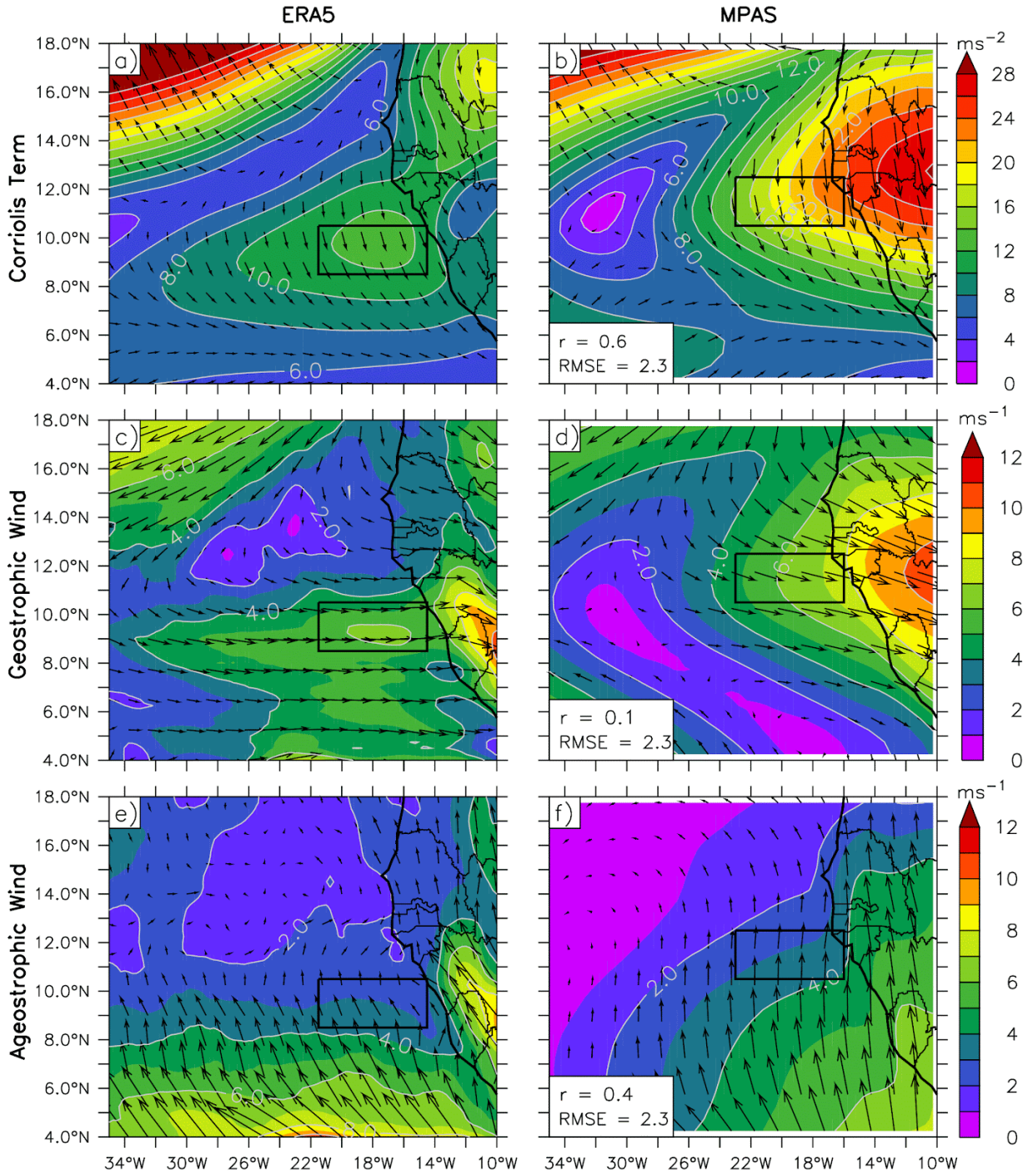

Figure 5.4: The spatial distribution of Coriolis term in equation (1 and 2), geostrophic wind and ageostrophic wind over the WAWJ domain in June to September (1985–2014) as depicted by ERA5 and MPAS. The arrows show the direction of the variables while the shading indicates the magnitude.

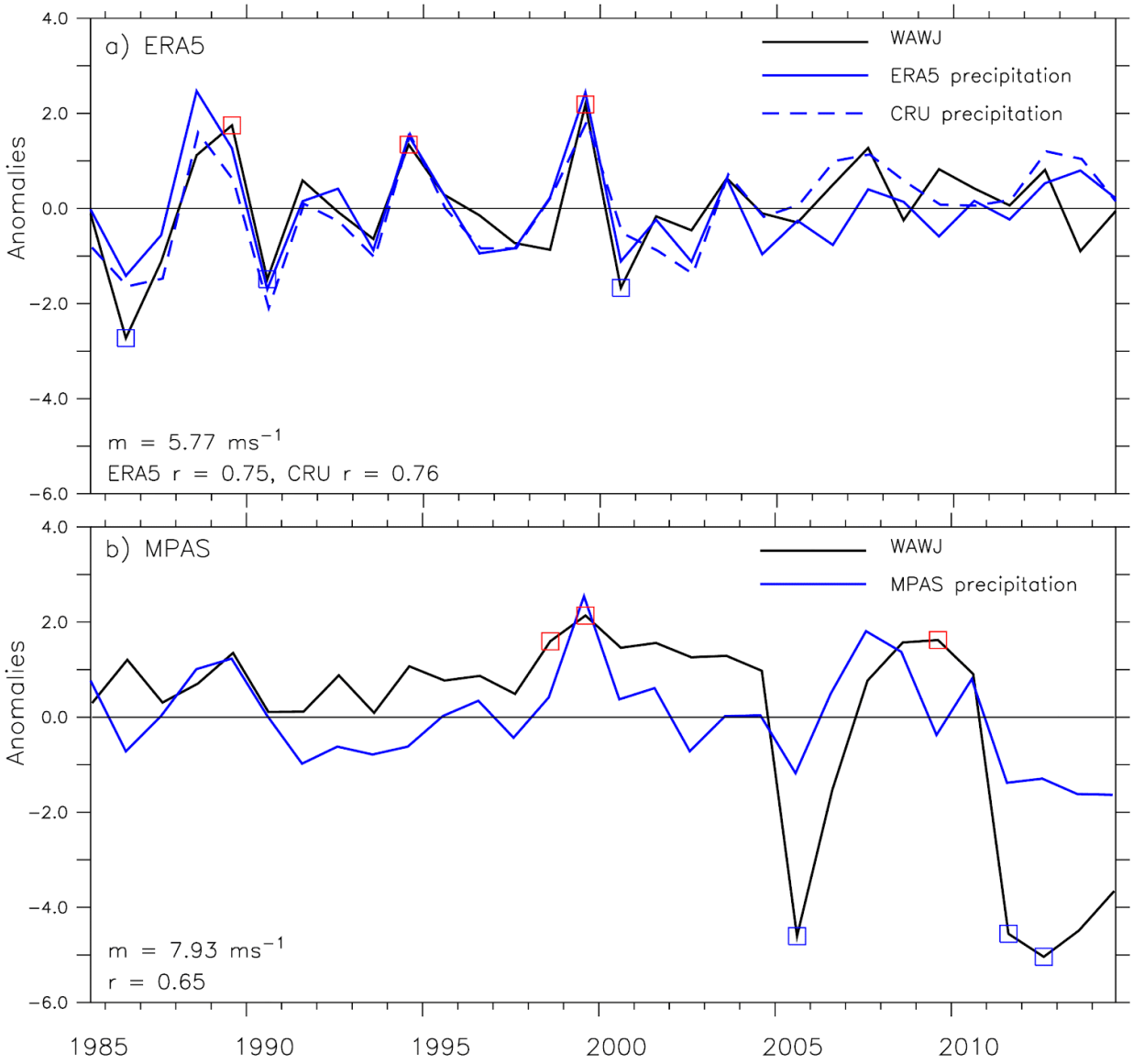

Figure 5.5: The interannual variation of WAWJ anomalies and Sahel precipitation in August. The jet anomalies are average values over the jet core area (i.e., white rectangle in Figure 5.2) while the Sahel precipitation (standardised anomaly) are average values over the Sahel region (as defined in Figure 3.1)

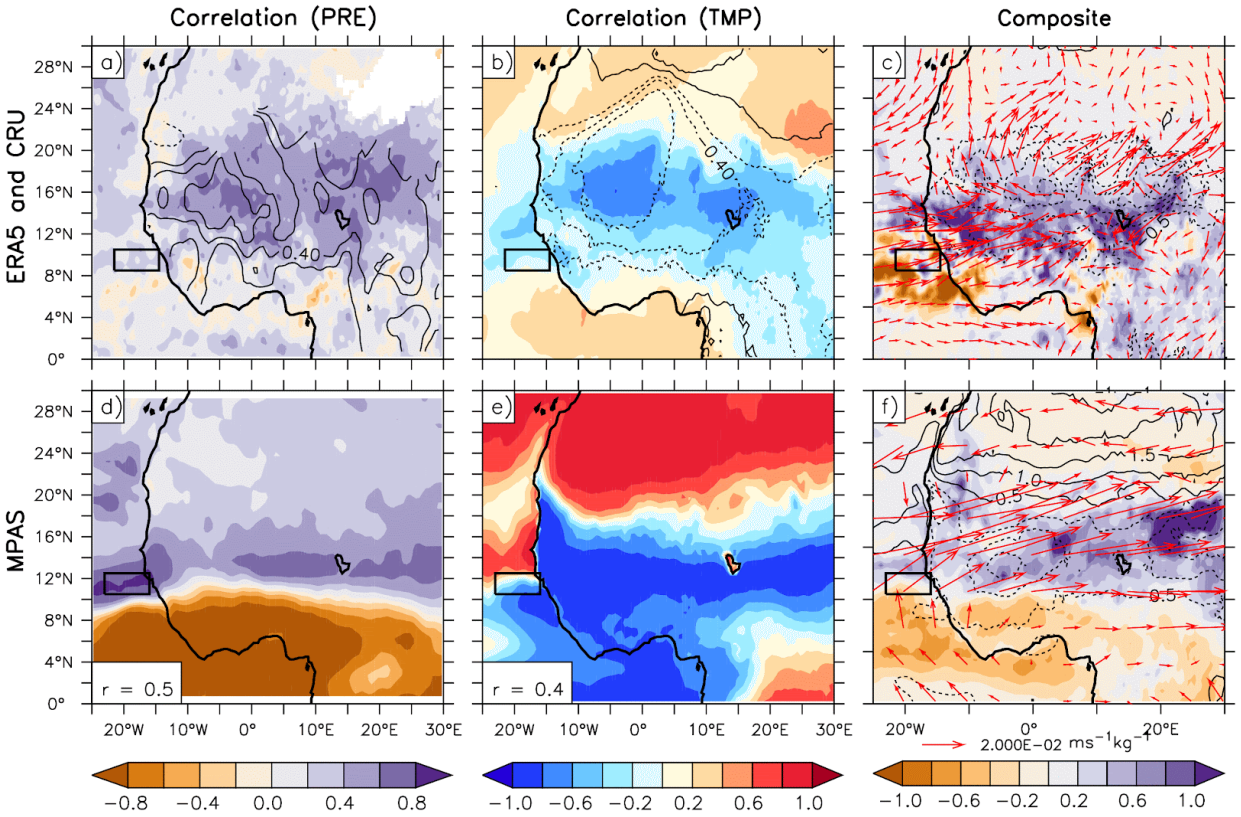

Figure 5.6: The spatial distribution of relationship between the interannual variabilities of the WAWJ and climate variables (i.e., precipitation and temperature) over West Africa (August 1985–2014) as observed by ERA5 and CRU (upper panels) and simulated by the MPAS (lower panels). In panels (a) and (b), the contours show the corresponding CRU results and in panels (d) and (e), the correlations (r) between simulated and observed patterns are indicated. The left panels show the correlation between WAWJ and precipitation; the middle panels show a correlation between the WAWJ and temperature; the right panels show the composites of moisture transport (arrows), precipitation (shaded), and temperature (contour) difference between the WAWJ strong years (1989, 1994, and 1999) and weak years (1986, 1990, and 2000) (strong years composite minus weak years composite).

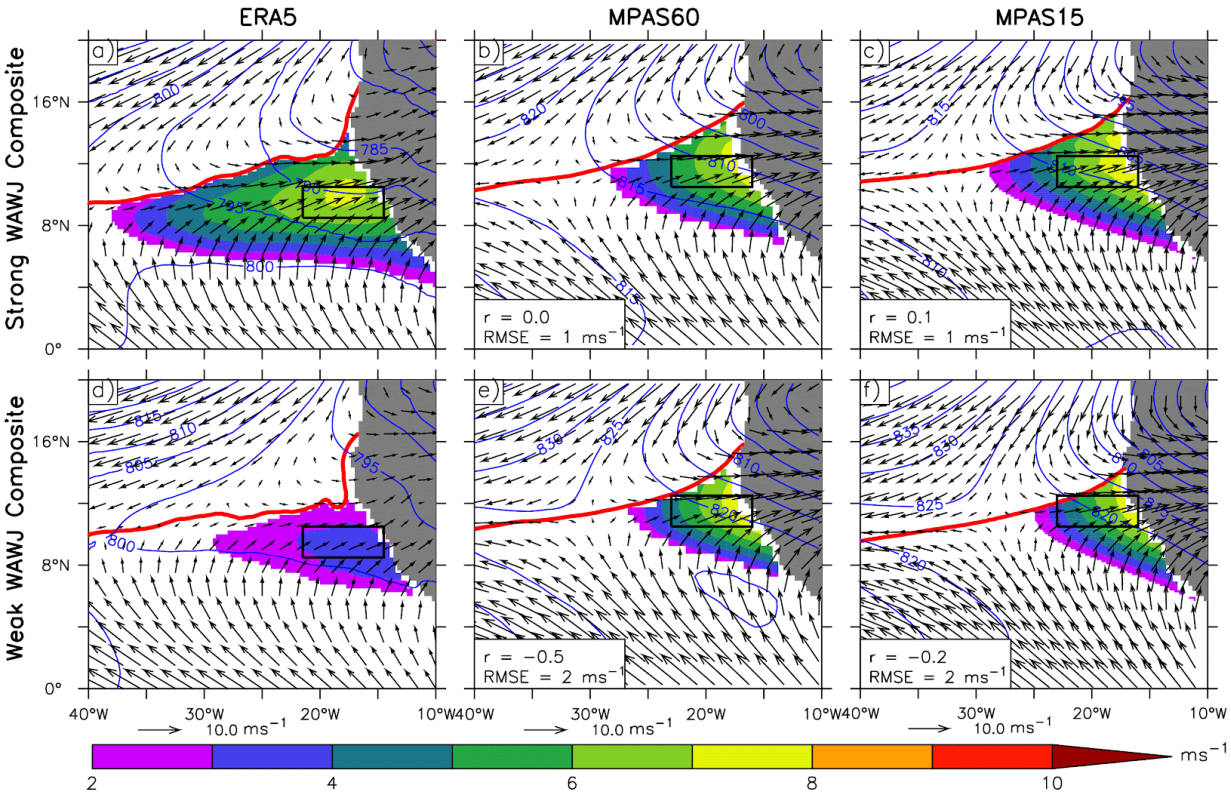

Figure 5.7: The composite of the spatial distribution of the WAWJ (shade), ITCZ (Red contour), geopotential height (gpm; blue contour), and winds (vectors) over West Africa during the WAWJ strong years (top panels) and weak years (bottom panels) as shown by ERA5 and simulated by MPAS60 and MPAS15. In reference to ERA5, the performance of MPAS60 and MPAS15 is quantified by correlation (r) and root-mean-square error (RMSE).

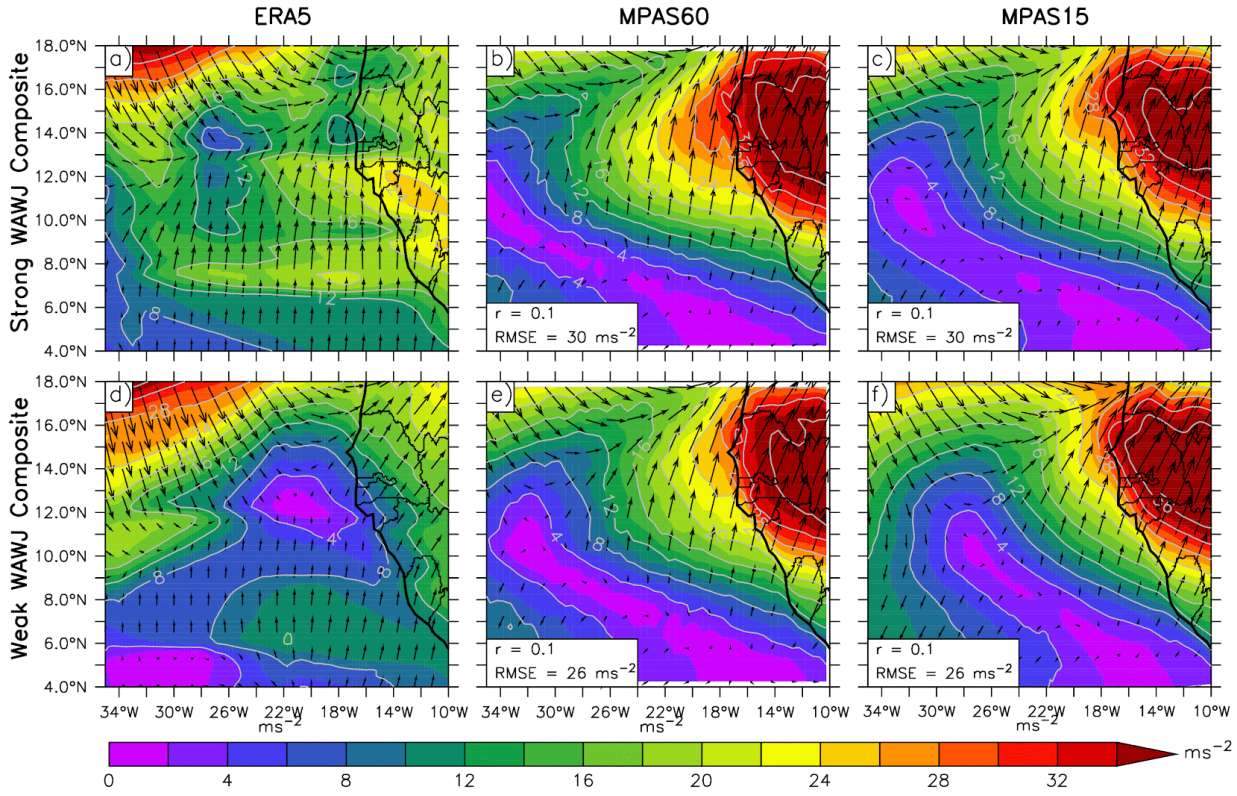

Figure 5.8: The composite of the spatial distribution of geopotential height gradient term direction (vector) and magnitude (shading; multiplied by 10^5) in the equation (1 and 2) over the WAWJ domain during the WAWJ strong years (top panels; 1989, 1994, and 1999) and weak years (bottom panels; 1986, 1990, and 2000) as shown by ERA5 and simulated by MPAS60 and MPAS15. In reference to ERA5, the performance of MPAS60 and MPAS15 is quantified by correlation (r) and root-mean-square error (RMSE).

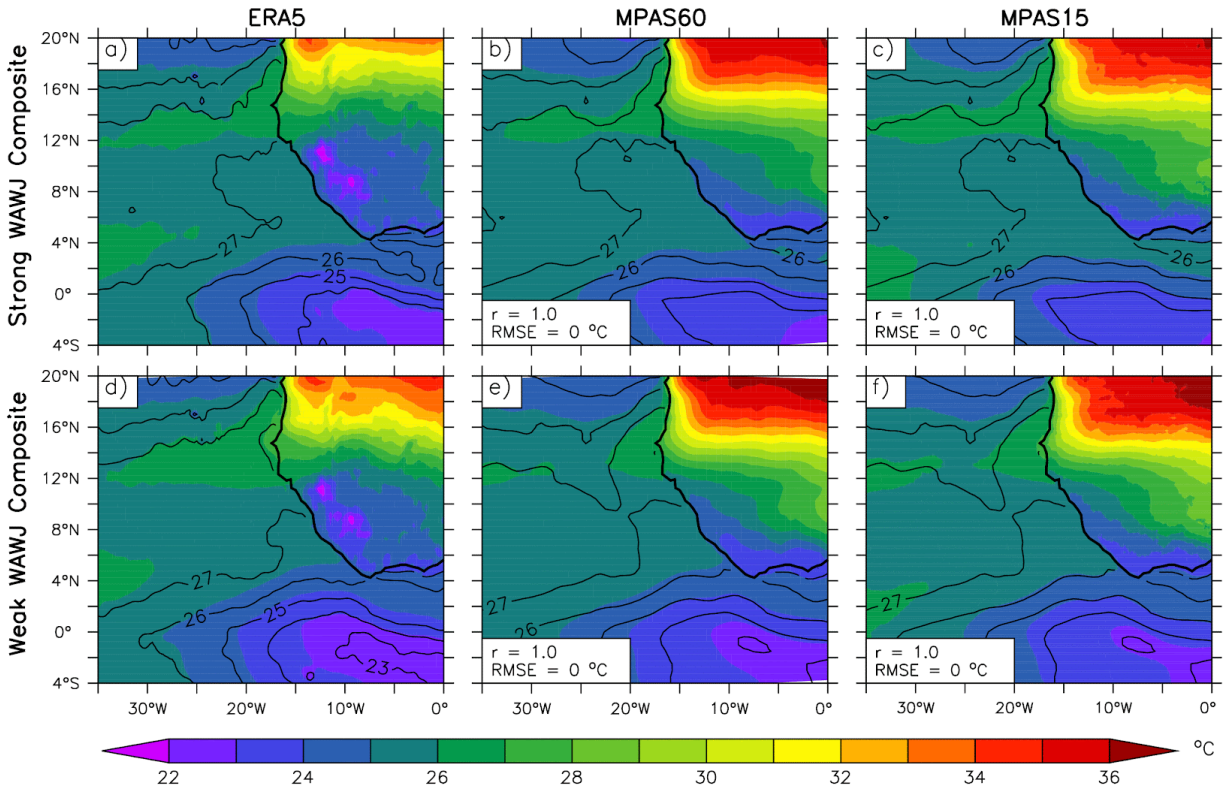

Figure 5.9: The composite of the spatial distribution of SST (contour, ºC) and 2–m temperature (shaded) over the WAWJ domain during the WAWJ strong years (top panels; 1989, 1994, and 1999) and weak years (bottom panels; 1986, 1990, and 2000) as shown by ERA5 and simulated by MPAS60 and MPAS15. In reference to ERA5, the performance of MPAS60 and MPAS15 is quantified by correlation (r) and root-mean-square error (RMSE).

Chapter 6: Conclusion

6.1 Summary

As part of efforts to improve the performance of MPAS in simulating West African climate systems and to enhance the projection of precipitation in the Sahel, the study has evaluated the capability of CMIP6 simulations and the MPAS model in simulating the WAWJ and the associated moisture transports over West Africa. The study analyzed the CRU, ERA5, and 26 CMIP6 datasets for a period of 35 years. This thesis has also conducted a climatological simulation and two sensitivity simulations with MPAS. The study, which defined WAWJ (one of the atmospheric features that modulate precipitation over the Sahel) as a low-level westerly jet over the eastern Atlantic and the West African coast, compared the characteristics of WAWJ in observational (CRU), reanalysis (ERA5), and simulation data. The study used standard statistical metrics to quantify the evaluation. It also quantifies the relationship between the jet and climate variables in the datasets with correlation analysis and uses composite analysis of the climate variables during the positive and negative modes of WAWJ to investigate the relationship.

The results of the study can be summarized below:

- ERA5 shows that the WAWJ has its core at 925 hPa and attains its maximum speed in August. Most CMIP6 simulations capture the temporal vertical and temporal structure of the jet but produce jets that develop too fast and are too strong with reference to ERA5 results.

- While most CMIP6 models agree with ERA5 on the spatial structure of WAWJ (covering $6^oN–12^oN$, $15^oW–35^oW$ with the core around 8^oN and 20^oW), more than 38% disagree with ERA5 on the spatial structure.

- The majority of the models reproduce a positive trend in the interannual variability of WAWJ as in ERA5 results, but some models show a negative trend in the interannual variability.

- In ERA5, the WAWJ has a strong positive correlation with precipitation over West Africa (especially over the Sahel) and a dipole correlation pattern with temperature over the sub-continent. Most CMIP6 simulations capture the correlation between the jet and temperature, but only a few of them capture the correlation between the jet and precipitation.

- Not all the CMIP6 simulations feature the two distinct increases in the moisture transports (i.e., the eastward and north-eastward transports) during the years of stronger WAWJ as in ERA5 results. Some of those that capture it do not translate the increase in moisture transport to a commensurable increase in precipitation north of 10^{o}N.

- MPAS gives credible simulations of the major features in temperature, precipitation, and wind fields over West Africa, except that it features wet and warm biases over the sub-continent and simulates a monsoon flow that is more zonal than observed.

- The model simulates the WAWJ, but the characteristics of the jet differ from the observed. The simulated WAWJ develops too early in the year. Its core is too strong, its area coverage is too small, and its location is too far north and too close to the coast.

- Both ERA5 and MPAS agree that the WAWJ is a sub-geostrophic flow because the PGF around the jet is higher than the Coriolis force, but while ERA5 attributes the formation of the jet to a localized PGF over the Atlantic Ocean, MPAS attributes the formation to the PGF from an extension of a continental trough to the coast.

- In agreement with ERA5, MPAS features a strong correlation between WAWJ and Sahelian precipitation, but the magnitude of the correlation is weaker than indicated in ERA5 because, although the jet transports moisture eastward into the sub-continent in both ERA5 and MPAS, the moisture flux is limited to the southern part of the Sahel in MPAS but is further transported to the northern part of the Sahel in ERA5.

- Increasing the horizontal resolution does not help MPAS in reproducing the localized PGF or in capturing the dynamics of WAWJ as in ERA5 results. It does not also help the model in distinguishing between strong and weak WAWJ years as indicated by ERA5.

These above results complement findings of previous studies on the dynamics and the roles of West African Westerly jet in rainfall variability over West Africa, especially over the Sahel, as well as the capability of GCMs in simulating atmospheric systems over West Africa. Nicholson (2013b) and Lélé et al. (2015) reported that the WAWJ enhances the westerly transport of moisture (from the eastern Atlantic) into the West African continent and northward reaching about 20^{o}N over the western Sahel. Furthermore, Pu & Cook (2012) and Lélé, (2014) have linked the repeated droughts over the Sahel to the negative anomalous moisture transport during the weaker WAWJ. Results of our study have shown that the WAWJ has a strong positive correlation with precipitation over West Africa (especially over the Sahel) and a dipole correlation pattern with temperature over the sub-continent due to the role of the Saharan heat-low in the formation of WAWJ and the influence of the jet on the temperature field through precipitation. In addition, the northeastward transport of moisture by WAWJ provides more moisture for the northeastward transport of moisture by the monsoon flow. The increase in moisture transport into the sub-continent increases precipitation and soil moisture, which results in lower temperatures within the 8^{o}N–20^{o}N band. The result of this thesis also shows that global climate models, like the CMIP6 and MPAS, struggle to simulate the characteristics and dynamics of WAWJ, as well as the influence of the jet on precipitation distribution over West Africa. The relative performance of the CMIP6 models may be influenced by different sources of uncertainty. One such uncertainty is the statistical or sampling uncertainty which could result in variances in different samples from the same model (Smith et al. 2009; NASEM et al. 2016; Paciorek et al. 2018; Abalos et al. 2021). Such uncertainty arises from limited sampling of the variability of a system, which can span a range of time scales from a few days to centuries, though it decreases with increasing sample size (Paciorek et al. 2018; Wehner et al. 2020). However, due to the computational constrains, the thesis evaluated only one 35-year record from each CMIP6 simulation. Technically, evaluating multiple 35-year record from each CMIP6 simulation could enhance the model performance because it would help delineate model biases (due model inadequacy) from the sampling uncertainty. In addition, the failure of MPAS to simulate WAWJ as observed could be attributed to the inability of the model to simulate the local PGF over the Atlantic Ocean, though the reason for the inability is still not clear.

The results of the thesis have several applications. The identified strengths and shortcomings of the climate models in simulating the characteristics of WAWJ and moisture transport over West Africa could guide the developer of these models on how to improve quality of seasonal

forecasting and climate projection over the region. For example, the inability of MPAS to capture the observed WAWJ despite the increase in resolution is an indication that more effort is needed on other areas of model development. The establishment of the strong relationship between WAWJ and Sahel rainfall in both observation and model simulations indicates the robustness of the relationship. Incorporating this relationship into existing empirical or statistical models for predicting the rainfall onset date, cessation dates and rainfall amount could improve the performance of the models. Furthermore, the thesis identified WAWJ as one of the most important but least understood rainfall-producing systems over West Africa. This motivates more studies on WAWJ. Better understanding of the jet would foster better seasonal rainfall prediction, which would help society, policymakers, and humanitarian agencies to make effective emergency response plans towards mitigating the devastating impacts of extreme events associated with rainfall variability in the region.

6.2 Suggestions for further research

Future studies can investigate how the results of the CMIP6 simulations are sensitive to model resolution. In addition, the biases identified in some of the CMIP6 models could be related to physics parameterization. For example, the inability of some of the models to translate the moisture transport by the jet to commensurable precipitation suggests that the convective parameterization schemes in the models might be too weak in translating the excess moisture into precipitation. Therefore, future studies could evaluate different physics parameterization schemes in those models. Furthermore, more studies and model developments are still needed to investigate why MPAS fails to capture the WAWJ dynamics. In addition, the biases identified in the temperature field, for example, the inability of MPAS to adequately capture the high-temperature band off the coast of Africa over the Atlantic Ocean could be due to inadequate mixing in the heat flux scheme of the model. Therefore, future studies could evaluate different heat flux parameterization schemes in the model. Also, future studies could investigate why the MPAS monsoon flow is more zonal than observed. This could shed more light on why precipitation along the ITCZ is too low. Nevertheless, the present study has shown that the MPAS model does not adequately capture the WAWJ, its interannual variability, and its north-eastward transport of moisture.

References

Aadhar, S., & Mishra, V. (2020). On the projected decline in droughts over south Asia in CMIP6 multimodel ensemble. Journal of Geophysical Research, 125(20). https://doi.org/10.1029/2020jd033587

Abalos, M., Calvo, N., Benito-Barca, S., Garny, H., Hardiman, S. C., Lin, P., ... & Yoshida, K. (2021). The Brewer–Dobson circulation in CMIP6. Atmospheric Chemistry and Physics, 21(17), 13571-13591.

Abatan, A. A. (2011). Iowa State University. https://search.proquest.com/openview/8bca905e47d79897bc17e6b5fca2f3a7/1?pq-origsite=gscholar&cbl=18750

Abiodun, B. J., Adeyewa, Z. D., Oguntunde, P. G., Salami, A. T., & Ajayi, V. O. (2012). Modeling the impacts of reforestation on future climate in West Africa. Theoretical and Applied Climatology, 110(1-2), 77–96.

Abiodun, B. J., Gutowski, W. J., Abatan, A. A., & Prusa, J. M. (2011). CAM-EULAG: A non-hydrostatic atmospheric climate model with grid stretching. Acta Geophysica, 59(6), 1158–1167.

Adaawen, S. (2021). Understanding Climate Change and Drought Perceptions, Impact and Responses in the Rural Savannah, West Africa. Atmosphere, 12(5), 594.

Afiesimama, E. A., Pal, J. S., Abiodun, B. J., Gutowski, W. J., & Adedoyin, A. (2006). Simulation of West African monsoon using the RegCM3. Part I: Model validation and interannual variability. In Theoretical and Applied Climatology (Vol. 86, Issues 1-4, pp. 23–37). https://doi.org/10.1007/s00704-005-0202-8

Ahmadalipour, A., & Moradkhani, H. (2018). Multi-dimensional assessment of drought vulnerability in Africa: 1960–2100. The Science of the Total Environment, 644, 520–535.

Ajibade, I., McBean, G., & Bezner-Kerr, R. (2013). Urban flooding in Lagos, Nigeria: Patterns of vulnerability and resilience among women. In Global Environmental Change (Vol. 23,

Issue 6, pp. 1714–1725). https://doi.org/10.1016/j.gloenvcha.2013.08.009

Akinsanola, A. A., Ogunjobi, K. O., Gbode, I. E., & Ajayi, V. O. (2015). Assessing the Capabilities of Three Regional Climate Models over CORDEX Africa in Simulating West African Summer Monsoon Precipitation. Advances in Meteorology, 2015. https://doi.org/10.1155/2015/935431

Akpoti, K., Antwi, E. O., & Kabo-bah, A. T. (2016). Impacts of Rainfall Variability, Land Use and Land Cover Change on Stream Flow of the Black Volta Basin, West Africa. Hydrology, 3(3), 26.

Alamirew, N. (2018). Comprehensive analysis of thermodynamics, dynamics and associated variability [University of Sussex]. https://ethos.bl.uk/OrderDetails.do?uin=uk.bl.ethos.751911

Albergel, C., Dutra, E., Munier, S., Calvet, J.-C., Munoz-Sabater, J., de Rosnay, P., & Balsamo, G. (2018). ERA-5 and ERA-Interim driven ISBA land surface model simulations: Which one performs better? Hydrology and Earth System Sciences Discussions, 1–37.

Algarra, I., Eiras-Barca, J., Miguez-Macho, G., Nieto, R., & Gimeno, L. (2019). On the assessment of the moisture transport by the Great Plains low-level jet. Earth System Dynamics, 10(1), 107–119.

Almazroui, M., Saeed, F., Saeed, S., Nazrul Islam, M., Ismail, M., Klutse, N. A. B., & Siddiqui, M. H. (2020). Projected Change in Temperature and Precipitation Over Africa from CMIP6. Earth Systems and Environment, 4(3), 455–475.

Amador, J. A. (2008). The Intra-Americas Sea low-level jet: overview and future research. Annals of the New York Academy of Sciences, 1146(1), 153–188.

Aneesh, S., & Sijikumar, S. (2016). Changes in the south Asian monsoon low level jet during recent decades and its role in the monsoon water cycle. Journal of Atmospheric and Solar-Terrestrial Physics, 138-139, 47–53.

Antwi-Agyei, P., Dougill, A. J., Doku-Marfo, J., & Abaidoo, R. C. (2021). Understanding climate services for enhancing resilient agricultural systems in Anglophone West Africa: The case of Ghana. Climate Services, 22, 100218.

Ardanuy, P. (1979). On the Observed Diurnal Oscillation of the Somali Jet. Monthly Weather Review, 107(12), 1694–1700.

Asumadu-Sarkodie, S., Owusu, P. A., & Jayaweera, H. M. P. C. (2015). Flood risk management in Ghana: A case study in Accra. https://open.metu.edu.tr/bitstream/handle/11511/68868/10.5281zenodo.812898.pdf

Atiah, W. A., Amekudzi, L. K., Aryee, J. N. A., Preko, K., & Danuor, S. K. (2020). Validation of Satellite and Merged Rainfall Data over Ghana, West Africa. Atmosphere, 11(8), 859.

Atiah, W. A., Mengistu Tsidu, G., Amekudzi, L. K., & Yorke, C. (2020). Trends and interannual variability of extreme rainfall indices over Ghana, West Africa. Theoretical and Applied Climatology, 140(3-4), 1393–1407.

Baas, P. (2009). Turbulence and low-level jets in the stable boundary layer. https://library.wur.nl/WebQuery/wurpubs/383383

Baas, P., Bosveld, F. C., Klein Baltink, H., & Holtslag, A. A. M. (2009). A Climatology of Nocturnal Low-Level Jets at Cabauw. Journal of Applied Meteorology and Climatology, 48(8), 1627–1642.

Bader, D. C., Leung, R., Taylor, M., & McCoy, R. B. (2019a). E3SM-Project E3SM1.0 model output prepared for CMIP6 CMIP historical [Data set]. Earth System Grid Federation. https://doi.org/10.22033/ESGF/CMIP6.4497

Bader, D. C., Leung, R., Taylor, M., & McCoy, R. B. (2019b). E3SM-Project E3SM1.1 model output prepared for CMIP6 CMIP historical [Data set]. Earth System Grid Federation. https://doi.org/10.22033/ESGF/CMIP6.11485

Bader, D. C., Leung, R., Taylor, M., & McCoy, R. B. (2020). E3SM-Project E3SM1.1ECA model output prepared for CMIP6 CMIP historical [Data set]. Earth System Grid Federation. https://doi.org/10.22033/ESGF/CMIP6.11486

Ballo, A., Omotosho, J. B., Klutse, N. A. B., Abiodun, B. J., & Coulibaly, A. (2021). The influence of quasi-biennial oscillation on West African Rainfall. Modeling Earth Systems and Environment. https://doi.org/10.1007/s40808-021-01185-6

Beauchemin, C. (2011). Rural–urban migration in West Africa: towards a reversal? Migration

trends and economic situation in Burkina Faso and Côte d'Ivoire. Population, Space and Place, 17(1), 47–72.

Beck, H. E., Pan, M., Roy, T., Weedon, G. P., Pappenberger, F., van Dijk, A. I. J. M., Huffman, G. J., Adler, R. F., & Wood, E. F. (2018). Daily evaluation of 26 precipitation datasets using Stage-IV gauge-radar data for the CONUS. Hydrology and Earth System Sciences Discussions, 1–23.

Berg, L. K., Riihimaki, L. D., Qian, Y., Yan, H., & Huang, M. (2015). The Low-Level Jet over the Southern Great Plains Determined from Observations and Reanalyses and Its Impact on Moisture Transport. Journal of Climate, 28(17), 6682–6706.

Berthou, S., Rowell, D. P., Kendon, E. J., Roberts, M. J., Stratton, R. A., Crook, J. A., & Wilcox, C. (2019). Improved climatological precipitation characteristics over West Africa at convection-permitting scales. Climate Dynamics, 53(3), 1991–2011.

Biasutti, M. (2013). Forced Sahel rainfall trends in the CMIP5 archive. Journal of Geophysical Research, 118(4), 1613–1623.

Bichet, A., & Diedhiou, A. (2018). Less frequent and more intense rainfall along the coast of the Gulf of Guinea in West and Central Africa (1981-2014). Climate Research, 76(3), 191–201.

Bojinski, S., Verstraete, M., Peterson, T. C., Richter, C., Simmons, A., & Zemp, M. (2014). The Concept of Essential Climate Variables in Support of Climate Research, Applications, and Policy. Bulletin of the American Meteorological Society, 95(9), 1431–1443.

Borvarán, D., Peña, A., & Gandoin, R. (2021). Characterization of offshore vertical wind shear conditions in Southern New England. Wind Energy, 24(5), 465–480.

Boyd, E., Cornforth, R. J., Lamb, P. J., Tarhule, A., Lélé, M. I., & Brouder, A. (2013). Building resilience to face recurring environmental crisis in African Sahel. Nature Climate Change, 3(7), 631–637.

Buontempo, C., Booth, B., & Moufouma-Okia, W. (2012). The climate of the Sahel. West African Studies Global Security Risks and West Africa Development Challenges: Development Challenges, 57.

https://books.google.com/books?hl=en&lr=&id=gW9C6LpaI_YC&oi=fnd&pg=PA57&dq=Buontempo+et+al.,+2012+sst+sahel&ots=Qd38Eakwyl&sig=IS4M_SLtagSeSzpgEEK0X5Q2BhQ

Burgering, L. M. T., Kleczek, M. A., & Steeneveld, G. J. (2013). Modeling orographic gravity wave drag in the stable boundary layer and determining the influence on cyclonic filling at the Northern Hemisphere during winter …. https://edepot.wur.nl/332362

Burpee, R. W. (1972). The Origin and Structure of Easterly Waves in the Lower Troposphere of North Africa. Journal of the Atmospheric Sciences, 29(1), 77–90.

Burrows, D. A., Ferguson, C. R., Campbell, M. A., Xia, G., & Bosart, L. F. (2019). An objective classification and analysis of upper-level coupling to the Great Plains low-level jet over the twentieth century. Journal of Climate, 32(21), 7127–7152.

Cadet, D. L., & Nnoli, N. O. (1987). Water vapour transport over Africa and the Atlantic ocean during summer 1979. Quarterly Journal of the Royal Meteorological Society, 113(476), 581–602.

Cai, S., & Yu, H. (2012). Analysis of different weather research and forecasting radiation schemes' impact on the numerical simulation of a typical mesoscale convective weather in China. In Journal of Atmospheric and Solar-Terrestrial Physics (Vol. 80, pp. 68–72). https://doi.org/10.1016/j.jastp.2012.02.021

Campbell, P. C., Bash, J. O., Herwehe, J. A., Gilliam, R. C., & Li, D. (2020). Impacts of tiled land cover characterization in the Model for Prediction Across Scales-Atmosphere (MPAS-A). Journal of Geophysical Research, D: Atmospheres, 125(15). https://doi.org/10.1029/2019JD032093

Campetella, C. M., & Vera, C. S. (2002). The influence of the Andes mountains on the South American low-level flow. Geophysical Research Letters, 29(17), 7–1 – 7–4.

Campion, B. B., & Venzke, J.-F. (2013). Rainfall variability, floods and adaptations of the urban poor to flooding in Kumasi, Ghana. In Natural Hazards (Vol. 65, Issue 3, pp. 1895–1911). https://doi.org/10.1007/s11069-012-0452-6

Chai, Z. (2020). CAS CAS-ESM1.0 model output prepared for CMIP6 CMIP historical [Data

set]. Earth System Grid Federation. https://doi.org/10.22033/ESGF/CMIP6.3353

Chauvin, F., Roehrig, R., & Lafore, J.-P. (2010). Intraseasonal Variability of the Saharan Heat Low and Its Link with Midlatitudes. Journal of Climate, 23(10), 2544–2561.

Cook, K. H. (1999). Generation of the African Easterly Jet and Its Role in Determining West African Precipitation. In Journal of Climate (Vol. 12, Issue 5, pp. 1165–1184). https://doi.org/10.1175/1520-0442(1999)012<1165:gotaej>2.0.co;2

Cook, K. H., & Vizy, E. K. (2006). Coupled Model Simulations of the West African Monsoon System: Twentieth- and Twenty-First-Century Simulations. In Journal of Climate (Vol. 19, Issue 15, pp. 3681–3703). https://doi.org/10.1175/jcli3814.1

Cook, K. H., & Vizy, E. K. (2010). Hydrodynamics of the Caribbean Low-Level Jet and Its Relationship to Precipitation. Journal of Climate, 23(6), 1477–1494.

Cook, K. H., Vizy, E. K., Launer, Z. S., & Patricola, C. M. (2008). Springtime Intensification of the Great Plains Low-Level Jet and Midwest Precipitation in GCM Simulations of the Twenty-First Century. In Journal of Climate (Vol. 21, Issue 23, pp. 6321–6340). https://doi.org/10.1175/2008jcli2355.1

Cornforth, R. J., Hoskins, B. J., & Thorncroft, C. D. (2009). The impact of moist processes on the African easterly jet-African easterly wave system. Quarterly Journal of the Royal Meteorological Society, 135(641), 894–913.

Couvreux, F., Guichard, F., & Bock, O. (2010). Synoptic variability of the monsoon flux over West Africa prior to the onset. Quarterly Journal of. https://rmets.onlinelibrary.wiley.com/doi/abs/10.1002/qj.473?casa_token=vnn5y9vnSkgAAAAA:7-vLHz29VsObOu0GNisw3iJGceFQP1-0wWO1MeoPaD3J514jtujdmBOpixsLFhdOQGyyf5ZR9AC-DvzuSA

Covey, C., AchutaRao, K. M., Cubasch, U., Jones, P., Lambert, S. J., Mann, M. E., Phillips, T. J., & Taylor, K. E. (2003). An overview of results from the Coupled Model Intercomparison Project. Global and Planetary Change, 37(1), 103–133.

Danabasoglu, G. (2019a). CMIP6.CMIP.NCAR.CESM2-WACCM.historical [Data set]. Earth System Grid Federation. https://doi.org/10.22033/ESGF/CMIP6.10071

Danabasoglu, G. (2019b). NCAR CESM2 model output prepared for CMIP6 CMIP historical [Data set]. Earth System Grid Federation. https://doi.org/10.22033/ESGF/CMIP6.7627

de Oliveira, C. P., Aímola, L., Ambrizzi, T., & Freitas, A. C. V. (2018). The influence of the regional Hadley and Walker circulations on precipitation patterns over Africa in El Niño, la Niña, and neutral years. Pure and Applied Geophysics, 175(6), 2293–2306. https://doi.org/10.1007/s00024-018-1782-4

Devereux, S. (2009). Why does famine persist in Africa? Food Security, 1(1), 25–35.

Devereux, S. (2019). Preventable famines. In An Economic History of Famine Resilience (pp. 203–224). https://doi.org/10.4324/9780429200632-11

Dezfuli, A. K., & Nicholson, S. E. (2011). A note on long-term variations of the African easterly jet. International Journal of Climatology, 31(13), 2049–2054.

Diasso, U., & Abiodun, B. J. (2017). Drought modes in West Africa and how well CORDEX RCMs simulate them. Theoretical and Applied Climatology, 128(1-2), 223–240.

Diatta, S., Diedhiou, C. W., Dione, D. M., & Sambou, S. (2020). Spatial Variation and Trend of Extreme Precipitation in West Africa and Teleconnections with Remote Indices. Atmosphere, 11(9), 999.

Dietz, A. J., Ruben, R., & Verhagen, A. (2006). The Impact of Climate Change on Drylands: With a Focus on West Africa. Springer Science & Business Media.

Diouf, A. A., Brandt, M., Verger, A., Jarroudi, M. E., Djaby, B., Fensholt, R., Ndione, J. A., & Tychon, B. (2015). Fodder Biomass Monitoring in Sahelian Rangelands Using Phenological Metrics from FAPAR Time Series. Remote Sensing, 7(7), 9122–9148.

Druyan, L. M. (2011). Studies of 21st-century precipitation trends over West Africa. International Journal of Climatology, 31(10), 1415–1424.

Druyan, L. M., & Fulakeza, M. (2018). Downscaling Atmosphere-Ocean Global Climate Model Precipitation Simulations over Africa Using Bias-Corrected Lateral and Lower Boundary Conditions. Atmosphere, 9(12), 493.

Du, Q., Faber, V., & Gunzburger, M. (1999). Centroidal Voronoi Tessellations: Applications

and Algorithms. SIAM Review, 41(4), 637–676.

Dwivedi, S., Yesubabu, V., & Ratnam, M. V. (2021). Variability of monsoon inversion over the Arabian Sea and its impact on rainfall. Aquatic Microbial Ecology: International Journal. https://rmets.onlinelibrary.wiley.com/doi/abs/10.1002/joc.6896?casa_token=QNr2u37SXOAAAAAA:pUjcXwhxwMbtxHChB_Mzud7HfXCfUa13YJEg_yP1K3YDWIh9vX7lFX80pDgmHDTyPTaft4O-_zeLaqbcCw

EC-Earth. (2019). EC-Earth-Consortium EC-Earth3 model output prepared for CMIP6 CMIP historical [Data set]. Earth System Grid Federation. https://doi.org/10.22033/ESGF/CMIP6.4700

EC-Earth-Veg. (2019). EC-Earth-Consortium EC-Earth3-Veg model output prepared for CMIP6 CMIP historical [Data set]. Earth System Grid Federation. https://doi.org/10.22033/ESGF/CMIP6.4706

Edwards, P. N. (2011). History of climate modeling. Wiley Interdisciplinary Reviews. Climate Change, 2(1), 128–139.

Egbebiyi, Egbebiyi, Crespo, & Lennard. (2019). Defining Crop–climate Departure in West Africa: Improved Understanding of the Timing of Future Changes in Crop Suitability. In Climate (Vol. 7, Issue 9, p. 101). https://doi.org/10.3390/cli7090101

Egbebiyi, T. S. (2016). Future changes in extreme rainfall events and African easterly waves over West Africa [University of Cape Town]. https://open.uct.ac.za/handle/11427/20581

Ek, M. B., Mitchell, K. E., Lin, Y., Rogers, E., Grunmann, P., Koren, V., Gayno, G., & Tarpley, J. D. (2003). Implementation of Noah land surface model advances in the National Centers for Environmental Prediction operational mesoscale Eta model. In Journal of Geophysical Research: Atmospheres (Vol. 108, Issue D22). https://doi.org/10.1029/2002jd003296

Elagib, N. A., Al Zayed, I. S., Gayoum Saad, S. A., Mahmood, M. I., Basheer, M., & Fink, A. H. (2021). Debilitating floods in the Sahel are becoming frequent. In Journal of Hydrology (Vol. 599, p. 126362). https://doi.org/10.1016/j.jhydrol.2021.126362

Essoungou, A.-M. (2013a). A messenger of peace and development goes to the Sahel. Africa

Renewal, 27(3), 20–21.

Essoungou, A.-M. (2013b). The Sahel: One region, many crises. Africa Renewal, 27(3), 22–23.

Eyring, V., Bony, S., Meehl, G. A., Senior, C. A., Stevens, B., Stouffer, R. J., & Taylor, K. E. (2016). Overview of the Coupled Model Intercomparison Project Phase 6 (CMIP6) experimental design and organization. In Geoscientific Model Development (Vol. 9, Issue 5, pp. 1937–1958). https://doi.org/10.5194/gmd-9-1937-2016

Falvey, M., & Garreaud, R. D. (2005). Moisture variability over the South American Altiplano during the South American Low Level Jet Experiment (SALLJEX) observing season. Journal of Geophysical Research, 110(D22). https://doi.org/10.1029/2005jd006152

FAO. (2012). Executive Brief: The Sahel Crisis 2012. Food and Agriculture Organization of the United Nations. http://www.fao.org/fileadmin/user_upload/sahel/docs/EXECUTIVE%20BRIEF%20TCE%206%20July.pdf

Ferguson, W. (1985). Integrating crops and livestock in West Africa. FAO Animal Production and Health Paper, 41. https://www.fao.org/3/x6543e/X6543E01.htm

Flaounas, E., Janicot, S., Bastin, S., & Roca, R. (2012). The West African monsoon onset in 2006: sensitivity to surface albedo, orography, SST and synoptic scale dry-air intrusions using WRF. Climate Dynamics, 38(3-4), 685–708.

Foltz, G. R., Brandt, P., Richter, I., Rodríguez-Fonseca, B., Hernandez, F., Dengler, M., Rodrigues, R. R., Schmidt, J. O., Yu, L., Lefevre, N., Da Cunha, L. C., McPhaden, M. J., Araujo, M., Karstensen, J., Hahn, J., Martín-Rey, M., Patricola, C. M., Poli, P., Zuidema, P., … Reul, N. (2019). The Tropical Atlantic Observing System. Frontiers in Marine Science, 6, 206.

Fontaine, B. (2003). Atmospheric water cycle and moisture fluxes in the West African monsoon: mean annual cycles and relationship using NCEP/NCAR reanalysis. Geophysical Research Letters, 30(3). https://doi.org/10.1029/2002gl015834

Fontaine, B., Janicot, S., & Moron, V. (1995). Rainfall Anomaly Patterns and Wind Field

Signals over West Africa in August (1958–1989). Journal of Climate, 8(6), 1503–1510.

Freitas, A. C. V., Aímola, L., Ambrizzi, T., & de Oliveira, C. P. (2017). Changes in intensity of the regional Hadley cell in Indian Ocean and its impacts on surrounding regions. Meteorology and Atmospheric Physics, 129(3), 229–246.

Gadde, S. N., & Stevens, R. J. A. M. (2021). Effect of low-level jet height on wind farm performance. Journal of Renewable and Sustainable Energy, 13(1), 013305.

Gallée, H. (2004). A high-resolution simulation of a West African rainy season using a regional climate model. In Journal of Geophysical Research (Vol. 109, Issue D5). https://doi.org/10.1029/2003jd004020

Gautam, M. (2006). Managing drought in sub-Saharan Africa: Policy perspectives. Resource /Energy Economics and Policy, 19.

Gbobaniyi, E., Sarr, A., Sylla, M. B., Diallo, I., Lennard, C., Dosio, A., Dhiédiou, A., Kamga, A., Klutse, N. A. B., Hewitson, B., Nikulin, G., & Lamptey, B. (2014). Climatology, annual cycle and interannual variability of precipitation and temperature in CORDEX simulations over West Africa. International Journal of Climatology, 34(7), 2241–2257.

Geist, H. J., & Lambin, E. F. (2004). Dynamic Causal Patterns of Desertification. Bioscience, 54(9), 817–829.

Gilliam, R. C., & Pleim, J. E. (2010). Performance Assessment of New Land Surface and Planetary Boundary Layer Physics in the WRF-ARW. Journal of Applied Meteorology and Climatology, 49(4), 760–774.

Giorgi, F. (2006). Regional climate modeling: Status and perspectives. Journal de Physique IV, 139, 101–118.

Giorgi, F., Coppola, E., Teichmann, C., & Jacob, D. (2021). Editorial for the CORDEX-CORE Experiment I Special Issue. Climate Dynamics, 57(5), 1265–1268.

Graef, F., & Haigis, J. (2001). Spatial and temporal rainfall variability in the Sahel and its effects on farmers' management strategies. Journal of Arid Environments, 48(2), 221–231.

Graves, A., Rosa, L., Nouhou, A. M., Maina, F., & Adoum, D. (2019). Avert catastrophe now in Africa's Sahel. Nature, 575(7782), 282–286.

Grist, J. P., & Nicholson, S. E. (2001). A Study of the Dynamic Factors Influencing the Rainfall Variability in the West African Sahel. In Journal of Climate (Vol. 14, Issue 7, pp. 1337–1359). https://doi.org/10.1175/1520-0442(2001)014<1337:asotdf>2.0.co;2

Grodsky, S. A. (2003). Near surface westerly wind jet in the Atlantic ITCZ. Geophysical Research Letters, 30(19). https://doi.org/10.1029/2003gl017867

Guedes do Nascimento, M., Herdies, D. L., & Oliveira de Souza, D. (2016). The south American water balance: The influence of low-level jets. Journal of Climate, 29(4), 1429–1449.

Gu, G., & Adler, R. F. (2004). Seasonal Evolution and Variability Associated with the West African Monsoon System. In Journal of Climate (Vol. 17, Issue 17, pp. 3364–3377). https://doi.org/10.1175/1520-0442(2004)017<3364:seavaw>2.0.co;2

Guha-Sapir, D., Hoyois, P., & Below, R. (2013). Annual disaster review 2012: The numbers and trends. Centre for Research on the Epidemiology of Disasters (CRED), Institute of Health and Society (IRSS), Universite Catholique de Louvain-Brussels, Belgium.

Guo, H., John, J. G., Blanton, C., McHugh, C., Nikonov, S., Radhakrishnan, A., Rand, K., Zadeh, N. T., Balaji, V., Durachta, J., Dupuis, C., Menzel, R., Robinson, T., Underwood, S., Vahlenkamp, H., Bushuk, M., Dunne, K. A., Dussin, R., Gauthier, P. P. G., … Zhang, R. (2018). NOAA-GFDL GFDL-CM4 model output historical [Data set]. Earth System Grid Federation. https://doi.org/10.22033/ESGF/CMIP6.8594

Gutowski, W. J., Ullrich, P. A., Hall, A., Leung, L. R., O'Brien, T. A., Patricola, C. M., Arritt, R. W., Bukovsky, M. S., Calvin, K. V., Feng, Z., Jones, A. D., Kooperman, G. J., Monier, E., Pritchard, M. S., Pryor, S. C., Qian, Y., Rhoades, A. M., Roberts, A. F., Sakaguchi, K., … Zarzycki, C. (2020). The Ongoing Need for High-Resolution Regional Climate Models: Process Understanding and Stakeholder Information. Bulletin of the American Meteorological Society, 101(5), E664–E683.

Hagos, S. M., & Cook, K. H. (2008). Ocean Warming and Late-Twentieth-Century Sahel Drought and Recovery. Journal of Climate, 21(15), 3797–3814.

Harris, I., Osborn, T. J., Jones, P., & Lister, D. (2020). Version 4 of the CRU TS monthly high-resolution gridded multivariate climate dataset. Scientific Data, 7(1), 109.

Hartman, A. T. (2018). An analysis of the effects of temperatures and circulations on the strength of the low-level jet in the Turkana Channel in East Africa. In Theoretical and Applied Climatology (Vol. 132, Issues 3-4, pp. 1003–1017). https://doi.org/10.1007/s00704-017-2121-x

Hassan, I., Kalin, R. M., White, C. J., & Aladejana, J. A. (2020). Selection of CMIP5 GCM Ensemble for the Projection of Spatio-Temporal Changes in Precipitation and Temperature over the Niger Delta, Nigeria. In Water (Vol. 12, Issue 2, p. 385). https://doi.org/10.3390/w12020385

Hastenrath, S. (1995). Recent advances in tropical climate prediction. Journal of Climate. https://journals.ametsoc.org/view/journals/clim/8/6/1520-0442_1995_008_1519_raitcp_2_0_co_2.xml

Heinzeller, D., Duda, M. G., & Kunstmann, H. (2016). Towards convection-resolving, global atmospheric simulations with the Model for Prediction Across Scales (MPAS) v3.1: an extreme scaling experiment. Geoscientific Model Development, 9(1), 77–110.

Hersbach, H., Bell, B., Berrisford, P., Hirahara, S., Horányi, A., Muñoz-Sabater, J., Nicolas, J., Peubey, C., Radu, R., Schepers, D., Simmons, A., Soci, C., Abdalla, S., Abellan, X., Balsamo, G., Bechtold, P., Biavati, G., Bidlot, J., Bonavita, M., … Jean-Noël Thépaut. (2020). The ERA5 global reanalysis. Quarterly Journal of the Royal Meteorological Society, 146(730), 1999–2049.

Hersbach, H., Bell, B., Berrisford, P., Biavati, G., Dee, D., Horányi, A., ... & Vamborg, F. (2019, January). The ERA5 Global Atmospheric Reanalysis at ECMWF as a comprehensive dataset for climate data homogenization, climate variability, trends and extremes. In Geophysical Research Abstracts (Vol. 21).

Hidalgo, H. G., Durán-quesada, A. M., Amador, J. A., & Alfaro, E. J. (2015). The caribbean low-level jet, the inter-tropical convergence zone and precipitation patterns in the intra-americas sea: a proposed dynamical mechanism. Geografiska Annaler: Series A, Physical Geography, 97(1), 41–59.

Hong, S.-Y., & Lim, J.-O. J. (2006). The WRF single-moment 6-class microphysics scheme (WSM6). Asia-Pacific Journal of Atmospheric Sciences, 42(2), 129–151.

Hosten, A. (2018). African Easterly Jet: Double Core Structure and Effect on Easterly Wave Development. https://fsu.digital.flvc.org/islandora/object/fsu%3A650281

Hourdin, F., Găinusă-Bogdan, A., Braconnot, P., Dufresne, J.-L., Traore, A.-K., & Rio, C. (2015). Air moisture control on ocean surface temperature, hidden key to the warm bias enigma. Geophysical Research Letters, 42(24), 10,885–10,893.

Huang, W. (2019). THU CIESM model output prepared for CMIP6 CMIP historical [Data set]. Earth System Grid Federation. https://doi.org/10.22033/ESGF/CMIP6.8843

Huang, X., Rhoades, A. M., Ullrich, P. A., & Zarzycki, C. M. (2016). An evaluation of the variable-resolutionCESMfor modeling California's climate. Journal of Advances in Modeling Earth Systems, 8(1), 345–369.

Iles, C. E., Vautard, R., Strachan, J., Joussaume, S., Eggen, B. R., & Hewitt, C. D. (2020). The benefits of increasing resolution in global and regional climate simulations for European climate extremes. Geoscientific Model Development, 13(11), 5583–5607.

Indeje, M., Semazzi, F. H. M., & Ogallo, L. J. (2000). ENSO signals in East African rainfall seasons. International Journal of Climatology, 20(1), 19–46.

Indeje, M., Semazzi, F. H. M., Xie, L., & Ogallo, L. J. (2001). Mechanistic Model Simulations of the East African Climate Using NCAR Regional Climate Model: Influence of Large-Scale Orography on the Turkana Low-Level Jet. Journal of Climate, 14(12), 2710–2724.

Issa Lélé, M., Leslie, L. M., & Lamb, P. J. (2015). Analysis of Low-Level Atmospheric Moisture Transport Associated with the West African Monsoon. Journal of Climate, 28(11), 4414–4430.

Iyakaremye, V., Zeng, G., Siebert, A., & Yang, X. (2021). Contribution of external forcings to the observed trend in surface temperature over Africa during 1901–2014 and its future projection from CMIP6 simulations. Atmospheric Research, 254, 105512.

Jackson, L. S., Finney, D. L., Kendon, E. J., Marsham, J. H., Parker, D. J., Stratton, R. A., Tomassini, L., & Tucker, S. (2020). The Effect of Explicit Convection on Couplings

between Rainfall, Humidity, and Ascent over Africa under Climate Change. Journal of Climate, 33(19), 8315–8337. https://doi.org/10.1175/JCLI-D-19-0322.1

Janicot, S. (1992). Spatiotemporal Variability of West African Rainfall. Part I: Regionalizations and Typings. In Journal of Climate (Vol. 5, Issue 5, pp. 489–497). https://doi.org/10.1175/1520-0442(1992)005<0489:svowar>2.0.co;2

Jenkins, G. S., Gaye, A. T., & Sylla, B. (2005). Late 20th century attribution of drying trends in the Sahel from the Regional Climate Model (RegCM3). Geophysical Research Letters, 32(22). https://doi.org/10.1029/2005gl024225

Jiao, D., Xu, N., Yang, F., & Xu, K. (2021). Evaluation of spatial-temporal variation performance of ERA5 precipitation data in China. Scientific Reports, 11(1), 17956.

Jnr, S. D. (2014). Land degradation and agriculture in the Sahel of Africa: causes, impacts and recommendations. Journal of Agricultural Science and Applications, 3(03), 67–73.

Joly, M., & Voldoire, A. (2009). Influence of ENSO on the West African Monsoon: Temporal Aspects and Atmospheric Processes. Journal of Climate, 22(12), 3193–3210.

Joly, M., & Voldoire, A. (2010). Role of the Gulf of Guinea in the inter-annual variability of the West African monsoon: what do we learn from CMIP3 coupled simulations? International Journal of Climatology, 30(12), 1843–1856.

Joseph, P. V., & Sijikumar, S. (2004). Intraseasonal Variability of the Low-Level Jet Stream of the Asian Summer Monsoon. Journal of Climate, 17(7), 1449–1458.

Jungclaus, J., Bittner, M., Wieners, K.-H., Wachsmann, F., Schupfner, M., Legutke, S., Giorgetta, M., Reick, C., Gayler, V., Haak, H., de Vrese, P., Raddatz, T., Esch, M., Mauritsen, T., von Storch, J.-S., Behrens, J., Brovkin, V., Claussen, M., Crueger, T., … Roeckner, E. (2019). MPI-M MPI-ESM1.2-HR model output prepared for CMIP6 CMIP historical [Data set]. Earth System Grid Federation. https://doi.org/10.22033/ESGF/CMIP6.6594

Karley, N. K. (2009). Flooding and physical planning in urban areas in West Africa: situational analysis of Accra, Ghana. Theoretical and Empirical Researches in Urban Management, 4(4 (13), 25–41.

Kayaga, S. M., Amankwaa, E. F., Gough, K. V., Wilby, R. L., Abarike, M. A., Codjoe, S. N. A., Kasei, R., Nabilse, C. K., Yankson, P. W. K., Mensah, P., Abdullah, K., & Griffiths, P. (2021). Cities and extreme weather events: impacts of flooding and extreme heat on water and electricity services in Ghana. Environment and Urbanization, 33(1), 131–150.

Kebe, I., Diallo, I., Sylla, M. B., De Sales, F., & Diedhiou, A. (2020). Late 21st century projected changes in the relationship between precipitation, African Easterly Jet, and African Easterly Waves. Atmosphere, 11(4), 353.

Kidson, J. W., & Newell, R. E. (1977). African rainfall and its relation to the upper air circulation. Quarterly Journal of the Royal Meteorological Society, 103(437), 441–456.

Kim, J. Y., Kang, J.-S., & Joh, M. (2021). GPU acceleration of MPAS microphysics WSM6 using OpenACC directives: Performance and verification. Computers & Geosciences, 146, 104627.

Kinuthia, J. H., & Asnani, G. C. (1982). A Newly Found Jet in North Kenya (Turkana Channel). Republic of Kenya, Meteorological Department, Institute for Meteorological Training and Research.

Klemp, J. B., Skamarock, W. C., & Dudhia, J. (2007). Conservative Split-Explicit Time Integration Methods for the Compressible Nonhydrostatic Equations. Monthly Weather Review, 135(8), 2897–2913.

Koike, T. (2019). 3. Mechanism, Trends and DRR Strategy of Heavy Rain Disaster in Western Japan. HELP Global Report on Water and Disasters, 28.

Komolafe, A. A., Adegboyega, S. A.-A., & Akinluyi, F. O. (2015). A review of flood risk analysis in Nigeria. American Journal of Environmental Sciences, 11(3), 157.

Kong, X., Wang, A., Bi, X., Sun, B., & Wei, J. (2022). The Hourly Precipitation Frequencies in the Tropical-Belt Version of WRF: Sensitivity to Cumulus Parameterization and Radiation Schemes. Journal of Climate, 35(1), 285–304.

Kramer, M., Heinzeller, D., Hartmann, H., van den Berg, W., & Steeneveld, G.-J. (2020). Assessment of MPAS variable resolution simulations in the grey-zone of convection against WRF model results and observations. Climate Dynamics, 55(1), 253–276.

Kumi, N., & Abiodun, B. J. (2018). Potential impacts of 1.5 °C and 2 °C global warming on rainfall onset, cessation and length of rainy season in West Africa. Environmental Research Letters: ERL [Web Site], 13(5), 055009.

Landu, K., Ruby Leung, L., Hagos, S., Vinoj, V., Rauscher, S. A., Ringler, T., & Taylor, M. (2014). The Dependence of ITCZ Structure on Model Resolution and Dynamical Core in Aquaplanet Simulations. Journal of Climate, 27(6), 2375–2385. https://doi.org/10.1175/JCLI-D-13-00269.1

Lavaysse, C., Flamant, C., Janicot, S., & Knippertz, P. (2010). Links between African easterly waves, midlatitude circulation and intraseasonal pulsations of the West African heat low. Quarterly Journal of the Royal Meteorological Society, 136(S1), 141–158.

Lawal, K. A., Stone, D. A., Aina, T., Rye, C., & Abiodun, B. J. (2015). Trends in the potential spread of seasonal climate simulations over South Africa. International Journal of Climatology, 35(9), 2193–2209.

Le Barbé, L., Lebel, T., & Tapsoba, D. (2002). Rainfall Variability in West Africa during the Years 1950–90. Journal of Climate, 15(2), 187–202.

Lebel, T., & Ali, A. (2009). Recent trends in the Central and Western Sahel rainfall regime (1990–2007). Journal of Hydrology, 375(1), 52–64.

Lebel, T., Delclaux, F., Le Barbé, L., & Polcher, J. (2000). From GCM scales to hydrological scales: rainfall variability in West Africa. Stochastic Environmental Research and Risk Assessment: Research Journal, 14(4), 275–295.

Lee, W.-L., & Liang, H.-C. (2020). AS-RCEC TaiESM1.0 model output prepared for CMIP6 CMIP historical [Data set]. Earth System Grid Federation. https://doi.org/10.22033/ESGF/CMIP6.9755

Le Houerou, H. N. (1980). The rangelands of the Sahel. Rangeland Ecology & Management. https://journals.uair.arizona.edu/index.php/jrm/article/viewFile/7010/6620

Lélé, M. I. (2014). Atmospheric Moisture Transport Associated with the West African Monsoon System: An Observational Study and Evaluation of a WRF Dynamical Downscaling Simulation. University of Oklahoma.

Lélé, M. I., & Leslie, L. M. (2016). Intraseasonal variability of low-level moisture transport over West Africa. Climate Dynamics, 47(11), 3575–3591.

Lélé, M. I., Leslie, L. M., & Lamb, P. J. (2015). Analysis of low-level atmospheric moisture transport associated with the West African monsoon. Journal of Climate, 28(11), 4414–4430.

Leung, L. R., Mearns, L. O., Giorgi, F., & Wilby, R. L. (2003). Regional climate research: Needs and opportunities. Bulletin of the American Meteorological Society, 84(1), 89–95.

Li, J., Sun, Z., Liu, Y., You, Q., Chen, G., & Bao, Q. (2021). Top-of-atmosphere radiation budget and cloud radiative effects over the Tibetan plateau and adjacent monsoon regions from CMIP6 simulations. Journal of Geophysical Research, 126(9). https://doi.org/10.1029/2020jd034345

Li, J., Miao, C., Wei, W., Zhang, G., & Hua, L. (2021). Evaluation of CMIP6 global climate models for simulating land surface energy and water fluxes during 1979–2014. Journal of Advances. https://agupubs.onlinelibrary.wiley.com/doi/abs/10.1029/2021MS002515

Lim, K.-S. S., Hong, S.-Y., Yoon, J.-H., & Han, J. (2014). Simulation of the Summer Monsoon Rainfall over East Asia Using the NCEP GFS Cumulus Parameterization at Different Horizontal Resolutions. Weather and Forecasting, 29(5), 1143–1154.

Liu, T., Li, J., & Zheng, F. (2015). Influence of the Boreal Autumn Southern Annular Mode on Winter Precipitation over Land in the Northern Hemisphere. Journal of Climate, 28(22), 8825–8839.

Liu, W., Cook, K. H., & Vizy, E. K. (2020). Role of the West African westerly jet in the seasonal and diurnal cycles of precipitation over West Africa. Climate Dynamics, 54(1-2), 843–861.

Lovato, T., & Peano, D. (2020). CMCC CMCC-CM2-SR5 model output prepared for CMIP6 CMIP historical [Data set]. Earth System Grid Federation. https://doi.org/10.22033/ESGF/CMIP6.3825

Lüdecke, H.-J., Müller-Plath, G., Wallace, M. G., & Lüning, S. (2021). Decadal and multidecadal natural variability of African rainfall. Journal of Hydrology: Regional

Studies, 34, 100795.

Macadam, I., Rowell, D. P., & Steptoe, H. (2020). Refining projections of future temperature change in West Africa. Climate Research, 82, 1–14.

Maoyi, M. L., & Abiodun, B. J. (2021). How well does MPAS-atmosphere simulate the characteristics of the Botswana High? Climate Dynamics, 57(7-8), 2109–2128.

Maranan, M., Fink, A. H., & Knippertz, P. (2018). Rainfall types over southern West Africa: Objective identification, climatology and synoptic environment. In Quarterly Journal of the Royal Meteorological Society (Vol. 144, Issue 714, pp. 1628–1648). https://doi.org/10.1002/qj.3345

Marengo, J. A. (2002). The South American low-level jet east of the Andes during the 1999 LBA-TRMM and LBA-WET AMC campaign. In Journal of Geophysical Research (Vol. 107, Issue D20). https://doi.org/10.1029/2001jd001188

Marengo, J. A., Soares, W. R., Saulo, C., & Nicolini, M. (2004). Climatology of the Low-Level Jet East of the Andes as Derived from the NCEP–NCAR Reanalyses: Characteristics and Temporal Variability. Journal of Climate, 17(12), 2261–2280.

Martin, E. R., & Schumacher, C. (2011). The Caribbean Low-Level Jet and Its Relationship with Precipitation in IPCC AR4 Models. Journal of Climate, 24(22), 5935–5950.

Masih, I., Maskey, S., Mussá, F. E. F., & Trambauer, P. (2014). A review of droughts on the African continent: a geospatial and long-term perspective. Hydrology and Earth System Sciences, 18(9), 3635–3649.

Mathon, V., & Laurent, H. (2001). Life cycle of Sahelian mesoscale convective cloud systems. Quarterly Journal of the Royal Meteorological Society, 127(572), 377–406.

M. B. Sylla, I. Diallo and J. S. Pal (August 28th 2013). West African Monsoon in State-of-the-Science Regional Climate Models, Climate Variability - Regional and Thematic Patterns, Aondover Tarhule, IntechOpen, DOI: 10.5772/55140. Available from: https://www.intechopen.com/chapters/44055

Mbow, C., Halle, M., El Fadel, R., & Thiaw, I. (2021). Land resources opportunities for a growing prosperity in the Sahel. Current Opinion in Environmental Sustainability, 48, 85–

92.

McOmber, C. (2020). Women and climate change in the Sahel (West African Papers). Organisation for Economic Co-Operation and Development (OECD). https://doi.org/10.1787/e31c77ad-en

Mestas-Nuñez, A. M., Enfield, D. B., & Zhang, C. (2007). Water Vapor Fluxes over the Intra-Americas Sea: Seasonal and Interannual Variability and Associations with Rainfall. Journal of Climate, 20(9), 1910–1922.

Meynadier, R., Bock, O., Guichard, F., Boone, A., Roucou, P., & Redelsperger, J.-L. (2010). West African Monsoon water cycle: 1. A hybrid water budget data set. Journal of Geophysical Research, 115(D19). https://doi.org/10.1029/2010jd013917

Michaelis, A. C., Lackmann, G. M., & Robinson, W. A. (2019). Evaluation of a unique approach to high-resolution climate modeling using the Model for Prediction Across Scales – Atmosphere (MPAS-A) version 5.1. In Geoscientific Model Development (Vol. 12, Issue 8, pp. 3725–3743). https://doi.org/10.5194/gmd-12-3725-2019

Mitchell, M. J., Arritt, R. W., & Labas, K. (1995). A Climatology of the Warm Season Great Plains Low-Level Jet Using Wind Profiler Observations. Weather and Forecasting, 10(3), 576–591.

Monerie, P.-A., Biasutti, M., & Roucou, P. (2016). On the projected increase of Sahel rainfall during the late rainy season. International Journal of Climatology, 36(13), 4373–4383.

Monerie, P.-A., Wainwright, C. M., Sidibe, M., & Akinsanola, A. A. (2020). Model uncertainties in climate change impacts on Sahel precipitation in ensembles of CMIP5 and CMIP6 simulations. Climate Dynamics, 55(5), 1385–1401.

Monin, A. (1954). Basic laws of turbulent mixing in the surface layer of the atmosphere. Contrib. Geophys. Inst. Acad. Sci. USSR, 151(163), e187.

Montini, T. L., Jones, C., & Carvalho, L. M. V. (2019). The south American low-level jet: A new climatology, variability, and changes. Journal of Geophysical Research, 124(3), 1200–1218.

Muhammed, I. (2013). Interannual Variability of TRMM RADAR Precipitation over West

Africa and the Sahel. FUTY Journal of the Environment, 1–14.

Muñoz, E., Busalacchi, A. J., Nigam, S., & Ruiz-Barradas, A. (2008). Winter and Summer Structure of the Caribbean Low-Level Jet. Journal of Climate, 21(6), 1260–1276.

Muñoz, E., & Enfield, D. (2011). The boreal spring variability of the Intra-Americas low-level jet and its relation with precipitation and tornadoes in the eastern United States. In Climate Dynamics (Vol. 36, Issues 1-2, pp. 247–259). https://doi.org/10.1007/s00382-009-0688-3

Naik, M., & Abiodun, B. J. (2016). Potential impacts of forestation on future climate change in Southern Africa. International Journal of Climatology, 36(14), 4560–4576.

NASA-GISS. (2018). NASA-GISS GISS-E2.1G model output prepared for CMIP6 CMIP historical [Data set]. Earth System Grid Federation. https://doi.org/10.22033/ESGF/CMIP6.7127

National Academies of Sciences, Engineering, and Medicine (NASEM), Division on Earth and Life Studies, Board on Atmospheric Sciences and Climate, & Committee on Extreme Weather Events and Climate Change Attribution. (2016). Attribution of Extreme Weather Events in the Context of Climate Change. National Academies Press. https://play.google.com/store/books/details?id=WWEpDQAAQBAJ

Niang, A., Becker, M., Ewert, F., Dieng, I., Gaiser, T., Tanaka, A., Senthilkumar, K., Rodenburg, J., Johnson, J.-M., Akakpo, C., Segda, Z., Gbakatchetche, H., Jaiteh, F., Bam, R. K., Dogbe, W., Keita, S., Kamissoko, N., Mossi, I. M., Bakare, O. S., … Saito, K. (2017). Variability and determinants of yields in rice production systems of West Africa. Field Crops Research, 207, 1–12.

Nicholson, S. (2016). The Turkana low-level jet: mean climatology and association with regional aridity. International Journal of Climatology, 36(6), 2598–2614.

Nicholson, S. E. (2000). The nature of rainfall variability over Africa on time scales of decades to millenia. Global and Planetary Change, 26(1), 137–158.

Nicholson, S. E. (2008). The intensity, location and structure of the tropical rainbelt over west Africa as factors in interannual variability. International Journal of Climatology, 28(13),

1775–1785.

Nicholson, S. E. (2009). On the factors modulating the intensity of the tropical rainbelt over West Africa. International Journal of Climatology, 29(5), 673–689.

Nicholson, S. E. (2013a). The West African Sahel: A review of recent studies on the rainfall regime and its interannual variability. International Scholarly Research Notices, 2013. https://downloads.hindawi.com/archive/2013/453521.pdf

Nicholson, S. E. (2013b). The West African Sahel: A review of recent studies on the rainfall regime and its interannual variability. ISRN Meteorology, 2013, 1–32.

Nicholson, S. E. (2019). A review of climate dynamics and climate variability in Eastern Africa. The Limnology, Climatology and Paleoclimatology of the East African Lakes, 25–56.

Nicholson, S. E., & Grist, J. P. (2001). A conceptual model for understanding rainfall variability in the West African Sahel on interannual and interdecadal timescales. International Journal of Climatology, 21(14), 1733–1757.

Nicholson, S. E., & Webster, P. J. (2007). A physical basis for the interannual variability of rainfall in the Sahel. Quarterly Journal of the Royal Meteorological Society, 133(629), 2065–2084.

Nicolini, M., Saulo, A. C., Torres, J. C., & Salio, P. (2002). Enhanced precipitation over southeastern South America related to strong low-level jet events during austral warm season. Meteorologica, Special Issue for the South American Monsoon System, 27(1), 59–69.

Noguer, M., Jones, R., & Murphy, J. (1998). Sources of systematic errors in the climatology of a regional climate model over Europe. Climate Dynamics, 14(10), 691–712.

Oguntunde, P. G., Lischeid, G., & Abiodun, B. J. (2018). Impacts of climate variability and change on drought characteristics in the Niger River Basin, West Africa. Stochastic Environmental Research and Risk Assessment: Research Journal, 32(4), 1017–1034.

Ojo, O. S., Adeyemi, B., & Ogolo, E. O. (2021). Geostatistical Distribution of Net Radiation at Different Sky Conditions over West Africa. Earth Systems and Environment, 5(1), 43-

57.

Okoloye, C. U., Aisiokuebo, N. I., Ukeje, J. E., Anuforom, A. C., & Nnodu, I. D. (2013). Rainfall Variability and the Recent Climate Extremes in Nigeria. Journal of Meteorology and Climate Science, 11(1), 49–57.

Okonkwo, C., Demoz, B., Sakai, R., Ichoku, C., Anarado, C., Adegoke, J., Amadou, A., & Abdullahi, S. I. (2015). Combined effect of El Niño southern oscillation and Atlantic multidecadal oscillation on Lake Chad level variability. In Cogent Geoscience (Vol. 1, Issue 1, p. 1117829). https://doi.org/10.1080/23312041.2015.1117829

Oliveira, M. I., Nascimento, E. L., & Kannenberg, C. (2018). A New Look at the Identification of Low-Level Jets in South America. Monthly Weather Review, 146(7), 2315–2334.

Omotosho, J. 'bayo, & Abiodun, B. J. (2007). A numerical study of moisture build-up and rainfall over West Africa. Meteorological Applications, 14(3), 209–225.

Onojeghuo, A. R., Balzter, H., & Monks, P. S. (2017). Tropospheric NO 2 concentrations over West Africa are influenced by climate zone and soil moisture variability. Atmospheric Chemistry and Physics Discussions, 1-21.

Osabohien, R., Iqbal, B. A., Osabuohien, E. S., Khan, M. K., & Nguyen, D. P. (2021). Agricultural trade, foreign direct investment and inclusive growth in developing countries: evidence from West Africa. Transnational Corporations Review, 1–12.

Paciorek, C. J., Stone, D. A., & Wehner, M. F. (2018). Quantifying statistical uncertainty in the attribution of human influence on severe weather. Weather and climate extremes, 20, 69-80.

Paeth, H., Capo-Chichi, A., & Endlicher, W. (2008). Climate change and food security in tropical West Africa—a dynamic-statistical modelling approach. Erdkunde, 101–115.

Paeth, H., Hall, N. M. J., Gaertner, M. A., Alonso, M. D., Moumouni, S., Polcher, J., Ruti, P. M., Fink, A. H., Gosset, M., Lebel, T., Gaye, A. T., Rowell, D. P., Moufouma-Okia, W., Jacob, D., Rockel, B., Giorgi, F., & Rummukainen, M. (2011). Progress in regional downscaling of west African precipitation. Atmospheric Science Letters, 12(1), 75–82.

Panthou, G., Vischel, T., & Lebel, T. (2014). Recent trends in the regime of extreme rainfall in

the Central Sahel. International Journal of Climatology, 34(15), 3998–4006.

Parish, T. R. (2000). Forcing of the Summertime Low-Level Jet along the California Coast. Journal of Applied Meteorology and Climatology, 39(12), 2421–2433.

Parish, T. R., Rodi, A. R., & Clark, R. D. (1988). A Case Study of the Summertime Great Plains Low Level Jet. Monthly Weather Review, 116(1), 94–105.

Park, S., & Shin, J. (2019). SNU SAM0-UNICON model output prepared for CMIP6 CMIP historical [Data set]. Earth System Grid Federation. https://doi.org/10.22033/ESGF/CMIP6.7789

Physical Geography. (n.d.). Retrieved December 14, 2021, from https://eros.usgs.gov/westafrica/physical-geography

Preethi, B., Sabin, T. P., Adedoyin, J. A., & Ashok, K. (2015). Impacts of the ENSO Modoki and other Tropical Indo-Pacific Climate-Drivers on African Rainfall. Scientific Reports, 5, 16653.

Pu, B., & Cook, K. H. (2010). Dynamics of the West African Westerly Jet. Journal of Climate, 23(23), 6263–6276.

Pu, B., & Cook, K. H. (2012a). Role of the West African westerly jet in Sahel rainfall variations. Journal of Climate, 25(8), 2880–2896.

Pu, B., & Cook, K. H. (2012b). Role of the West African Westerly Jet in Sahel Rainfall Variations. Journal of Climate, 25(8), 2880–2896.

Quenum, G. M. L. D., Quenum, G. M. L., Klutse, N. A. B., Dieng, D., Laux, P., Arnault, J., Kodja, J. D., & Oguntunde, P. G. (2019). Identification of Potential Drought Areas in West Africa Under Climate Change and Variability. In Earth Systems and Environment (Vol. 3, Issue 3, pp. 429–444). https://doi.org/10.1007/s41748-019-00133-w

Raj, J., Bangalath, H. K., & Stenchikov, G. (2019). West African Monsoon: current state and future projections in a high-resolution AGCM. Climate Dynamics, 52(11), 6441–6461.

Ranjha, R., Svensson, G., Tjernström, M., & Semedo, A. (2013). Global distribution and seasonal variability of coastal low-level jets derived from ERA-Interim reanalysis. Tellus.

Series A, Dynamic Meteorology and Oceanography, 65(1), 20412.

Ranjha, R., Tjernström, M., Semedo, A., Svensson, G., & Cardoso, R. M. (2015). Structure and variability of the Oman coastal low-level jet. In Tellus A: Dynamic Meteorology and Oceanography (Vol. 67, Issue 1, p. 25285). https://doi.org/10.3402/tellusa.v67.25285

Redelsperger, J.-L., Diongue, A., Diedhiou, A., Ceron, J.-P., Diop, M., Gueremy, J.-F., & Lafore, J.-P. (2002). Multi-scale description of a Sahelian synoptic weather system representative of the West African monsoon. Quarterly Journal of the Royal Meteorological Society, 128(582), 1229–1257.

Ridley, J., Menary, M., Kuhlbrodt, T., Andrews, M., & Andrews, T. (2019). MOHC HadGEM3-GC31-LL model output prepared for CMIP6 CMIP historical [Data set]. Earth System Grid Federation. https://doi.org/10.22033/ESGF/CMIP6.6109

Ridout, J. (2013). Physics Parameterization for Seasonal Prediction. NAVAL RESEARCH LAB MONTEREY CA MARINE METEOROLOGY DIV. https://apps.dtic.mil/sti/citations/ADA598266

Ridout, J. A., Barton, N. P., Janiga, M. A., Reynolds, C. A., May, J. C., Rowley, C., & Bishop, C. H. (2021). Surface radiative flux bias reduction through regionally varying cloud fraction parameter nudging in a global coupled forecast system. Journal of Advances in Modeling Earth Systems, 13(4). https://doi.org/10.1029/2019ms002006

Rife, D. L., Pinto, J. O., Monaghan, A. J., Davis, C. A., & Hannan, J. R. (2010). Global Distribution and Characteristics of Diurnally Varying Low-Level Jets. Journal of Climate, 23(19), 5041–5064.

Ringler, T. D., Jacobsen, D., Gunzburger, M., Ju, L., Duda, M., & Skamarock, W. (2011). Exploring a Multiresolution Modeling Approach within the Shallow-Water Equations. Monthly Weather Review, 139(11), 3348–3368.

Ringler, T. D., Thuburn, J., Klemp, J. B., & Skamarock, W. C. (2010). A unified approach to energy conservation and potential vorticity dynamics for arbitrarily-structured C-grids. Journal of Computational Physics, 229(9), 3065–3090.

Ringler, T., Ju, L., & Gunzburger, M. (2008). A multiresolution method for climate system

modeling: application of spherical centroidal Voronoi tessellations. Ocean Dynamics, 58(5-6), 475–498.

Roehrig, R., Bouniol, D., Guichard, F., Hourdin, F., & Redelsperger, J.-L. (2013). The Present and Future of the West African Monsoon: A Process-Oriented Assessment of CMIP5 Simulations along the AMMA Transect. Journal of Climate, 26(17), 6471–6505.

Rong, X. (2019). CAMS CAMS_CSM1.0 model output prepared for CMIP6 CMIP historical [Data set]. Earth System Grid Federation. https://doi.org/10.22033/ESGF/CMIP6.9754

Rosegrant, M. W., Cai, X., & Cline, S. A. (2002). World Water and Food to 2025: Dealing with Scarcity. Intl Food Policy Res Inst.

Ruchith, R. D., & Ernest Raj, P. (2015). Features of nocturnal low level jet (NLLJ) observed over a tropical Indian station using high resolution Doppler wind lidar. Journal of Atmospheric and Solar-Terrestrial Physics, 123, 113–123.

Rummukainen, M. (2010). State-of-the-art with regional climate models. Wiley Interdisciplinary Reviews. Climate Change, 1(1), 82–96.

Salio, P., Nicolini, M., & Zipser, E. J. (2007). Mesoscale Convective Systems over Southeastern South America and Their Relationship with the South American Low-Level Jet. Monthly Weather Review, 135(4), 1290–1309.

Sathiyamoorthy, V., & Mahesh, C. (2013). Characteristics of low clouds over the Arabian Sea. Journal of. https://doi.org/10.1002/2013JD020553

Saulo, A. C., Nicolini, M., & Chou, S. C. (2000). Model characterization of the South American low-level flow during the 1997–1998 spring–summer season. Climate Dynamics, 16(10), 867–881.

Semmler, T., Danilov, S., Rackow, T., Sidorenko, D., Barbi, D., Hegewald, J., Sein, D., Wang, Q., & Jung, T. (2018). AWI AWI-CM1.1MR model output prepared for CMIP6 CMIP historical [Data set]. Earth System Grid Federation. https://doi.org/10.22033/ESGF/CMIP6.2686

Shapiro, A., Gebauer, J., & Fedorovich, E. (2016). A Baroclinic Nocturnal Low-Level Jet over the Great Plains. AGU Fall Meeting Abstracts, 2016, A12C – 01.

Shiferaw, B., Tesfaye, K., Kassie, M., Abate, T., Prasanna, B. M., & Menkir, A. (2014). Managing vulnerability to drought and enhancing livelihood resilience in sub-Saharan Africa: Technological, institutional and policy options. In Weather and Climate Extremes (Vol. 3, pp. 67–79). https://doi.org/10.1016/j.wace.2014.04.004

Shiru, M. S., Chung, E.-S., Shahid, S., & Alias, N. (2020). GCM selection and temperature projection of Nigeria under different RCPs of the CMIP5 GCMS. Theoretical and Applied Climatology, 141(3-4), 1611–1627.

Shvili, J. (2021, May 17). West African Countries. World Atlas; WorldAtlas. https://www.worldatlas.com/geography/west-african-countries.html

Sinkovits, R. S., & Duda, M. G. (2016). Optimization and parallel load balancing of the MPAS Atmosphere Weather and Climate Code. Proceedings of the XSEDE16 Conference on Diversity, Big Data, and Science at Scale, 1–6.

Skamarock, W. C., & Klemp, J. B. (2008). A time-split nonhydrostatic atmospheric model for weather research and forecasting applications. Journal of Computational Physics, 227(7), 3465–3485.

Skamarock, W. C., Klemp, J. B., Duda, M. G., Fowler, L. D., Park, S.-H., & Ringler, T. D. (2012). A Multiscale Nonhydrostatic Atmospheric Model Using Centroidal Voronoi Tesselations and C-Grid Staggering. Monthly Weather Review, 140(9), 3090–3105.

Smith, E. N., Gebauer, J. G., Klein, P. M., Fedorovich, E., & Gibbs, J. A. (2019). The Great Plains Low-Level Jet during PECAN: Observed and Simulated Characteristics. Monthly Weather Review, 147(6), 1845–1869.

Smith, E. N., Gibbs, J. A., Fedorovich, E., & Klein, P. M. (2018). WRF Model Study of the Great Plains Low-Level Jet: Effects of Grid Spacing and Boundary Layer Parameterization. Journal of Applied Meteorology and Climatology, 57(10), 2375–2397.

Smith, R. L., Tebaldi, C., Nychka, D., & Mearns, L. O. (2009). Bayesian modeling of uncertainty in ensembles of climate models. Journal of the American Statistical Association, 104(485), 97-116.

Song, J., Liao, K., Coulter, R. L., & Lesht, B. M. (2005). Climatology of the Low-Level Jet at

the Southern Great Plains Atmospheric Boundary Layer Experiments Site. Journal of Applied Meteorology and Climatology, 44(10), 1593–1606.

Song, Z., Qiao, F., Bao, Y., Shu, Q., Song, Y., & Yang, X. (2019). FIO-QLNM FIO-ESM2.0 model output prepared for CMIP6 CMIP historical [Data set]. Earth System Grid Federation. https://doi.org/10.22033/ESGF/CMIP6.9199

Son, J.-H., & Seo, K.-H. (2020). Mechanisms for the Climatological Characteristics and Interannual Variations of the Guinea Coast Precipitation: Early Summer West African Monsoon. Atmosphere, 11(4), 396.

Stefanidis, S., Dafis, S., & Stathis, D. (2020). Evaluation of Regional Climate Models (RCMs) Performance in Simulating Seasonal Precipitation over Mountainous Central Pindus (Greece). WATER, 12(10), 2750.

Stouffer, R. J., Eyring, V., Meehl, G. A., Bony, S., Senior, C., Stevens, B., & Taylor, K. E. (2017). CMIP5 Scientific Gaps and Recommendations for CMIP6. In Bulletin of the American Meteorological Society (Vol. 98, Issue 1, pp. 95–105). https://doi.org/10.1175/bams-d-15-00013.1

Sultan, B., Baron, C., Dingkuhn, M., Sarr, B., & Janicot, S. (2005). Agricultural impacts of large-scale variability of the West African monsoon. Agricultural and Forest Meteorology, 128(1), 93–110.

Sultan, B., & Janicot, S. (2000). Abrupt shift of the ITCZ over West Africa and intra-seasonal variability. Geophysical Research Letters, 27(20), 3353–3356.

Sultan, B., Janicot, S., & Diedhiou, A. (2003). The West African Monsoon Dynamics. Part I: Documentation of Intraseasonal Variability. Journal of Climate, 16(21), 3389–3406.

Swathi, M. S., Izumo, T., Lengaigne, M., Vialard, J., & Ramesh Kumar, M. R. (2020). Remote influences on the Indian monsoon low-level jet intraseasonal variations. In Climate Dynamics (Vol. 54, Issues 3-4, pp. 2221–2236). https://doi.org/10.1007/s00382-019-05108-1

Sylla, M. B., Dell'Aquila, A., Ruti, P. M., & Giorgi, F. (2010). Simulation of the intraseasonal and the interannual variability of rainfall over West Africa with RegCM3 during the

monsoon period. International Journal of Climatology, 30(12), 1865–1883.

Sylla, M. B., Gaye, A. T., Pal, J. S., Jenkins, G. S., & Bi, X. Q. (2009). High-resolution simulations of West African climate using regional climate model (RegCM3) with different lateral boundary conditions. Theoretical and Applied Climatology, 98(3-4), 293–314.

Sylla, M. B., Giorgi, F., Ruti, P. M., Calmanti, S., & Dell'Aquila, A. (2011). The impact of deep convection on the West African summer monsoon climate: a regional climate model sensitivity study. Quarterly Journal of the Royal Meteorological Society, 137(659), 1417–1430.

Sylla, M. B., Nikiema, P. M., Gibba, P., Kebe, I., & Klutse, N. A. B. (2016). Climate Change over West Africa: Recent Trends and Future Projections. In Adaptation to Climate Change and Variability in Rural West Africa (pp. 25–40). https://doi.org/10.1007/978-3-319-31499-0_3

Tang, Y., Rumbold, S., Ellis, R., Kelley, D., Mulcahy, J., Sellar, A., Walton, J., & Jones, C. (2019). MOHC UKESM1.0-LL model output prepared for CMIP6 CMIP historical [Data set]. Earth System Grid Federation. https://doi.org/10.22033/ESGF/CMIP6.6113

Tarek, M., Brissette, F. P., & Arsenault, R. (2020). Evaluation of the ERA5 reanalysis as a potential reference dataset for hydrological modelling over North America. Hydrology and Earth System Sciences, 24(5), 2527–2544.

Tarhule, A. (2005). Damaging rainfall and flooding: The other Sahel hazards. Climatic Change, 72(3), 355–377.

Taylor, C. M., Belušić, D., Guichard, F., Parker, D. J., Vischel, T., Bock, O., Harris, P. P., Janicot, S., Klein, C., & Panthou, G. (2017). Frequency of extreme Sahelian storms tripled since 1982 in satellite observations. Nature, 544(7651), 475–478.

Tennant, W. J., & Reason, C. J. C. (2005). Associations between the Global Energy Cycle and Regional Rainfall in South Africa and Southwest Australia. Journal of Climate, 18(15), 3032–3047.

Thorncroft, C. D., & Blackburn, M. (1999). Maintenance of the African easterly jet. Quarterly

Journal of the Royal Meteorological Society, 125(555), 763–786.

Tompkins, A. M., Diongue-Niang, A., Parker, D. J., & Thorncroft, C. D. (2005). The African easterly jet in the ECMWF Integrated Forecast System: 4D-Var analysis. Quarterly Journal of the Royal Meteorological Society, 131(611), 2861–2885.

Torres-Alavez, J. A., Das, S., Corrales-Suastegui, A., Coppola, E., Giorgi, F., Raffaele, F., Bukovsky, M. S., Ashfaq, M., Salinas, J. A., & Sines, T. (2021). Future projections in the climatology of global low-level jets from CORDEX-CORE simulations. Climate Dynamics, 57(5-6), 1551–1569.

Touzé-Peiffer, L., Barberousse, A., & Le Treut, H. (2020). The Coupled Model Intercomparison Project: History, uses, and structural effects on climate research. Wiley Interdisciplinary Reviews. Climate Change, 11(4). https://doi.org/10.1002/wcc.648

Trenberth, K. E., Dai, A., van der Schrier, G., Jones, P. D., Barichivich, J., Briffa, K. R., & Sheffield, J. (2013). Global warming and changes in drought. Nature Climate Change, 4(1), 17–22.

TRS Briefing1. (2021). Next generation climate models: a step change for net zero and climate adaptation. The Royal Society-Climate Change, 11.

Tschakert, P., Sagoe, R., Ofori-Darko, G., & Codjoe, S. N. (2010). Floods in the Sahel: an analysis of anomalies, memory, and anticipatory learning. In Climatic Change (Vol. 103, Issues 3-4, pp. 471–502). https://doi.org/10.1007/s10584-009-9776-y

Tuttle, J. D., & Davis, C. A. (2006). Corridors of Warm Season Precipitation in the Central United States. Monthly Weather Review, 134(9), 2297–2317.

United Nations. (2019). World Population Prospects, The 2019 Revision - Volume I: Comprehensive Tables. Department of Economics and Social Affairs, 9789210046428, 392.

USAID. (2018). CLIMATE RISKS IN WEST AFRICA: REGIONAL RISK PROFILE. Https://reliefweb.int/report/world/climate-Risk-Profile-West-Africa. https://reliefweb.int/report/world/climate-risk-profile-west-africa

USGS EROS. (2016). West African: Land use and land cover Dynamics. USGS EROS.

https://eros.usgs.gov/westafrica/node/157

Vellinga, M., Roberts, M., Vidale, P. L., Mizielinski, M. S., Demory, M.-E., Schiemann, R., Strachan, J., & Bain, C. (2016). Sahel decadal rainfall variability and the role of model horizontal resolution. Geophysical Research Letters, 43(1), 326–333.

Vichot-Llano, A., Martinez-Castro, D., Bezanilla-Morlot, A., Centella-Artola, A., Gil-Reyes, L., Torres-Alavez, J. A., Corrales-Suastegui, A., & Giorgi, F. (2021). Caribbean Low-Level Jet future projections using a multiparameter ensemble of RegCM4 configurations. International Journal of Climatology, joc.7319. https://doi.org/10.1002/joc.7319

Visser, S. M., & Sterk, G. (2007). Nutrient dynamics—wind and water erosion at the village scale in the Sahel. Land Degradation & Development, 18(5), 578–588.

Viswanadhapalli, Y., Dasari, H. P., Dwivedi, S., Madineni, V. R., Langodan, S., & Hoteit, I. (2020). Variability of monsoon low-level jet and associated rainfall over India. International Journal of Climatology, 40(2), 1067–1089.

Vizy, E. K., & Cook, K. H. (2009). A mechanism for African monsoon breaks: Mediterranean cold air surges. Journal of Geophysical Research, 114(D1). https://doi.org/10.1029/2008jd010654

Vizy, E. K., & Cook, K. H. (2019). Observed relationship between the Turkana low-level jet and boreal summer convection. Climate Dynamics, 53(7-8), 4037–4058.

Vogel, L. (2010). Food crisis escalates in Africa's Sahel region. CMAJ: Canadian Medical Association Journal = Journal de l'Association Medicale Canadienne, 182(12), E555–E556.

Volodin, E., Mortikov, E., Gritsun, A., Lykossov, V., Galin, V., Diansky, N., Gusev, A., Kostrykin, S., Iakovlev, N., Shestakova, A., & Emelina, S. (2019a). INM INM-CM4-8 model output prepared for CMIP6 CMIP historical [Data set]. Earth System Grid Federation. https://doi.org/10.22033/ESGF/CMIP6.5069

Volodin, E., Mortikov, E., Gritsun, A., Lykossov, V., Galin, V., Diansky, N., Gusev, A., Kostrykin, S., Iakovlev, N., Shestakova, A., & Emelina, S. (2019b). INM INM-CM5-0 model output prepared for CMIP6 CMIP historical [Data set]. Earth System Grid

Federation. https://doi.org/10.22033/ESGF/CMIP6.5070

Wang, C. (2002). Atlantic Climate Variability and Its Associated Atmospheric Circulation Cells. Journal of Climate, 15(13), 1516–1536.

Wang, C. (2007). Variability of the Caribbean Low-Level Jet and its relations to climate. Climate Dynamics, 29(4), 411–422.

Wang, C., Graham, R. M., Wang, K., Gerland, S., & Granskog, M. A. (2018). Comparison of ERA5 and ERA-Interim near surface air temperature and precipitation over Arctic sea ice: Effects on sea ice thermodynamics and evolution. The Cryosphere Discussions, 1–28.

Wang, C., Graham, R. M., Wang, K., Gerland, S., & Granskog, M. A. (2019). Comparison of ERA5 and ERA-Interim near-surface air temperature, snowfall and precipitation over Arctic sea ice: effects on sea ice thermodynamics and evolution. The Cryosphere, 13(6), 1661–1679.

Wang, Y., Leung, L. R., McGREGOR, J. L., Lee, D.-K., Wang, W.-C., Ding, Y., & Kimura, F. (2004). Regional Climate Modeling: Progress, Challenges, and Prospects. 気象集誌. 第2輯, 82(6), 1599–1628.

Weaver, S. J., & Nigam, S. (2011). Recurrent Supersynoptic Evolution of the Great Plains Low-Level Jet. Journal of Climate, 24(2), 575–582.

Wehner, M., Gleckler, P., & Lee, J. (2020). Characterization of long period return values of extreme daily temperature and precipitation in the CMIP6 models: Part 1, model evaluation. Weather and Climate Extremes, 30, 100283.

Wicker, L. J., & Skamarock, W. C. (2002). Time-Splitting Methods for Elastic Models Using Forward Time Schemes. Monthly Weather Review, 130(8), 2088–2097.

Wu, C.-H., Wang, S.-Y. S., & Hsu, H.-H. (2017). Large-scale control of the Arabian Sea monsoon inversion in August. Climate Dynamics. https://doi.org/10.1007/s00382-017-4029-7

Wu, T., Chu, M., Dong, M., Fang, Y., Jie, W., Li, J., Li, W., Liu, Q., Shi, X., Xin, X., Yan, J., Zhang, F., Zhang, J., Zhang, L., & Zhang, Y. (2018). BCC BCC-CSM2MR model output

prepared for CMIP6 CMIP historical [Data set]. Earth System Grid Federation. https://doi.org/10.22033/ESGF/CMIP6.2948

Xavier, A., Kottayil, A., Mohanakumar, K., & Xavier, P. K. (2018). The role of monsoon low-level jet in modulating heavy rainfall events. International Journal of Climatology, 38, e569–e576.

Yukimoto, S., Koshiro, T., Kawai, H., Oshima, N., Yoshida, K., Urakawa, S., Tsujino, H., Deushi, M., Tanaka, T., Hosaka, M., Yoshimura, H., Shindo, E., Mizuta, R., Ishii, M., Obata, A., & Adachi, Y. (2019). MRI MRI-ESM2.0 model output prepared for CMIP6 CMIP historical [Data set]. Earth System Grid Federation. https://doi.org/10.22033/ESGF/CMIP6.6842

Yu, Y. (2019). CAS FGOALS-f3-L model output prepared for CMIP6 CMIP historical [Data set]. Earth System Grid Federation. https://doi.org/10.22033/ESGF/CMIP6.3355

Zarzycki, C. M., Jablonowski, C., & Taylor, M. A. (2014). Using Variable-Resolution Meshes to Model Tropical Cyclones in the Community Atmosphere Model. Monthly Weather Review, 142(3), 1221–1239.

Zhang, C., & Wang, Y. (2017). Projected Future Changes of Tropical Cyclone Activity over the Western North and South Pacific in a 20-km-Mesh Regional Climate Model. Journal of Climate, 30(15), 5923–5941.

Zhang, Z., & Moore, J. C. (2015). Chapter 14 - Climate and Earth System Models. In Z. Zhang & J. C. Moore (Eds.), Mathematical and Physical Fundamentals of Climate Change (pp. 457–472). Elsevier.

Zhao, C., Leung, L. R., Park, S.-H., Hagos, S., Lu, J., Sakaguchi, K., Yoon, J., Harrop, B. E., Skamarock, W., & Duda, M. G. (2016). Exploring the impacts of physics and resolution on aqua-planet simulations from a nonhydrostatic global variable-resolution modeling framework. Journal of Advances in Modeling Earth Systems, 8(4), 1751–1768.

Zhao, C., Xu, M., Wang, Y., Zhang, M., Guo, J., Hu, Z., Ruby Leung, L., Duda, M., & Skamarock, W. (2019). Modeling extreme precipitation over East China with a global variable-resolution modeling framework (MPASv5.2): impacts of resolution and physics. In Geoscientific Model Development (Vol. 12, Issue 7, pp. 2707–2726).

https://doi.org/10.5194/gmd-12-2707-2019

Zhao, T., Chen, H., Pan, B., Ye, L., Cai, H., Zhang, Y., & Chen, X. (2021). Correspondence relationship between ENSO teleconnection and anomaly correlation for GCM seasonal precipitation forecasts. Climate Dynamics. https://doi.org/10.1007/s00382-021-05925-3

Zheng, D., van der Velde, R., Su, Z., Booij, M. J., Hoekstra, A. Y., & Wen, J. (2014). Assessment of Roughness Length Schemes Implemented within the Noah Land Surface Model for High-Altitude Regions. Journal of Hydrometeorology, 15(3), 921–937.

Zheng, T., Feng, S., Davis, K. J., Pal, S., & Morguí, J.-A. (2021). Development and evaluation of CO2 transport in MPAS-A v6.3. In Geoscientific Model Development (Vol. 14, Issue 5, pp. 3037–3066). https://doi.org/10.5194/gmd-14-3037-2021

Zhongming, Z., Linong, L., Wangqiang, Z., Wei, L., & Others. (2019). The CMIP6 landscape. http://resp.llas.ac.cn/C666/handle/2XK7JSWQ/187509

Wang, C. (2002). Atlantic climate variability and its associated atmospheric circulation cells. Journal of climate, 15(13), 1516-1536.